SOD1 A4V MUTATION INCREASES Nav1.3 CHANNEL EXCITABILITY on *XENOPUS* LAEVIS OOCYTE

by

Elif Kubat Öktem

B.S., in Molecular Biology and Genetics, Boğaziçi University, 2004

M.S., in Biomedical Engineering, Boğaziçi University, 2008

Submitted to the Institute of Biomedical Engineering

in partial fulfillment of the requirements

for the degree of

Doctor

of

Philosophy

Boğaziçi University

2016

SOD1 A4V MUTATION INCREASES Nav1.3 CHANNEL EXCITABILITY on *XENOPUS* LAEVIS OOCYTE

APPROVED BY:

Prof. Dr. Yekta Ülgen (Thesis Advisor)	.....
Prof. Dr. Ata Akın (Thesis Co-advisor)	.....
Prof. Dr. Nazlı Başak	.....
Prof. Dr. Mustafa Cengiz Yakıcıer	.....
Assoc. Prof. Dr. Bora Garipcan	.....
Assist. Prof. Dr. Esin Öztürk Işık	.....

DATE OF APPROVAL: 14 April 2016

ACKNOWLEDGMENTS

First of all I would like to express my sincere gratitude to Prof. Dr. Robert Brown Jr., for starting up this PhD thesis journey from Turkey to USA. This thesis wouldn‘t have been existed unless he had given me opportunity to work in his project. I would also thank to my coadvisor, Prof. Dr. Ata Akın for the continuous support of my Ph.D study and related research, motivation and his patience. His guidance helped me in all the time of my research. I could not have imagined having a better mentor for my Ph.D study.

I also want to thank to my advisor Prof. Dr. Yekta Ülgen for his comments and support for this thesis. Besides my advisor and co advisor, I would like to thank the rest of my thesis committee: Prof. Dr. Nazlı Başak, Prof. Dr. Mustafa Cengiz Yakıcıer, Associate Prof. Dr. Bora Garipcan and Assistant Prof. Dr. Esin Öztürk Işık for their insightful comments and encouragement.

My sincere thanks also goes to Prof. Dr. William Kobertz who provided me an opportunity to join his team as a guest researcher, and who gave access to the laboratory and research facilities. Without his precious support it would not be possible to conduct this research. He definitely made his lab, my second home in UMASS Medical School. I also want to thank to Prof. Dr. Ahmet Ademoğlu, Prof. Dr. Gürkan Öztürk, Associate Prof. Dr. Hanefi Özbek, Associate Prof. Dr. Chris Ahern, Associate Prof. Dr. Daryl Bosco, Associate Prof. Dr. Jennifer A Kearney, Nick Wightman and Joshua Chang for their valuable additions to this thesis.

I should state my thanks to Dr. Karen Mruk, my ‘sensei‘ for her help with everything which includes making me an electrophysiologist from scratch to editing the manuscript. A good friend, a teacher, a sister, a colleague, an abroad survival adviser, are only some aspects coming to my mind about her.

I would like to thank to Dr. Hülya Gündeşli, Evren Kocabaş Argon and Özge Yıldız for being my family in USA; life was easier and more fun with them. I also appreciate my friends in Turkey; Pınar Özel, Betül Polat, Dr. Sinem Burcu Erdoğan, Fatma Şimşek, Ayşe Sena Kabaş Sarp, İlknur Yurtsever and Seda Dumlu for their friendship, support and comments during this journey.

I would very much like to thank my family for their support and encouragements, especially my husband Kürşat Öktem, for being there whenever, wherever and whoever.

Last but not least, I should thank to my little son Ahmet Emir Öktem, for teaching me being a mother and a graduate student at the same time; for making me a more powerful and a happier woman.

ACADEMIC ETHICS AND INTEGRITY STATEMENT

I, Elif Kubat Öktem, hereby certify that I am aware of the Academic Ethics and Integrity Policy issued by the Council of Higher Education (YÖK) and I fully acknowledge all the consequences due to its violation by plagiarism or any other way.

Name :

Signature:

Date:

ABSTRACT

SOD1 A4V MUTATION INCREASES Nav1.3 CHANNEL EXCITABILITY on *XENOPUS* LAEVIS OOCYTE

Amyotrophic lateral sclerosis (ALS) is a lethal, paralytic disease caused by degeneration of motor neurons in the spinal cord, brain stem and motor cortex. Mutations in the gene encoding copper/zinc superoxide dismutase (SOD1) are present in 20 % of familial ALS and 2 % of all ALS cases. The most common SOD1 gene mutation in North America is a missense mutation substituting valine for alanine (A4V). In this study, sodium channel currents in oocytes expressing either wild type or mutant (A4V) SOD1 protein were analyzed. In this study elicited on *Xenopus* Laevis oocyte, it is demonstrated that the A4V mutation confers a propensity to hyperexcitability on a voltage dependent sodium channel (Na_v) mediated by heightened total Na^+ conductance and a hyperpolarizing shift in the voltage dependence of Na_v 1.3 activation. To estimate the impact of these channel effects on excitability in an intact neuron, these changes were simulated in the program NEURON; this shows that the changes induced by mutant SOD1 increase the spontaneous firing frequency of the simulated neuron. These findings are consistent with the view that excessive excitability of neurons is one component in the pathogenesis of this disease.

Keywords: Na_v channel, amyotrophic lateral sclerosis, hyperexcitability, superoxide dismutase, oocyte

ÖZET

SOD1 A4V MUTASYONU *XENOPUS* LAEVIS OOSİTİNDE Nav1.3 KANALININ EKSİTASYONUNU ARTIRIR

Amyotrofik lateral skleroz (ALS), omurilik, beyin sapı ve motor korteksteki motor nöronların dejenerasyonu ile gerçekleşen, ölümcül ve paralitik bir hastalıktır. Aileden gelen ALS vakalarının % 20'sinde ve toplam ALS vakalarının % 2'sinde bakır-çinko süperoksit dismutaz (SOD1) proteinindeki mutasyonlara rastlanır. SOD1 geninde görülen en yaygın mutasyon, alanin aminoasitinin valin aminoasitine (A4V) dönüştüğü missense mutasyonlardır. *Xenopus* Laevis oositinde yapılan bu çalışmada, A4V mutasyonunun voltaja duyarlı sodyum kanalında, toplam Na^+ geçirgenliğinde ve Na_v 1.3 'ün voltaja bağımlı aktivasyonunda hiperpolarize bir kaymaya neden olduğu gösterilmiştir. Kanal etkisinin eksitasyona olan etkisini nöronda göstermek için deneysel sonuçları NÖRON programında simule edilmiştir ve mutant SOD1 proteininin simule edilen nöronda simultane aksiyon potansiyelini artırdığı gözlemlenmiştir. Bu sonuçlar, hastalığın patojenitesinde, motor nöronlardaki aşırı eksitasyon olduğu görüşüyle tutarlıdır.

Anahtar Sözcükler: Voltaja duyarlı sodyum kanalı, amyotrofik lateral skleroz, hipereksitasyon, süperoksit dismutaz, oosit

TABLE OF CONTENTS

LIST OF FIGURES

LIST OF TABLES

LIST OF SYMBOLS

A_1	Approximate Portion-1 of the Inactivated Currents
A_2	Approximate Portion-2 of the Inactivated Currents
Bottom	Minimum Value of I/Imax
C	Fast Inactivation Equation Constant
C_m	Membrane Capacitance
E_k	Equilibrium Potential
E_K	Equilibrium Potential of Potassium Ions
E_L	Equilibrium Potential of Chloride Ions
E_{Na}	Equilibrium Potential of Sodium Ions
g_K	Conductance of Potassium Ions
$\bar{g_K}$	Maximum Specific Potassium Channel Conductance
G_K	Voltage dependent Conductance of Potassium Ions
g_L	Conductance of Chloride Ions
G_L	Voltage Independent Leakage Conductance
g_{Na}	Conductance of Sodium Ions
$\bar{g_{Na}}$	Maximum Specific Sodium Channel Conductance
G_{Na}	Voltage dependent Conductance of Sodium Ions
h	Sodium Conductance Inactivation State Parameter
I_{ext}	Externally Applied Current
I_{ion}	Ionic Current
I/I_{max}	Ratio of Current at a Specific Time Point to the Maximum Current
K	Recovery from Fast Inactivation Rate Constant
L	Length of the Segment
m	Sodium Conductance Activation State Parameter
n	Potassium Conductance State Parameter
$nseg$	Number of Segments
$Plateau$	I/Imax Value at Infinite Times
R_a	Radius of the Segment

slope	Steepness of the Curve
t	Time
T_1	Time Constant-1
T_2	Time Constant-2
Top	Maximum Value of I/Imax
V	Voltage
$V_{1/2}$	Potential Where Current Achieves Half-Maximal Value
V_m	Membrane Potential
α_h	Sodium Channel α Component of h Gating State
α_m	Sodium Channel α Component of m Gating State
β_h	Sodium Channel β Component of h Gating State
β_m	Sodium Channel β Component of m Gating State

LIST OF ABBREVIATIONS

ALS	Action Potential
ALS	Amyotrophic Lateral Sclerosis
diam	Diameter
DIV	Days in Vitro
EMG	Electromyography
EEC	El Escorial Criteria
fALS	Familial Amyotrophic Lateral Sclerosis
FTLD	Frontotemporal Lobe Degeneration
NMJ	Neuromuscular Junction
RP	Resting Potential
SALS	Sporadic Amyotrophic Lateral Sclerosis
SOD1	Cu-Zn Superoxide Dismutase
TEVC	Two Electrode Voltage Clamp
TTX	Tetrodotoxin

1. INTRODUCTION

1.1 Motivation and objectives

Amyotrophic lateral sclerosis (ALS) is a lethal paralytic disease in which death occurs within an average of 1.5 years of diagnosis. Toxic gain of function autosomal dominant mutations in the gene encoding cytosolic Cu/Zn superoxide dismutase 1 (SODl) are known to be responsible for 2 % of all familial amyotrophic lateral sclerosis cases. This 32 kDA protein is a free radical scavenger with its positively charged active site. Voltage gated sodium channels (Na_v) are responsible for action potentials which start with the voltage dependent influx of Na^+ to the cell with their 3 states related to membrane potential namely as; activation, inactivation and deactivation within a few milliseconds.

There exist many hypothesis about how SOD1 protein mutations lead to ALS; hyperexcitability of the motor neurons is one of the most popular view of nowadays. Although how mutant SOD1 mutations lead to hyperexcitability is still on debate, the fact that the only accepted ALS drug, riluzole, is indeed a Na_v channel blocker, encourages scientists to attach importance to hyperexcitability theory of ALS.

In this study, it was hypothesized that mutant SOD1 leads to the hyperexcitability and excessive firing of motor neurons. To test this hypothesis, Na_v channel 1.3 isoform and the most severe SOD1 mutation, which is A4V were used for electrophysiological experiments. The experimental results were then simulated with 'NEURON' simulation program to estimate the impact of electrophysiological results.

The goal of this study was; *To characterize the effect of human SOD1 wild type and mutant hSOD1^{A4V} protein on native Na_v channel conductance and functionality in terms of hyperexcitability.*

1.2 Problem Statement

ALS is the most frequent adult onset disease and death occurs within an average of 1.5 years of diagnosis. Identification of the pathogenic events in SOD1 -ALS is essential for the development of therapies. One of these therapies, are the Na_v channel inhibitors (riluzole, mexiletine). However, today, Na_v channel inhibitors, are not effective in delaying onset of ALS and riluzole. The only accepted ALS drug, riluzole, extends the patient survival only about 3 months, by mainly blocking $PICNa^+$ and excitability to a great extent. The reason for this drug‘s limited treatment capacity could be suggested that excitability changes are seen very early even in the first postnatal days, much before the observed symptoms and subsequent applications of riluzole can‘t heal the disease effectively. So, discovery of more specific drugs targeting hyperexcitability even at embryonic stages is a challenge today. Considering different sodium channel isoforms are expressed and dominate at different stages of development, this challenge could only be overcome by investigating Na_v channel excitability on the individual isoform manner and trying to invest drugs specific for the early stage isoforms.

1.3 Contribution of the Thesis

The exact mechanism explaining how SOD1 mutations cause ionic channel activity and motor neuron degeneration are still on debate. The general theory is that; if increased persistent sodium current leads to cell degeneration in SOD1 mutated ALS, then drugs that decrease this current should be neuroprotective. Overall, it could be speculated that persistent sodium channels have an important role in the development of intrinsic hyperexcitability. Although excitability changes of $hSOD1^{G93A}$ mutations on Na_v channels are reported in literature because of the availability of $hSOD1^{G93A}$ mutant mice commercially, there is no excitability change comparison study of one of the most important $hSOD1^{A4V}$ mutations in an isolated system with one Na_v channel isoform specific for embryonic stages of development. So, this study is the first

study which investigates the effect of most severe SOD1 mutation (hSOD1^{A4V}) on an early-stage developmental Na$_v$ channel isoform (Na$_v$1.3) in an isolated system.

In this study, chapter 2 consists of theoretical background of literature on which this project's hypothesis was built. The chapter starts with a brief introduction on the disease amyotrophic lateral sclerosis, SOD1 protein and continues with voltage gated sodium channels. Following them, some background information about the methods used, such as two electrode voltage clamp (TEVC), usage of *Xenopus* Laevis oocyte and Hodgkin- Huxley equations were described. Finally, the chapter is completed with providing examples of previous electrophysiological studies of ALS related neurophysiological defects.

Chapter 3 contains all the methods related to experimental parts of the project. In Chapter 4, results of the previous methods are given. Mathematical modeling of the data is presented in Chapter 5. Chapter 6 includes discussions and comments about this study. Chapter 7 concludes the project and gives some new directions for the proposed study.

2. BACKGROUND

2.1 Amyotrophic Lateral Sclerosis

2.1.1 General Properties of ALS

Amyotrophic lateral sclerosis (ALS) is a lethal paralytic disease caused by motor neuron death in the spinal cord, brain stem and motor cortex [1]. Today, it is the most frequent adult onset disease and death occurs within an average of 1.5 years of diagnosis [2]. Taking account the short period of prognosis, 1 in every 800 patients is assumed to have ALS in his lifetime [3, 4]. ALS is observed clinically at late stages, at almost always after the fourth decade of life and mortality is inevitable after 2-5 years of disease onset. Disease duration is highly variable even between patients from one family, with the same mutation, suggesting that other factors play a role in modification of the phenotype [5]. Although both upper and lower motor neurons are affected in this disease; autonomic nervous, cognitive and sensational functions remain intact. Eye movement and pelvic floor muscles remain unaffected during the disease and brings about the idea of selective motor neuron degeneration [6]. In addition to the motor neuron degeneration, frontotemporal dementia is seen in approximately 1 out of 6 patients. This case is accepted as ALS with frontotemporal lobe degeneration (FTLD) [7]. Clinical prognosis of the disease is determined with muscle twitching and muscle weakness. Hyperreflexivity of facial muscles for bulbar onset, hyperreflexivity of limbs for spinal onset can be examined. Diagnosis of the disease is performed with clinical examination, electromyography (EMG) and El Escorial criteria (EEC) which was developed in 1990 [8].

Four body regions were specified for the EEC as;

1. Brain stem
2. Cervical

3. Thoracal

4. Lumbosacral

Environmental factors also might play a role in the etiology of the ALS cases. Severe exposure to some chemicals and heavy metals [9], and viral infection [10] are some of these environmental factors. Also, ALS cases are seen at higher ratios in some geographically isolated groups such as soccer players [11] and Chamarro people living in Guam. A plant, which is common in Guam, produces neurotoxin beta-methylamino-L-alanine (BMAA). This plant is the food of flying fox. Because Guam people feed on flying fox at considerable amounts; this potent neurotoxin is found in the brain tissue of Guam People [12] which could be speculated to be a reason for this disease‘s high frequency among those people. The classification of ALS cases according to the disease signs in these four regions is summarized in Table 2.1 which is modified from [8].

Table 2.1
El Escorial Table

Classification	**Clinical Presentation**
Definite ALS	lower and upper motor neuron in at least 3 body sign
Probable ALS	lower and upper motor neuron in at least 2 body sign
Clinically probable, laboratory supported ALS	lower and upper motor neuron in 1 body sign also electromyographic signs of active and chronic degeneration in at least 2 extremities
Possible ALS	Signs of lower and upper motor neuron in 1 body region only or upper motor neuron signs in 2 body region only or upper motor neuron signs in 2 or more body regions
UMN signs: spasticity, hyperreflexivity LMN signs: weakness, atrophy, fasciculation	

2.1.2 Etiology of ALS

The disease could occur in two categories as familial (FALS) and sporadic (SALS) in of which familial cases are about 10 % of all cases. Although these two groups are clinically indifferent, FALS is almost always autosomal dominant and patients without affected relatives are known to be in sporadic form [7]. ALS Online Genetics Database (ALSOD) (Table 2.2 is summarizing all the genetic loci related to ALS susceptibility.

Table 2.2
ALS Online Genetics Database (ALSOD)

Locus	Gene	Chromosome
ALS 1	SOD1	21q22.11
ALS 2	ALS2	2q33.2
ALS 3	ALS3	18q21
ALS 4	SETX	9q34.13
ALS 5	SPG11	15q14
ALS 6	FUS	16p11.2
ALS 7	ALS7	20p13
ALS 8	VAPB	20q13.33
ALS 9	ANG	14q11.1
ALS 10	TARDBP	1p36.22
ALS 11	FIG4	6q21
ALS 12	OPTN	10p13
ALS 13	ATXN2	12q23-q24.1
ALS 14	VCP	9p13
ALS 15	UBQLN2	Xp11.21
ALS 16	SIGMAR1	9p13
ALS 17	CHMP2B	3p12.1

Locus	Gene	Chromosome
ALS 18	PFN1	17p13.3
ALS 19	ERBB4	2q33.3-q34
ALS 20	HNRNPA1	12q13.1
ALS 21	MATR3	5q31.2
ALS-FTD2	CHCHD10	22q11.23
ALS-FTD1	C9orf72	9p21.2
ALS	UNC13A	19p13.12
ALS	DAO	12q24
ALS	DCTN1	2p13
ALS	NEFH	22q12.1-q13.1
ALS	PRPH	12q12
ALS	SQSTM1	5q35
ALS	TAF15	17q11.1-q11.2
ALS	SPAST	2p24
ALS	ELP3	8p21.1
ALS	LMNB1	5q23.2

2.2 SOD1

SOD1 is a 32000 Da homodimer protein keeping a structure of an eight stranded barrel with three extended loop regions; consisting of 153 amino acids in its whole structure [1]. The structure of SOD1 protein is indicated in Figure 2.1 which is modified from [13]. In this figure, The zinc and copper atoms are shown in cyan and orange, respectively.

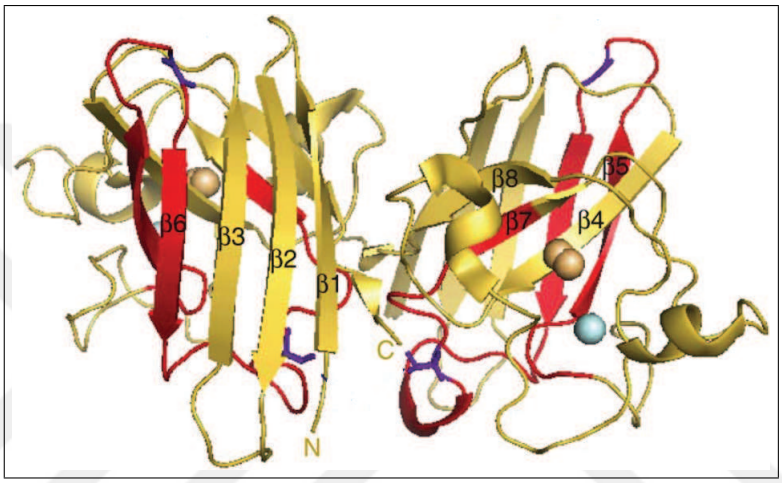

Figure 2.1 SOD1 Structure

SOD1 protein functions as a free radical scavenger with its positively charged active site. The superoxide anion is drawn into the positively charged active site and reacts with copper and is dismutated to hydrogen peroxide H_20_2 in a two step reaction [14]. Catalase or glutathione peroxidase in the cytoplasm converts hydrogen peroxide to H_20 [1]. This reaction is illustrated in Figure 2.2 which is modified from [14].

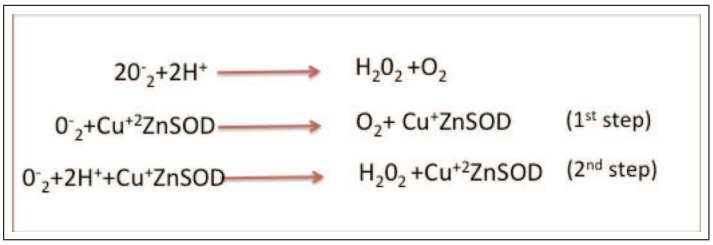

Figure 2.2 SOD1 Activity Equations

Toxic gain of function autosomal dominant mutations in the gene encoding cytosolic Cu/Zn superoxide dismutase 1 (SODl) are known to be responsible for 2 %

of FALS cases [15] although full activity is observed in most of these mutations [16]. Mutations at each fundamental structural element such as loop regions, disulfide bond, metal sides, inter monomer interface throughout this enzyme is assumed to lead to FALS linked ALS [17]. Up to date, more than 160 mutations of this protein have been found to be pathogenic [7] and all of these mutations cause autosomal dominant ALS, except for D90A mutation, which behaves as a recessive mutation [18]. These mutations are shown in Figure 2.3 which is modified from [5].

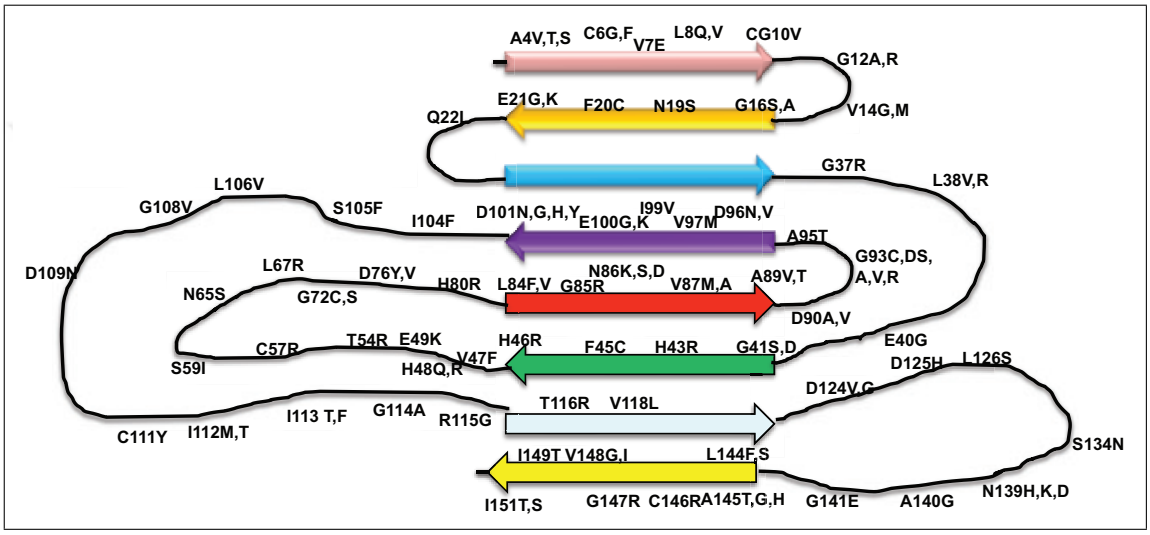

Figure 2.3 SOD1 Mutations

One of these mutations, A4V (Alanine 4 to Valine), is described by a rapid symptom onset and relatively fast progression, with a mean survival of usually 1 to 2 years [2]. Biochemical studies show that, this mutation reduces enzyme activity by 50 % [1]. Reduced thermal stability of the Apo protein is also observed [19], although catalytic and metal binding activities are not different compared to wild type Apo protein. Because of the severity of hSOD1^{A4V} mutations, functional studies of the effects of this mutation are also of importance. This mutation decreases half-life of enzyme activity correlating with the reduction of SOD1 activity. Thus, activity level is reduced while the protein gets less stable [20].

The ability of SOD1 mutants to cause neurodegeneration is not related to the loss of dismutase function [5]. This idea is strengthened by some observations such as;

1. The SOD1 mutant toxicity can not be inverted by SOD1 wild type coexpression [5].

2. SOD1 knock out mice do not cause neurodegeneration [21].

3. Full enzymatic activity of near wild type levels is acquired in most of these mutants [16].

Although the mechanisms explaining SOD1 mutations causing selective motor neuron death have not been put forward; A) misfolding (aberrant oligomerization) and B) aggregation of mutant SOD1 molecules are thought to be the reasons for gained toxic gain of function [5]. Numerous studies exist demonstrating SOD1 mutants destabilize native fold or quaternary structure [17, 22]. In other words, ALS could be speculated as one of the members of protein conformational disorders such as Alzheimer‘s. Also certain mutations lead to higher aggressiveness, accordingly; increased aggregation time leads to decreased survival time [23, 24]. Misfolding (Aberrant oligomerization) is an effect of some SOD1 mutations. The aggregation propensity and instability are demonstrated in Figure 2.4 which is taken from [24].

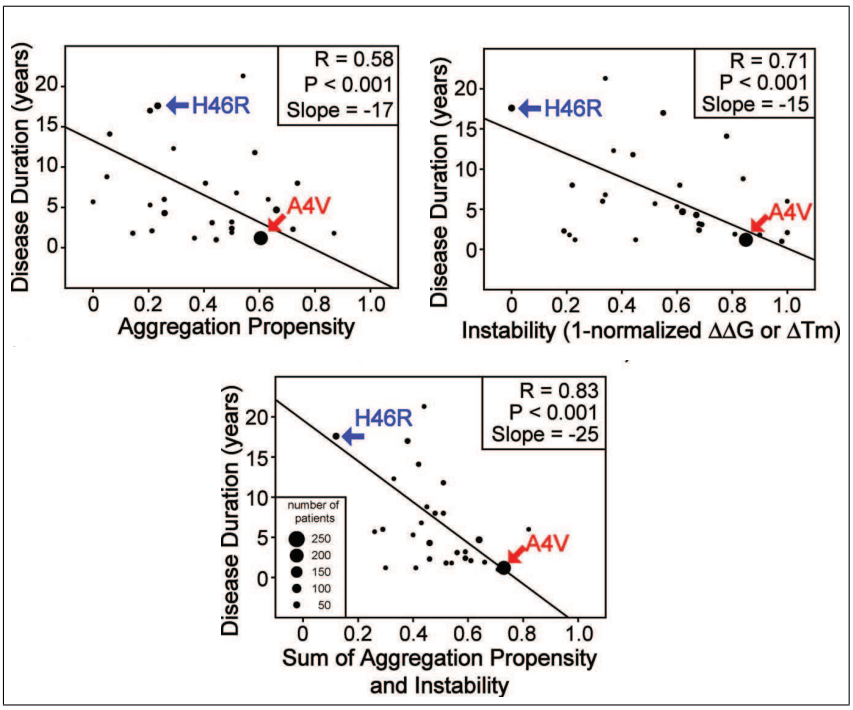

Figure 2.4 SOD1 Mutations Leading to Aggregation and Instability

SOD1 is a highly stable protein in its mature, homodimeric form and it rests on its extreme stability on the Zn^{+2} coordination (His-63, His-71, His-80, and Asp-83), which defends the eight-stranded Greek key beta-barrel. Copper ion (His-46, His-48, His-120, His-63) coordination and disulfide bridge between Cys-57 and Cys-146 do not impart monomer thermodynamic stability but assists dimer formation. The maturation events of SOD1 are interdependent such as; metal binding supports disulfide bond, disulfide bond assists dimerization and dimerization assigns SOD1 more durable to metal loss and disulfide bond degradation [25].

SOD1 aggregation starts with dimer dissociation and followed by metal loss (and/or disulfide reduction) resulting in non-native oligomer assembly. The rate of SOD1 aggregation is elevated with the decreased protein net charge magnitude, beta sheet gaining, alpha helix lose, and elevated hydrophobicity [24]. Post translation modification and apo monomer stability loses are the two additional mechanisms by which SOD1 mutations contribute to protein aggregation. Aggregation could be in two ways as; detergent resistant aggregates and soluble oligomers [5]. As discussed, disulfide bridge and metal binding both contribute to the intramolecular stability of SOD1 protein. Aggregate formation is associated with disulfide bridge weakening and Cysteine molecules at positions 6 and 11 contribute to the aggregate formation. Insoluble aggregates in brain and spinal cord are observed with the disease onset and increase in number with the disease progress which brings the idea that these molecules are by themselves toxic [26]. However, the fact that other instable protein form, which is the soluble oligomers are seen numerously since birth in motor neurons [27] would be an indicator of presence of these small toxic structures throughout life. The disease is revealed when the body no longer compensates with the toxic effects of these molecules. However, none of these mechanisms are directly proven [5].

Motor neuron death characterization of SOD1 related FALS is not clear. The situation occurs in two ways. In the first one, the current model for ALS has both characterization of apoptosis (which is programmed cell death of the cell itself) and necrosis (which is cell death caused by external factors other than the cell itself). Which one weighs more than the other is totally cell dependent [28]. In the second situation,

the cell goes through either cell autonomous or cell non autonomous process. In the cell autonomous process, the motor neuron dies independent of surrounding cells. However, recent studies show that non-neuronal cells are also important in ALS pathogenesis and progression [29]. More interestingly, mutant SOD1 expression in skeletal muscle causes disease progression and brings the idea of 'dying back' hypothesis where motor neuron is not the dying point. According to this hypothesis, the disease causing toxic signals are transferred from muscle to NMJ (neuromuscular junction) and from NMJ to motor neuron axons in a retrograde manner [30].

2.3 Voltage Gated Sodium (Na_v) Channels

2.3.1 General Information About Na_v Channels and Their Subunits

The first time voltage gated sodium channels Na_v introduced was 1952 when Hodgkin and Huxley performed some experiments about action potential of squid axon [31]. They demonstrated that action potential started with the voltage dependent influx of Na^+ to the cell and endured about 1-2 ms and ended with K^+ outflow from the cell to rebuild the original cell membrane electrical balance [32].

During 1970s, Armstong and Hille introduced some models of sodium channel function [33]; however the literal structure remained unsolved. Also some laboratories used neurotoxins in order to study the voltage dependent gating of sodium channels. It was 1980 when photoaffinity labeling technique was used to determine protein subunits of sodium channels [34]. According to that study, sodium channels have a 260 kDa α subunit and 30-40 kDa β subunits. α subunit is a trans membrane protein with around 2,000 amino acid residues and is composed of 4 homologous repeats. These repeats contain 6 transmembrane segments where both N and C termini of the residues lay on the membrane cytoplasmic site. β subunits consist of a C terminal intracellular segment, a single transmembrane segment and an N terminal extracellular segment [32] demonstrated as a cartoon in Figure 2.5.

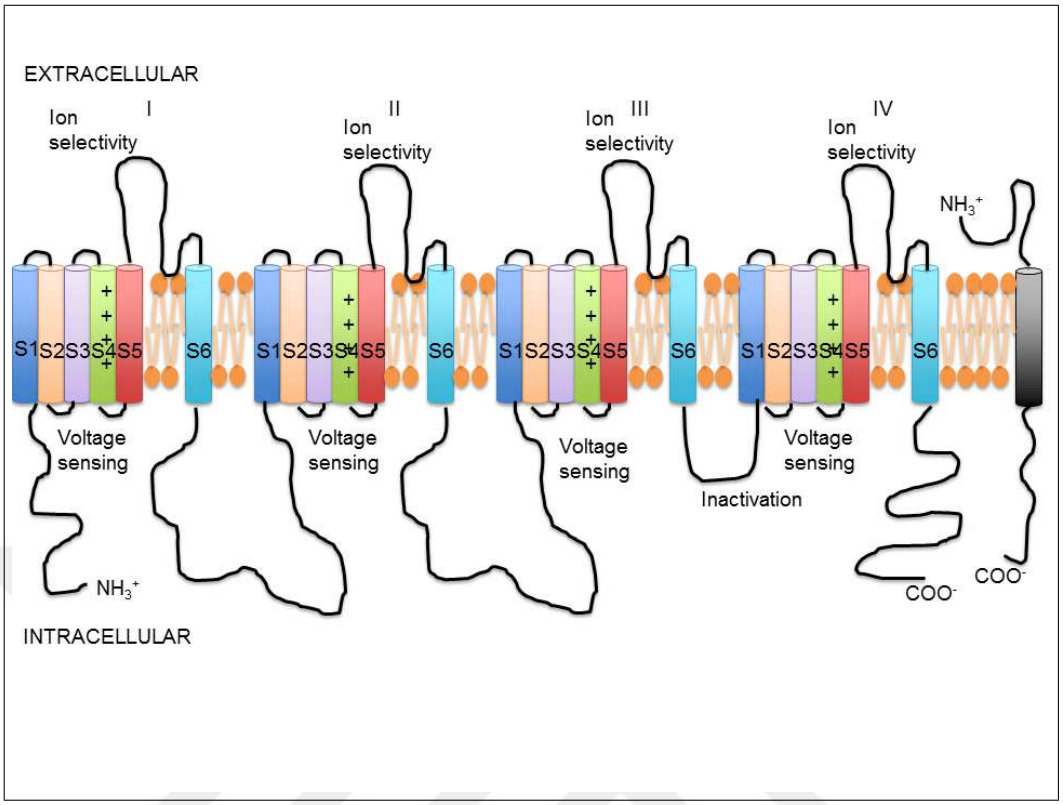

Figure 2.5 Sodium Channel Subunits

Among the genes responsible for α subunit transcription, 10 genes could be classified as a single family Na_v 1. Most of these isoforms could be expressed in exogenous systems [35]. Among them, peripheral nervous system channels are Na_v 1.7, Na_v 1.8, Na_v 1.9 whereas central nervous system channels are Na_v 1.2 , Na_v 1.3 and Na_v 1.6. Na_v 1.5 is mainly found in the heart; (Na_v) 1.4 is a skeletal muscle sodium channel [32]. The 10^{th} sodium channel protein is not voltage gated and it senses salt. This 'concentration sensitive' but not 'voltage sensitive ' isoform may introduce various crucial cellular effects [35]. Table 2.3 is summarizing the mammalian Na^+ channel genes. β subunit can be in different isoforms as; $\beta 1$, $\beta 2$, $\beta 3$, $\beta 4$. Brain sodium channels consist of a α subunit with non-covalently associated $\beta 1$ and $\beta 3$ subunits; a disulfide linked $\beta 2$ and $\beta 4$ subunits [36]. Expression of only α subunit is sufficient for channel functionality. Although β subunits don't change the functionality of the channel, they modulate the kinetics voltage dependence of activation and inactivation [37] as shown in Figure 2.6. Figure 2.6A is rat skeletal muscle SKM1 whereas Figure 2.6B is rat brain III. β subunits have a role in sodium channel localization on the cell membrane [38].

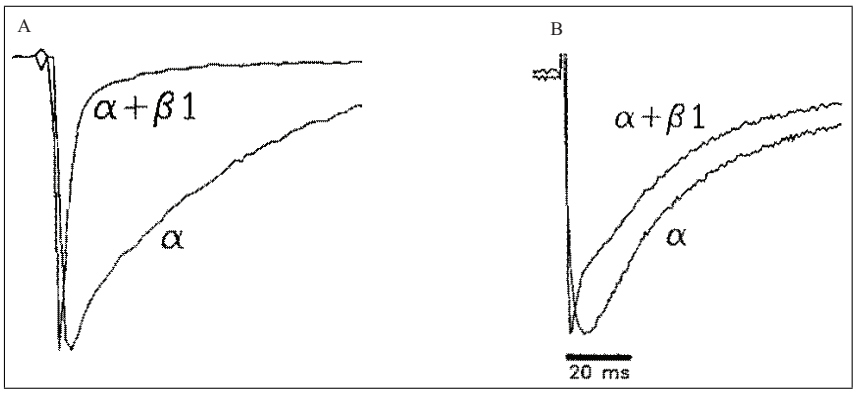

Figure 2.6 Modification of Sodium Channel with β Subunit

Table 2.3
Mammalian Na^+ Channel Genes

Isoform Name	Gene Symbol	Human Chromosome Location	Primary Tissues
Na_v 1.1	SCN1A	2q24	CNS neurons
Na_v 1.2	SCN2A	2q23-24	CNS neurons
Na_v 1.3	SCN3A	2q24	CNS neurons
Na_v 1.4	SCN4A	17q23-25	SkM
Na_v 1.5	SCN5A	3p21	Uninnervated SkM, heart
Na_v 1.6	SCN8A	12q13	CNS neurons
Na_v 1.7	SCN9A	2q24	PNS neurons
Na_v 1.8	SCN10A	3p22-24	DRG neurons
Na_v 1.9	SCN11A	3p21-24	DRG neurons
Na_v X	SCN7A,SCN6A	2q21-23	Uterus, astrocytes

According to Sato et. al. [39], Na_v channel has a bell shaped outer surface with 135 A^0 in height, a square shaped bottom with 100 A^0 side length, half spherical top with a diameter of 65 A^0. The upper 65 A^0 region has four small holes working as the extracellular Na^+ ion doors. These small holes are connected to the central pore, which is the ion permeation pore. At the lower pore, the central pore branches into four bigger holes working as cytoplasmic Na^+ ion doors which is modified from [35]. There are also four small peripheral holes other than the central pole residing in each repeat of the channel [35] as shown in Figure 2.7. These peripheral holes create internal hydrophilic environment for the sliding helix movement model of the channel [39].

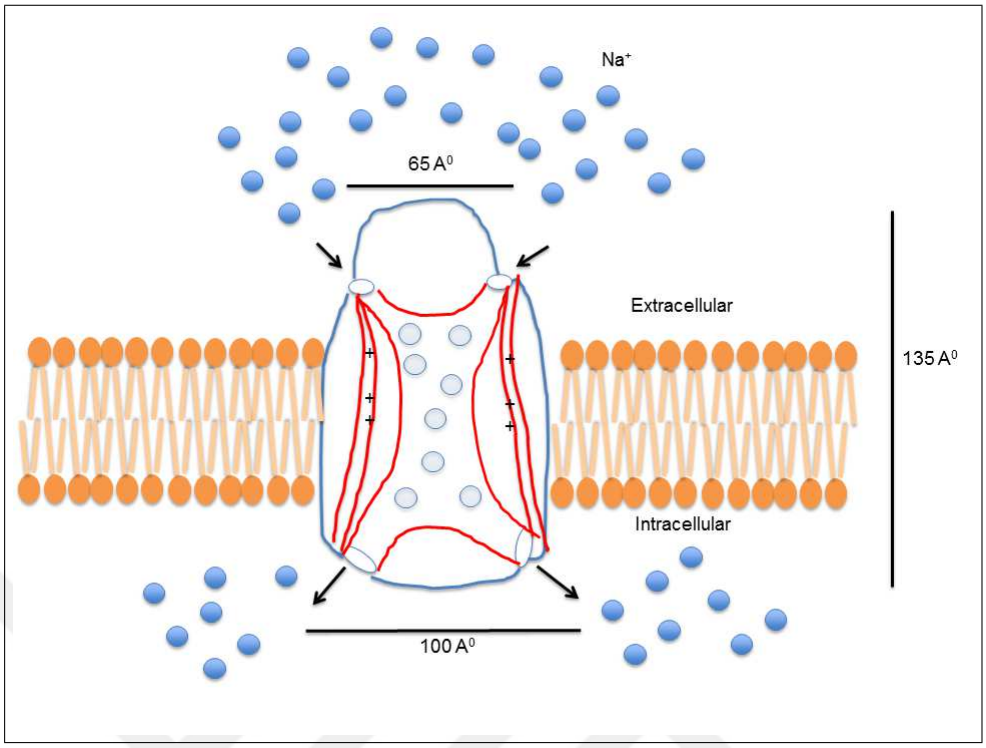

Figure 2.7 Sodium Channel Pores

Sodium channels possess spatial and temporal plasticity although localization borders can be observed sharply in a myelinated axon rode of Ranviers which are central places for saltatory conduction whereas they are much less denser at axon membrane intermodal places [40].

2.3.2 Sodium Channel Functions and its Functionality Elements

Voltage gated sodium channels (Na_v) are responsible for fast upstroke of action potential in nerve and muscle fibers. They have three important features as:

1. Voltage dependent activation in response to depolarization
2. Inactivation during a maintained depolarization
3. High selectivity of the channel pore to Na^+ ions [41].

1. ACTIVATION GATE:

   Hodgkin and Huxley explained activation of sodium channels as movement of three electrically charged particles across the membrane [31]. 6 to 8 positive charged residues at the fourth transmembrane segment of each repeat play an important role as voltage sensors in voltage dependent activation of the channel by the movement of charged residues within the membrane. The transmembrane segment usually contains arginine or lysine at every third position with two uncharged residues interrupting between them [41]. The fourth transmembrane segment of each repeat is called as S4 segment and it does not reside only on sodium channels but also on other cation-selective channels. Although the complete mechanism is not fully understood, sliding helix model is suggested to explain the S4 segment movement through the channel as illustrated in Figure 2.8 which is modified from [42].

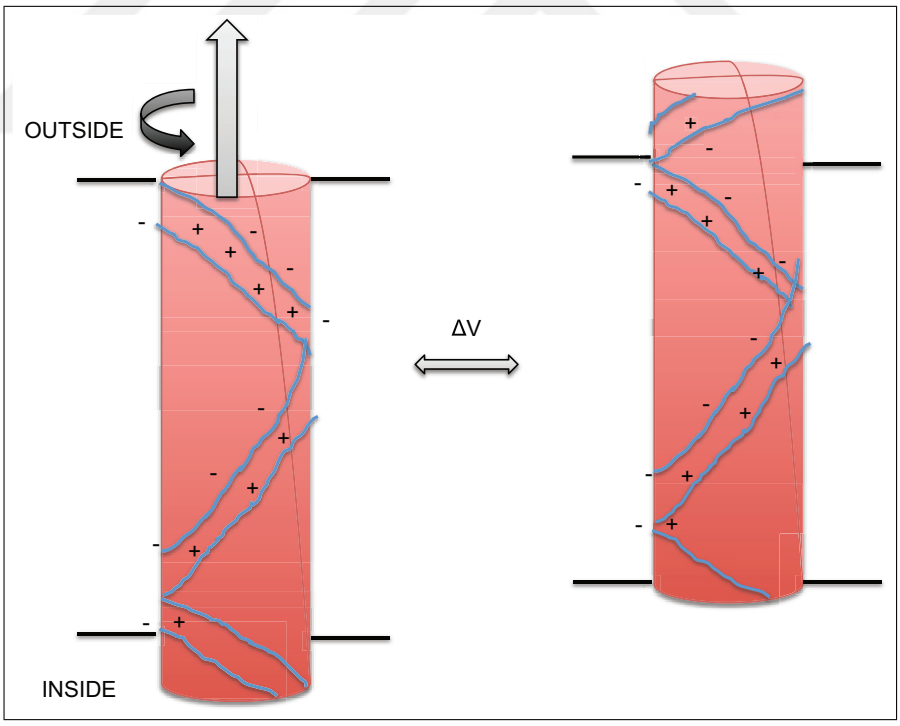

Figure 2.8 Sliding Helix Model

2. SELECTIVITY LOOP: The lining of the ion pore is made by the extracellular loop which links between segment 5 and segment 6 of each repeat. Positively charged tetrodotoxin (TTX) which is normally a Na_v channel blocker, binds

to the outer mouth of the channel. The binding of TTX is achieved by the negatively charged glutamate residue at position 387 (E387). When this residue is mutated to a neutral glycine molecule experimentally, TTX binding is inhibited. This experimental result indicates that negatively charged glutamate residue is a receptor site and forms the outer opening of the pore [41]. The amino acid residue mutations of this loop also control ion selectivity [32]. According to the crystal structure of the pore, it contains;

(a) A voluminous extracellular funnel

(b) An ion selectivity filter

(c) A water filled central cavity

(d) An intracellular activation gate [43].

3. INACTIVATION GATE: According to Hodgkin and Huxley [31], during action potential, sodium channels open and then inactivate in 1-2 ms. This fast inactivation process is important in repetitive firing of action potentials as well as nerve and muscle cell excitability management. There are two modes of inactivation as fast and slow. Intracellular loop between repeats 3 and 4 are responsible for fast inactivation. Hinged Lid model (Figure 2.9) explains how this short loop bends at a pair of glycine residues to fold into the intracellular opening of the pore and prevents sodium flow [44]. According to this model, the inactivation gate is placed on the cytoplasmic site of the membrane and the movement of it into the inner mouth of the pore inhibits the ion flux by enclosing the pore. Three hydrophobic residues, isoleucine-phenylalanine-methionine, (IFM) form the inactivation loop. Slow inactivation is kinetically and structurally distinct from fast inactivation although its exact mechanism is not fully understood. Mutations at the cytoplasmic ends of segment 5 and segment 6 inhibit slow inactivation [45].

2.3.3 Sodium Channel Gating States

Sodium channels are a member of an ion channel superfamily which are gated (membrane potential related open and close mechanism). 3 states related to membrane

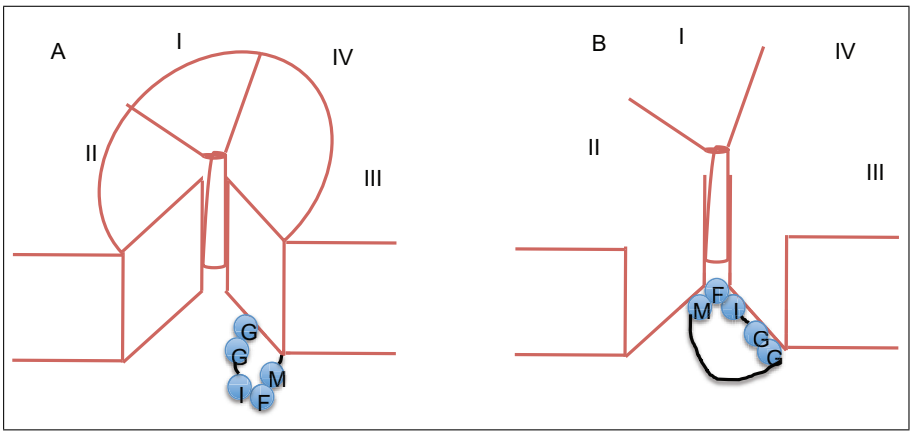

Figure 2.9 Hinged Lid Model

potential are observed among these channels as activation, inactivation and deactivation within a few milliseconds, shown in Figure 2.10. Closed state turns into the open (activation) state with a sudden local Na^+ influx upon depolarization. During this event, channel protein moves in an outward direction in accordance with sliding helix model as discussed before. Action potential uprise phase is characterized by this rapid influx of Na^+ ions. Inactivation linkers form the consequent gating process which is also called inactivation process. The inactivated channel should undergo recovery from inactivation before opening process. During sodium channel inactivation and voltage gated potassium channel activation part of action potential, the cellular membrane is repolarized. Sodium channels may go through deactivation (from open to closed state) during recovery from inactivation. Also, sodium channels may undergo a slower inactivation process where membrane depolarization takes a longer time [41].

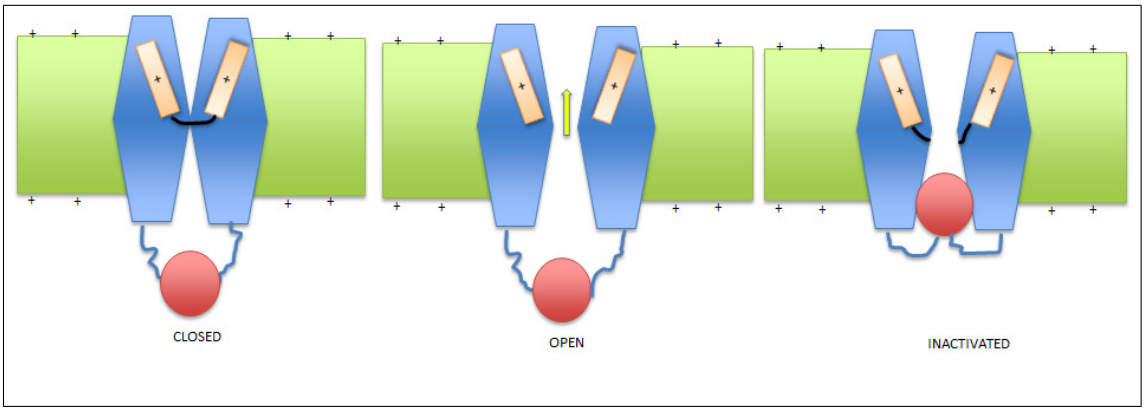

Figure 2.10 Sodium Channel Gating States

2.3.4 Drug Receptor Sites and Toxins of Sodium Channels

Na_v channel aminoacid residues in the S6 of repeats 1, 3 and 4 are responsible for the binding of local antiepileptics, anaesthetics and antiarrhythmics. These residues line the inner surface of the S6 segments and would block the pore [32]. Toxins of sodium channel could be grouped into five according to their binding sites. Most of these toxins bind to the activation or inactivation sites. Among these groups, only TTX (tetrodotoxin) binds to the outer pore of the channel. Some of these binding sites are also local places for Na_v channel disease mutations [35]. These sites are shown in Figure 2.11 which is modified from [35].

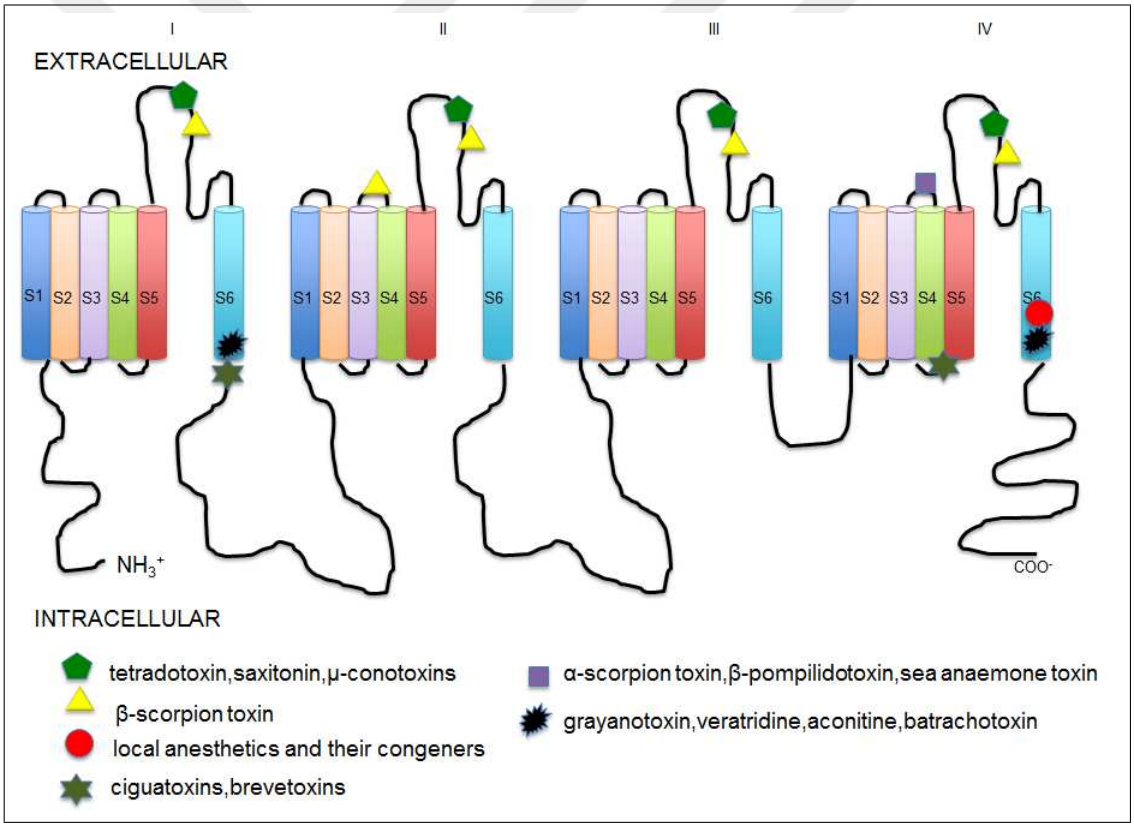

Figure 2.11 Sodium Channel Drug Receptors

2.3.5 Sodium Channel Diseases

Sodium channel related tissues are of important for having excitable cells responsible for generation and propagation of action potentials [41]. Hence, sodium channel disorders were one of the first ion channel diseases. These diseases lead to various symptoms ranging from mild to life threatening. The severity of these symptoms primarily depends on mutant protein expression levels at the tissues and sodium channel electrophysiological characteristics. Table 2.4 is a summary of sodium channel diseases which is modified from [32, 36].

Although some sodium channel diseases possess recessive inheritance, most of them are dominant with gain of function mutations [32]. For example, Na_v 1.4 mutations in skeletal muscle damages fast and/or slow inactivation and increase channel activity resulting in paramyotonia congenita and hyperkalaemic periodic paralysis by [46]. However, there also exists loss of function mutations. Dravet syndrome could be given as an example of loss of function mutation causing sodium channel disease. In this disease, Na_v 1.1 channel mutations cause discriminating damage to the GABAergic inhibitory neurons and result in epilepsy by producing hyperexcitability [47]. Not only α subunits, but also different β subunits/isoforms could be responsible for sodium channel related diseases [48].

Sodium channel diseases could be classified into two as;

1. Muscle sodium channel disorders:

   Two symptoms which are specific for muscle are myotonia and periodic paralysis. Muscle membrane excitability with continual action potentials and retarded muscle relaxation are some characteristics of myotonia. Weakness is seen as a symptom in paramyotonia congenital, whereas it is not seen in potassium aggravated myotonias (PAM) [49] where K^+ rich diet makes the symptoms worse. In contrast, periodic paralysis is characterized by a paucity of action potentials with an ephemeral state of inexcitability or hypoexcitability [50].

Table 2.4
(Na_v) Channel Diseases

GENE	CHANNEL	DISEASE
SCN1A	Na_v 1.1	Benign neonatal convulsions
SCN1A	Na_v 1.1	Generalized epilepsy with febrile seizures
SCN1A	Na_v 1.1	Dravet syndrome
SCN1A	Na_v 1.1	Familial Hemiplegic Migrane type III
SCN2A	Na_v 1.2	Benign Familial Neonatal -infantile Seizures
SCN4A	Na_v 1.4	K+ Sensitive Normokalaemic Periodic Paralysis
SCN4A	Na_v 1.4	Hyperkalaemic Periodic Paralysis
SCN4A	Na_v 1.4	Hypokalaemic Periodic Paralysis typeII
SCN4A	Na_v 1.4	Paramyotonia Congenita
SCN5A	Na_v 1.5	Brugada Syndrome
SCN5A	Na_v 1.5	Long QT Syndrome type III
SCN9A	Na_v 1.7	Congenital Indifference to Pain
SCN9A	Na_v 1.7	Paroxysmal Extreme Pain Disorder
SCN9A	Na_v1.7	Erythromelalgia
SCN1B	β1	Dravet syndrome
SCN1B	β1	Febrile Seizures
SCN1B	β1	Traumatic Nerve Injury
SCN1B	β1	Temporal Lobe Epilepsy
SCN2B	β2	Traumatic Nerve Injury
SCN2B	β2	Inflammatory Pain
SCN2B	β2	Post-traumatic Neuropathic Pain
SCN2B	β2	Multiple Sclerosis
SCN3B	β3	Traumatic Nerve Injury
SCN3B	β3	Temporal Lobe Epilepsy
SCN4B	β4	Huntington‘s Disease

2. Brain sodium channel disorders:

   Diseases known as generalized epilepsy with febrile seizures [48] and multiple sclerosis [51] could be given as examples of neurological diseases caused by Na_v channel mutations.

2.4 Persistent Current

During action potential, a fast inactivating sodium current is observed through the cell membrane. In addition to this current, some subthreshold sodium currents, namely as persistent sodium currents are observed [35]. So, when a depolarizing current is applied to cells, it also creates a plateau potential that overlasts the stimulus by several hundred milliseconds. Fast action potentials and plateau responses in the same cell are a result of two distinguishable sodium conductance mechanisms as;

1. Spikes generated by Hogkin Huxley inactivating sodium conductance
2. Plateu responses generated by noninactivating sodium conductance [52].

According to Crill [52], there is evidence of the existence of a more persistent sodium channel accompanying transient sodium current resulting from depolarization. This current possesses varying amplitude changing with clamp potential amplitude, noticeable first at potentials around -70 mV (activates around resting membrane potentials), extending an ultimate amplitude around -40 mV, with a >50 % of its detectable amplitude when the transient sodium current is inactivated [53]. This more slowly inactivating, persistent sodium current can also be blocked by tetrodotoxin (TTX) which is a transient sodium channel blocker, and is dissipated when extracellular sodium is replaced by choline and can‘t be blocked by calcium channel blocker cadmium. It is also very fast, exists within 3-4 ms [52]. The resistance of this current to inactivations brings the idea of its crucial role in repetitive firing of neurons. The reason for the existence of persistent currents can be hypothesized in 3 cases as [52]:

1. Window current hypothesis: According to Hodgkin-Huxley, there is a a small membrane potential at a tiny range where the m (activation) and h (inactivation) gates overlap [31]. The current at this range is called "window current". However, according to the studies, activation curve for persistent sodium conductance has a conductance maximum at -50 mV and does not decrease at even positive potentials whereas window current has a maximum at -50 mV, decreasing fast to zero with further depolarizing voltages [53].

2. Production of this current by special type of sodium channels: in literature, persistent sodium current is activated 10 mV negative to transient sodium current and this result can be interpreted as, different sodium channel subtypes could be responsible for persistent current [52]. This theory could be best tested by isolation of different subtypes pharmacologically or *Xenopus* oocyte system.

3. Transient sodium channel inactivation property: the channel with transient sodium current could also behave like a persistent sodium current channel when it fails to inactivate. This inactivation current is rare [54]. Those noninactivating currents play an important role in adjusting repetitive firing, increasing dentritic depolarizations, creating after depolarization potentials and plateau potentials [52].

2.4.1 Potential Mechanisms That Determine ALS Hyperexcitability

Increases in $PICNa^{+}$ (Persistent inward Na^{+} current) and $PICCa^{+2}$ (Persistent inward Ca^{+2} current) and accompanying variations in synaptic inputs, neuronal morphology and excitability have been observed in early developmental phases of mutant SOD1 mice motor neurons and interneurons [55]. $PICNa^{+}$ forms only 1-5 % of total current because the $PICNa^{+}$ is generated from the same typical fast $PICNa^{+}$ current and can be activated at similar voltages around resting potential [52, 56].

Elevations in $PICNa^{+}$ and $PICCa^{+2}$ could trigger a cascade of events responsible for glutamate excitotoxicity resulted from hyperexcitability. $PICNa^{+}$ and $PICCa^{+2}$

would induce post and pre- synaptic membrane depolarizations which would further lead to Ca^{+2} and Na^{+} influxes through other receptors like other Ca_v channels, NMDA and AMPA receptors committing to excitotoxicity [55]. This cascade of events are shown in Figure 2.12. In this figure (Modified from [55]), Small increases in PICNa via Na_v channels and PICCa via Ca_v channels would increase neuronal excitability synaptic transmission, resulting in toxic influxes of additional positive ions through Ca_v channels, NMDA and AMPA receptors. Limited Ca^{+2} buffering protein capacity of motor neurons forces the mitochondria to perform the buffering task, resulting in mitochondrial dysfunction. In addition to this, excess Ca^{+2} in the cytoplasm also activates expression of plasticity-related genes which would together with the disruption of the harmony between hyperpolarization and depolarization, damage local circuitry and networks, cause minor behavioral changes.

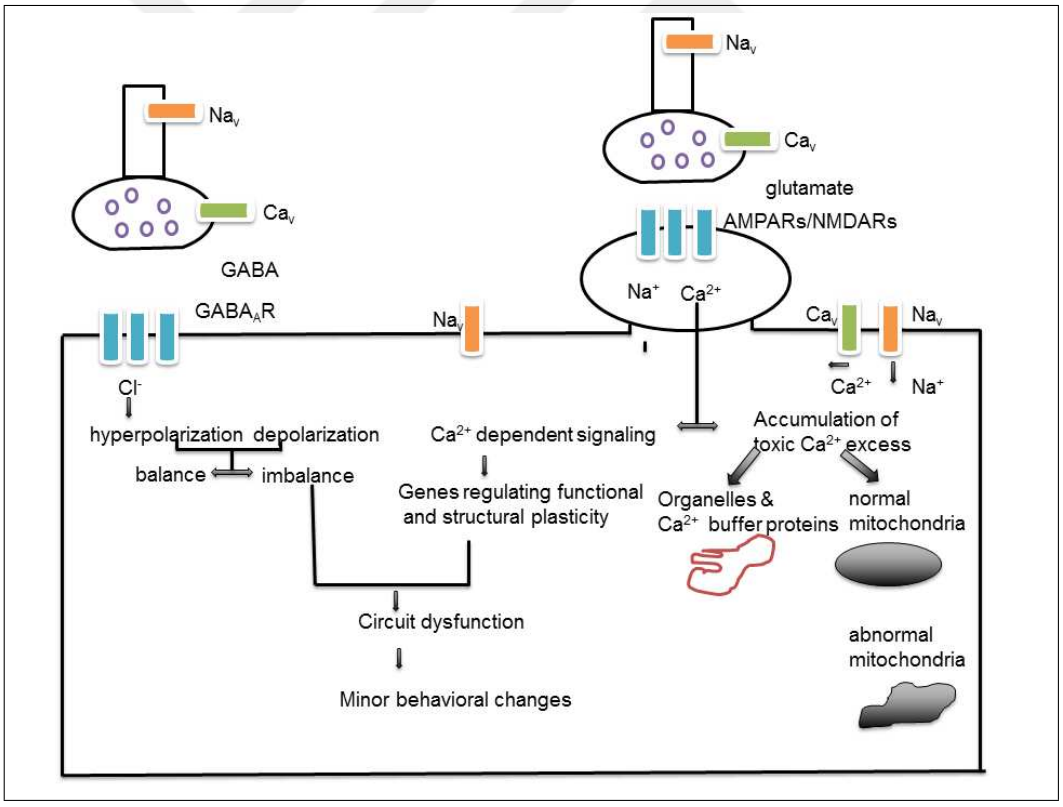

Figure 2.12 SOD1-PICNa$^+$ Relation

Some protein kinases, reactive oxygen and nitrogen species (ROS/ RNS) modify PICNa$^+$ [57, 58, 56]. Alterations in Na_v channel functionality is more important compared to other protein changes influenced by ROS. For instance, ROS decrease

function of NMDA, AMPA and L type Ca_v channels. Today, Na_v channel inhibitors, are not effective in delaying onset of ALS and riluzole. The only accepted ALS drug, extends the patient survival only about 3 months. Experiments done with riluzole demonstrate that the drug blocks Na_v channels, blocks $PICNa^+$ and excitability to a great extent [59, 60, 61, 62, 63]. The reason for this drug's limited treatment ability could be suggested that the alterations of motor and interneurons are seen very early even in the first postnatal days, much before the observed symptoms and subsequent applications of riluzole can't heal the disease effectively [55].

2.5 *Xenopus* Laevis Oocyte

2.5.1 General Properties of *Xenopus* Oocyte

South African clawed frog *Xenopus* laevis was used for early embryological studies and cell division regulation mechanisms in parallel with investigation of ion channels at a controlled in vivo environment [64]. Gurdon was the first person that synthesized exogenous proteins in the oocytes [65]. There exist mainly five types of oocyte studies to explore ion channels with two electrode voltage clamp (TEVC), patch clamp techniques or some other biochemical applications [66]. These are:

1. mRNA from isolated whole organs are injected to oocytes and analyzed free from other responses.
2. mRNA from a cDNA library is in vitro transcribed and injected to oocytes.
3. Defined mutations or chimeric molecules between close channels are constructed and injected to oocytes.
4. Human disorder causing mutations are determined functionally.
5. Potential drug effects on channels are screened with new generation high tech systems.

Both neurotransmitter and voltage activated ion channels could be synthesized in the oocyte system where some factors should be considered whether *Xenopus* oocyte expression system is the appropriate tool to use. Some advantages of the system are [66]:

1. Oocytes do not express a large quantity of endogenous channels so, when an exogenous channel is injected, it could be studied without the contamination of endogenous ones. Even if this case is not true for all situations, the current from injected exogenous channel is much larger than the endogenous one which makes it possible to record the exogenous channel without contamination from oocyte native current. Also, exogenous protein injection lowers the endogenous membrane protein synthesis rate because of the competition between oocyte endogenous mRNA [67].

2. Some channels can only be expressed in this expression systems instead of mammalian cells and injection success for mammalian cells depend on cell type.

3. The ratio of the RNA encoding each channel subunit can be adjusted in a more controlled fashion compared to the mammalian expression systems so that the roles of different subunits can be investigated.

4. Some specific analysis methods such as cut-open oocyte voltage clamp which is a high resolution technique which is important for fast ionic and gating current recordings.

5. Mutations and second messenger studies fit well with this expression system because injection and electrophysiology can be performed in a semi-automated mode. Also, multiple proteins and second messengers can be injected simultaneously during recording.

Considering the other side of the coin, some disadvantages of this expression system could be listed as [66, 64]:

1. All channels can‘t be expressed in this system. However, this problem is not unique to the use of *Xenopus* oocytes, it is a common problem of all expression systems.

2. Accessibility of a pharmacological agent is less because of the oocyte membrane, vitelline membrane around the surface and follicle cells around the oocyte cells. This requires more concentration of the drug applications compared to the native mammalian cells.

3. Oocyte studies require preparations and equipment beyond a traditional laboratory and performance of the expression depends on the oocyte quality which would oscillate due to the seasonal factors and ambient temperature.

4. Injected channels are not in their native environments and functional properties of these channels as well as cellular trafficking of these proteins would be different compared to the mammalian cells, especially neurons.

5. Different batches of oocytes would cause the diversity of results, notably in quantification of proteins, levels of internal secondary messengers and resting potential of membranes. All of these factors alter the exogenous channel assets. Comparison of different batches and oocytes as much as possible would be a solution to this problem.

Most of the electrophysiological studies are implemented with fully grown (stages 5 and 6) in *Xenopus* oocytes. The diameter of stage 6 oocytes are 1.2 to 1.3 mm and their surface is seen as two halves; melanin pigment containing dark brown animal hemisphere and yellowish white vegetal hemisphere. These two hemispheres have distinct properties as [64]:

1. There are more microvilli, membrane junctions between cytoplasm membrane and endoplasmic reticulum (ER) and cytoskeletal contractile structures in the animal hemisphere. Sperm penetration into the egg appears usually through animal hemisphere.

2. Vegetal hemisphere resides most of the oocyte RNA and membrane lipid lateral movement is faster in this hemisphere.

2.5.2 Human Voltage Dependent Na_v 1.3 Channel Expression of Oocytes

The currents from injected Na_v channel RNA is similar to the source Na_v channels is many aspects as tetrodotoxin (TTX) blockage, inactivation after a few milliseconds and 20 pS single channel conductances [64]. Sodium channel excitation disorders have been studied in skeletal muscle (Na_v 1.4) [49], brain [48] and sensory neurons (Na_v 1.7) [68]. Hundreds of mutations in Na_v 1.1 and Na_v 1.2 have been associated with epilepsy [69, 70, 71]. Among these channels, the expression levels of Na_v 1.3 are slightly different in rodent and human brains. In rodent central nervous system (CNS), this isoform is prevalent in embryonic and neonatal, and ephemeral in adults [72, 73, 74]. However, usage of this isoform in cloning and mutagenesis experiments is slightly difficult because of the instability of this isoform in the hosting cell. This is the most important reason why Na_v 1.5 cardiac isoform is preferred to this isoform for Na_v channel function experiments in oocyte [75, 76]. Also, injury to Na_v 1.3 isoform introduces a non inactivating, persistent current [77].

2.6 Electrophysiological Analysis of *Xenopus* Laevis Oocyte with Two Electrode Voltage Clamp (TEVC) Technique

All of the common electrophysiological methods can be applied to oocytes, along with patch clamp and whole cell recording of both single channel and macroscopic currents. Single channel kinetics, also alterations caused by mutations and chemical applications to the channels could be studied with the patch clamp single channel measurements to the divitellinized oocytes [78]. Single channel or multichannel patch clamp recordings could be carried out in three configurations as;

1. Cell attached
2. Inside out
3. Outside out

Whole cell recordings are mostly done with TEVC (two electrode voltage clamp) technique which enables the study of the voltage dependence and kinetics of the channels [64]. In contrast to patch clamp recording where a single electrode is used for both current and voltage, voltage and current injections are done with different electrodes in TEVC. This technique could be executed in two ways as current clamp and voltage clamp. Voltage clamp mode includes measurement of the ion channels on the whole cell while keeping the membrane potential at a certain level; in contrast to the current clamp mode which consists of measurement of membrane potential while keeping the current through those channel at a certain level.

Considering the general equipment for this technique; a high compliance amplifier is needed for the experimental set-up because high quantities of current need to be measured unlike patch clamp. The amplifier output demonstrates the current change at the monitor of an oscilloscope or computer and could be archived at a storage device. KCl /agarose bridges connect the Ag/AgCl ground electrodes to the extracellular solution in the chamber. A graphic recorder, a vibration isolation table, a Faraday cage, a perfusion system, an experimental chamber, a microscope and micromanipulators are other devises for the experimental set-up [78].

Some advantages of this technique are [78, 64, 66]:

1. The large size of the oocyte enables the procedure easy to learn and quick to implement. Related to this, electrodes are easy to prepare and recording from all oocytes could be possible if the oocytes are healthy.
2. Perfusion of the external medium could be adjusted easier than patch clamp.

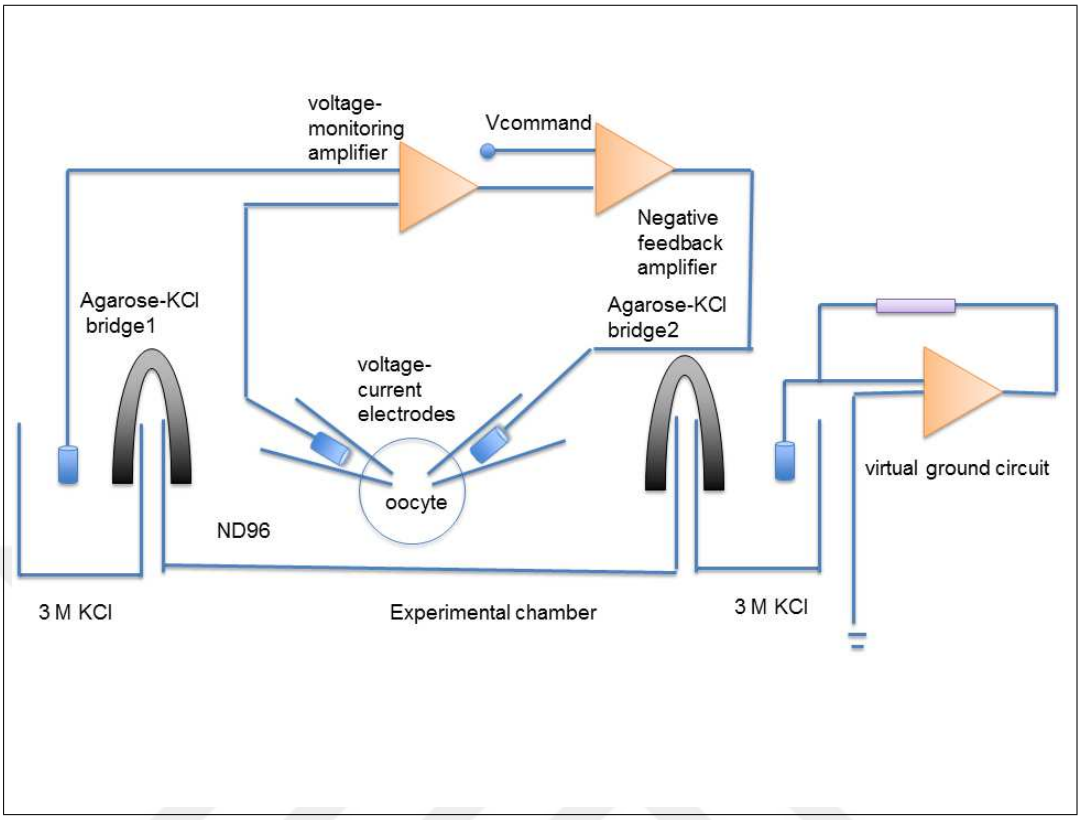

Figure 2.13 Two Electrode Voltage Clamp Technique Set-up

3. Recording with TEVC could be stable over long periods so it is ideal for long protocols, such as slow inactivation of Na_v channels.

4. TEVC makes it possible to record a large variety of currents ranging from 10 nA to 100 μA, depending on the RNA injected.

5. The cytoplasm of the oocyte is not damaged and the intracellular environment remains intact with this technique.Thus, it is an economical method such that the same pair of electrodes could be used to measure many numerous cells.

6. Both TEVC and patch clamp experiments could be done on the same oocyte.

7. Stable and long lasting recordings are possible with this technique.

8. Ion channel activity is recorded one or a few days after injection and while doing the experiment.

9. The current or voltage change at different protocols, under different solutions and solution concentrations could be analyzed with this technique.

10. The technique is advantageous especially over small cells transfected with exogenous DNA, where expression levels are not easy to determine.

11. The injected RNA amount could be precisely adjusted with this technique so that expressed protein levels could be adjusted easily.

Several disadvantages of this technique [78, 64] as:

1. The expressed proteins in the oocyte could be processed differently in the mammalian cells than oocytes. So, it is important to compare the functional properties of the exogenous proteins expressed in oocytes with the proteins in the original tissue. Alternatively, the processing could be traced carefully with biochemical approaches.

2. The resolution of voltage dependent current fast kinetic components are relatively poor.

3. The large size of the oocyte leads to a large membrane capacitance of around 150-200 nF with a slow clamp settling period during membrane potential alterations.

Although a difference of resting potential (RP) exists among oocytes of different frogs and different batches, and many factors including electrode penetration could alter the exact value of RP, the oocyte membrane acquires an active Na^+ - K^+ pump. When required measurement are done, it has been observed that *Xenopus* oocytes have an RP changing in the range between -40 to - 60 mV. Defollication of the oocyte also changes the RP value because of the damage applied during this process. That is the reason why freshly defollicated oocytes are recommended to heal for a few hours before starting the electrophysiological experiments for ion channel studies. These healed oocytes have RP's changing between -45 to -65 mV [64]. Currents measured are desired not to exceed 10 μA and it is advised to start the measurement 0.5 to 1.5 ms after voltage clamp, in order to get accurate measurements. One of the microelectrodes of TEVC should be shielded with a metal wire and connected to the common ground and the shield should be kept dry [78].

2.7 Previous Electrophysiological Studies of ALS Related Neurophysiological Defects

Hyperexcitability studies related to SOD1 mutation related ALS could be grouped into 3 regarding the brain area of degenerated neurons:

1. Spinal Cord: According to the study done by Hadzipasic et al., [79] at even early in life, month 4, mutant hSOD1^{G85R} causes elevated firing that interrupts fast twitch muscle lost. In addition to this, Martin and his colleagues [80] demonstrated that mutant SOD1 diminished dentritic elongation and amplified hyperexcitability of murine embryonic lumbar motor neuron slices. Also, mutant protein increased persistent Na^{+} - Ca^{+2} currents and normal development rate of with postnatal, neonatal and juvenile motor neurons [81] whereas it reduced glysine induced current and IPSC on embryonic motor neurons [82]. To add this, firing frequency and persistent Na_v current were augmented with mutant hSOD1^{G93A} [83, 60, 84, 85]. The same mutation caused voltage gated Na_v channels to have a quicker recovery from fast inactivation period compared to the control with or without free radical scavenger addition [86]. In addition to the Na_v current studies, SALS patient immunoglobins given to rat spinal cord motor neurons resulted in $V_{1/2}$ depolarizing shift of Ca_v current without any toxicity or maximum Ca^{+2} conductance [87]. Van Damme and his colleagues observed that AMPA receptor excitotoxicity related to high Ca^{+2} concentration inside the cell results in ALS. When NBQX was applied to mutant spinal cord motor neurons, kainate currents were inhibited and prolonged survivals were obtained [88]. Related to excitotoxicity and Ca^{+2} conductance, oculomotor neurons found to have a high Ca^{+2} buffering capacity leading to less vulnerability to ALS [89].

2. Bain Stem: In addition to the riluzole effect study on wild type murine brain stem preparation [63] and stress induction study [61], hyperexcitability of postnatal hSOD1^{G93A} mice much before symptoms were observed according to the patch clamp experiments [90].

3. Motor cortex: Accompanying Zona et. al., [91] and Pieri et. al., studies [92] investigating the effect of the mutant protein on Na^+ current, increased membrane expression of N type Ca_v channels and net calcium depolarization influx was observed [93] on motor cortex mouse primary cells.

Also, Wainger and his colleagues [94] suggested that hSOD1^{A4V} mutations reduces K^+ current where its activator retigabine inhibits hyperexcitability on their study with human IPSCs.

Riluzole, which is known to be the only therapeutic agent for ALS is also suggested decrease repetitive firing according to some studies [63, 62, 91, 61]. This drug was proved to induce a reversible and dose-dependent decrease of the hyperexcitability and a negative shift of the steady-state inactivation curve for the Na^+ currents on neocortical neurons from rat with whole cell patch clamping technique [91]. Also, Bellingham and his colleagues observed that riluzole reduced persistent Na_v - Ca_v currents and repetitive firing using whole cell patch clamping technique on wild type murine brain stem motor neurons [63]. According to Schuster et. al., [62], riluzole inhibited 50 % of persistent sodium currents and depressed repetitive firing on a study done with primary mouse spinal cord culture with hSOD1^{G93A} mutations using whole cell patch clamp recordings. Cifra and his friends [61] put neonatal murine brainstem slices on excitotoxic stress and concluded that riluzole protected glia and motor neurons from boosted firing related to excitotoxicity if it is applied early after stress.

According to these hyperexcitability studies, various mechanisms account for the pathophysiology of motor neuron degeneration in ALS as;

1. Intrinsic motor neuron hyperexcitation [79, 94, 63, 80, 85, 95, 62, 96, 81, 82, 97, 92, 84, 86, 60, 83, 87, 85, 88, 89, 59, 91, 98]
2. Mutant SOD1 hosting neuron and interneuron interaction [99, 100, 90].
3. Mutant SOD1 hosting glia, specifically astrocytes [61, 101].

3. METHODOLOGY

The methodology of this study is outlined in Figure 3.1:

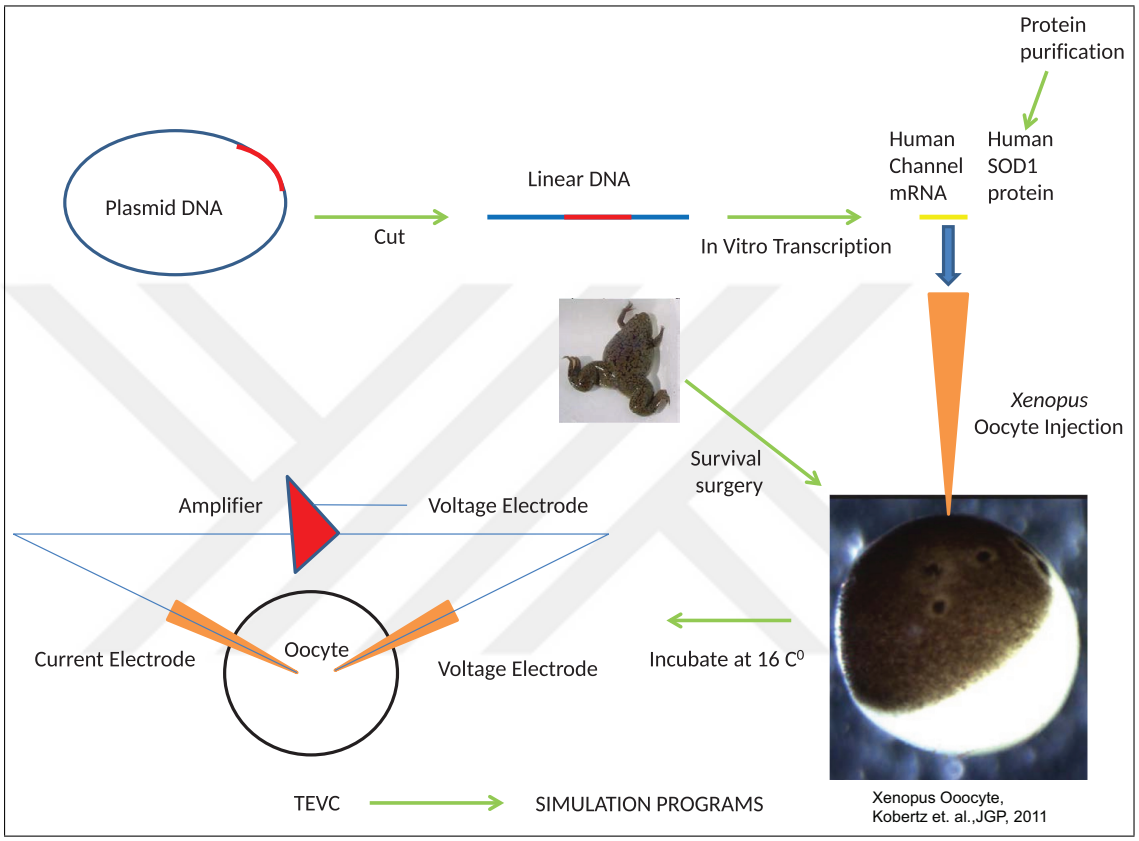

Figure 3.1 Outline of the Study

3.1 Molecular Biology

Human Na_v 1.3 α subunit isoform 2 (NCBI Reference Sequence: NP001075145.1) DNA was obtained from J.A Kearney (Vanderbilt University, Nashville, TE). The β subunit DNA was obtained from C. Ahern (University of British Columbia, Vancouver, Canada). The constructs were linearized with the appropriate restriction enzyme (New England Biolabs) and cRNA was synthesized using in vitro run-off transcription with T7 polymerase (Promega).

3.2 hSOD1^{WT}/ hSOD1^{A4V} Expression and Purification

The pET3d vectors with human wild type (hSOD1^{WT}) and mutant (hSOD1^{A4V}) SOD1 cDNA were expressed in BL21 (DE3) PlysS cells. To express the SOD1 protein, the bacterial culture was incubated with 1 mM isopropyl β-D-thiogalactopyranoside (Sigma) in the presence of 200 μM copper (II) chloride (Sigma) and 200 μM zinc chloride (Sigma) for 3 h at 37°C (WT) or 30°C (A4V). The protein was harvested when the culture achieved an optical density (A600) between 0.6 and 0.8; hSOD1^{WT} and hSOD1^{A4V} proteins were harvested and purified from cell pellets [20, 102].

3.3 Immunoblotting

Immunoblots of individual and groups of oocytes were washed with PBS and lysed in RIPA buffer. Lysates were sonicated and cleared by centrifugation at 12,000 rpm for 5 min. The protein content of the cleared lysate was quantified by BCA colorimetric assay (Thermo, USA). For denaturing Western analyses, 5 μg of total protein was loaded on 12 % Tris-glycine gels (Invitrogen, USA) in Tris-Glycine SDS running buffer (Invitrogen, USA) and transferred to nitrocellulose membrane using i-BlotÂő (Invitrogen, USA). Membranes were blocked for 1 h in blocking solution (LiCor, USA) containing 0.1 % Tween-20. Sheep anti human SOD1 antibody (The Binding Site) was incubated at 4°C overnight at a 1:2000 dilution. After washing in PBS containing 0.1 % Tween-20, blots were incubated for 1 h with fluorophore-conjugated donkey anti-sheep antibody (LiCor, USA) prior to visualization and analysis by the Odyssey infrared imaging system (LiCor, USA).

3.4 Electrophysiology

Oocytes were surgically removed from *Xenopus* laevis as previously described [24]. The extraction procedure and care of *Xenopus* laevis were approved by the

University of Massachusetts Institutional Animal Care and Use Committee. Twenty-four hours after surgery, oocytes were first microinjected with mRNA (6 ng α subunit, 1.2 ng β1subunit) then subsequently with 25 ng of purified hSOD1 protein. Injection set-up is shown in Figure 3.2.

Figure 3.2 Injection Set-up

Microinjected oocytes were stored in antibiotic-supplemented ND96 buffer [103]. Microinjected oocytes are indicated in Figure 3.3

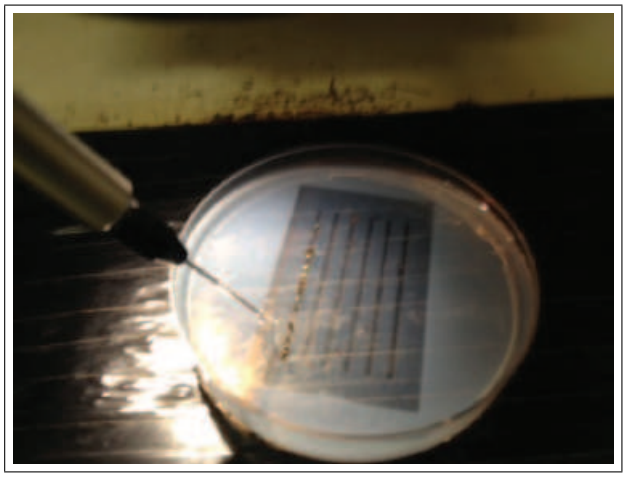

Figure 3.3 Oocytes on Agar Plate

Currents were measured 18 h after injection using two-electrode voltage clamp (OC-725; Warner Instrument Corp.); the data were acquired with Digidata 1322A

(Axon Instruments) running pClamp 9 (Axon Instruments) at room temperature. Electrodes were filled with: 3 M KCl, 10 mM HEPES and 5 mM EGTA, pH 7.6. Currents were measured in ND96 recording buffer (pH 7.6) containing: 96 mM NaCl, 5 mM HEPES, 2 mM KOH, 1 mM $MgCl_2$, and 0.3 mM $CaCl_2$. TEVC set-up is demonstrated in Figure 3.4.

Figure 3.4 TEVC Set-up

3.4.1 Total Current

The quantification of total current through the oocytes, the voltage dependence of activation and the kinetics of fast inactivation were evaluated with a protocol in which oocytes were depolarized from a holding potential of -100 mV to a range of potentials from -80 to +60 mV in 10 mV increments for 50 ms. Voltage step depolarizations were delivered every 5 s. Data analysis was performed with Clampfit 9 (Axon Instruments) and Prism 5 software (Graphpad). The amplitude of current was measured at each potential and normalized such that the maximal current in oocytes injected with mRNA alone was equal to 1. The currents from potentials -80 mV to +60 mV of each oocyte from the protein injected group (WT or mutant) were normalized to the mRNA control group. For this and all other electrophysiology experiments, the Grubbs test was used to exclude any outliers. Data are presented as mean ± SEM.

Differences between values were examined by ANOVA followed by Tukey's multiple comparison test with statistical significance established at $p < 0.05$.

3.4.2 Voltage-Dependence of Activation

Current-voltage relationships were measured by holding at -100 mV and stepping to a series of test potentials for 50 ms in 10 mV increments, followed by a tail pulse at -100 mV. Voltage step depolarizations were delivered every 5 s to allow for channels closing between depolarizations. To measure the voltage dependence of activation, maximum currents at each potential were normalized to the maximum peak current. Normalized tail currents were plotted versus the test potential to produce activation curves and fit to the Boltzmann equation where V is the applied pulse potential, $V_{1/2}$ is the half maximal activation, slope is the steepness of the curve as:

$$I/Imax = 1/(1 + e^{V_{1/2} - V/slope}) \tag{3.1}$$

This was calculated for each individual experiment. Within each experiment set (control, hSOD1^{WT}, hSOD1^{A4V}) the $V_{1/2}$ values were then averaged to obtain the mean $V_{1/2}$ for that set.

3.4.3 Voltage-Dependence of Inactivation

Oocytes were held at -100 mV. A conditioning pulse was applied to a range of potentials from -120 to 0 mV in 20-mV increments for the duration of 500 ms, followed by a test pulse to -30 mV for 50 ms. Voltage step depolarizations were delivered every 5 s to allow for channel closing. Peak current at each test pulse was normalized to the current of the conditioning pulse. Normalized values were plotted against the test pulse voltage and the data were fit with a Boltzmann sigmoidal function where V is the applied pulse potential, $V_{1/2}$ is the half maximal inactivation, slope is the

steepness of the curve, Top and Bottom are the maximum and minimum values of I/Imax respectively. The equation was:

$$I/Imax = Bottom + (Top - Bottom)/(1 + e^{V_{1/2} - V/slope}) \tag{3.2}$$

3.4.4 Kinetics of Fast Inactivation

Oocytes were held at a holding potential of -100 mV. Oocytes were depolarized to a range of potentials from -80 to +60 mV in 10 mV increments for 50 ms. Voltage step depolarizations were delivered every 5 s to allow for channels closing between depolarizations. To evaluate the kinetics of fast inactivation, the decay phase of current traces acquired by a depolarizing step to -30 mV, -20 mV, -10 mV, 0 mV and 10 mV from a holding potential of -100 mV were fitted best by the sum of two exponential standard functions where A_1 and A_2 are the approximate portion of the inactivated currents, t is time, T_1 and T_2 are the respective time constants and C is the equation constant as:

$$I = A_1 \times e^{(-t/T_1)} + A_2 \times e^{(-t/T_2)} + C \tag{3.3}$$

The function consisted of a fast component, which forms the transient Na^+ current, and a long lasting, slow, component, which forms PICNa^+.

3.4.5 Recovery from Fast Inactivation

Oocytes were held at -100 mV. A depolarization pulse was applied from the holding potential to a step potential of 0 mV for 50 ms to induce inactivation. A second depolarizing pulse (also from -100 to 0 mV) was applied to activate the Na^+ current. The inter-pulse interval was initially 50 ms and was increased by 1 ms steps to define the rate of recovery. The entire protocol entailed 40 sweeps. The time courses for recovery

from fast inactivation data were evaluated by normalizing the current amplitude during the second depolarization test pulse to that of the first depolarization test pulse. The data were fit to the one phase decay function where Plateau is the I/Imax value at infinite times and K is the rate constant as:

$$I/Imax = (I/Imax - Plateau) \times e^{(-K \times time)} + Plateau \tag{3.4}$$

All experiments were conducted using three different batches of oocytes; typically three conditions were tested (control, hSOD1^{WT} and hSOD1^{WT}) on subsets of equivalent numbers of oocytes from each batch.

4. RESULTS

To study the impact of WT and mutant (A4V) SOD1 protein on the properties of Na_v 1.3, an oocyte expression system was used. A4V variant of SOD1 was elected to study because this is the most common SOD1 gene mutation in North America and because it has an aggressive clinical course, with survival typically about one year [2]. As described above, electrophysiological studies were performed approximately 18 hours after injecting purified SOD1 protein together with the cDNA expressing the α and β subunits of $Na_v1.3$.

4.1 Immunoblotting

Firstly, it was documented that hSOD1 protein (both WT and A4V) could be detected by Western blotting in oocyte extracts not only immediately after injection but also at 18 hr post-injection. Also, expression and trafficking of $Na_v1.3$- $\beta1$ complexes were confirmed, by measuring current; uninjected oocytes have negligible sodium currents. It is demonstrated in the following figure that, exogenous hSOD1 and $hNa_v1.3$ are expressed trafficked properly in *Xenopus* oocytes. As seen in Figure 4.1A, hSOD1 protein was identified in extracts from injected oocytes by Western blot analysis. The first three lanes represent 5 μg total protein from 23 oocyte lysates whereas the following two lanes represent 5 μg total protein from a single oocyte lysate. There is a non-specific band at 15 kD that is present in both injected and uninjected oocytes. In Figure 4.1B, representative traces from oocytes that were uninjected or injected with Na_v 1.3 mRNA are shown. Proper assembly and trafficking of Na_v 1.3 channels was confirmed by the presence of Na^+ current elicited from a single pulse to 0 mV from a holding potential of -100 mV. Dotted line indicates zero current; scale bar is 1 μA and 10 ms. Lastly, hSOD1 protein was identified in oocyte extracts immediately after injection and up to 24 hours post-injection and shown in Figure 4.1C, where each lane contains 5 μg total protein from a single oocyte lysate.

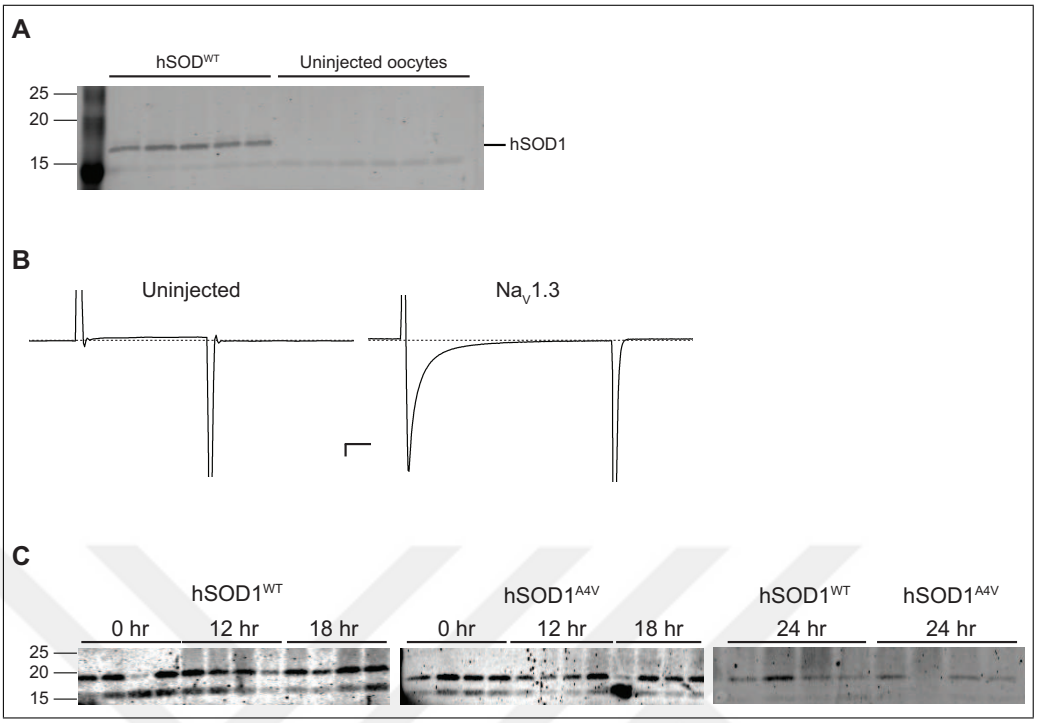

Figure 4.1 Exogenous hSOD1 and hNa$_v$1.3 are Expressed in Xenopus Ooyctes.

4.2 Electrophysiology

4.2.1 Total Current

The influence of hSOD1^{WT} vs hSOD1^{A4V} on peak Na$_v$ 1.3 currents elicited by -100 mV to a range of test potentials were compared. In Figure 4.2, SOD1 protein increases Na$_v$1.3- β1 channel current from oocytes co-injected with different hSOD1 proteins. The effect of hSOD1^{WT} vs hSOD1^{A4V} protein on peak Na$_v$1.3- β1 channel currents was compared for depolarizations from -100 mV to a range of test potentials. Values are normalized to oocytes injected with only α and β subunit mRNA (without exogenous hSOD1). For all but two test voltages (-40 and 10 mV), the peak Na^+ current in the presence of hSOD1^{A4V} exceeded that seen with hSOD1^{WT}. Data are presented as the mean $\pm$ SEM from multiple oocytes (Table 4.1). Asterisks indicate significant difference between data using hSOD1^{A4V} and either hSOD1^{WT} or no hSOD1 (ANOVA with Tukey's post test *** $p < 0.001$, ** $p < 0.01$, * $p < 0.05$).

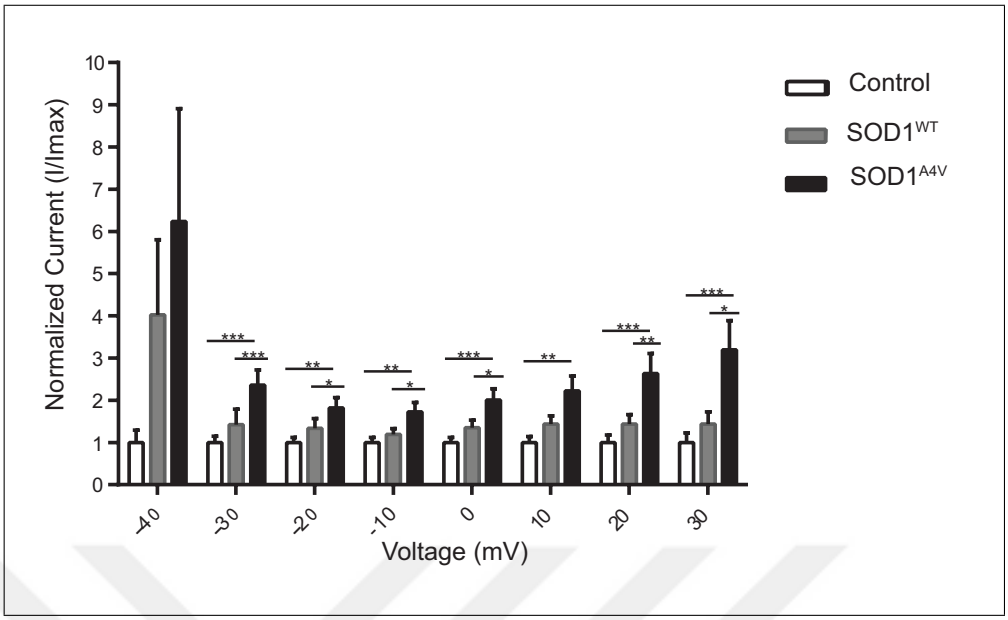

Figure 4.2 SOD1 Protein Increases $Na_v1.3$- $\beta 1$ Channel Current.

4.2.2 Voltage Dependence of Activation

To determine whether this increase in current was due to a shift in the voltage sensitivity of $Na_v1.3$- β channel complexes, channel current was measured at different voltages. The threshold and voltage dependence of activation for the peak sodium current were similar for control and complexes injected with $hSOD1^{WT}$. By contrast, in the presence of the mutant $hSOD1^{A4V}$ protein there was a significant hyperpolarizing shift of the midpoint of activation ($V_{1/2}$). There also was a slight decrease in the voltage-dependence (slope) of $Na_v1.3$- $\beta 1$ complexes that was not significant (Figure 4.3). In Figure 4.3, SOD1 protein induces a hyperpolarizing shift in the voltage dependence of $Na_v1.3$- $\beta 1$ channel activation. In Figure 4.3A, time course of $Na_v1.3$- $\beta 1$ currents are shown. $Na_v1.3$ currents elicited from a holding potential of -100 mV by 50 ms steps to potentials of -80 to 60 mV are displayed for oocytes injected with only α and β subunit channel mRNA, or α and β subunit mRNA combined with either $hSOD1^{WT}$ or $hSOD1^{A4V}$ protein (scale bar: x = 0.2 ms, y = 2 μA). Current-voltage curves for $Na_v1.3$- $\beta 1$ complexes are indicated in Figure 4.3B. Current tracings over time are normalized to the maximum current. The threshold and voltage dependence of activation for the peak sodium current were similar for complexes injected with $hSOD1^{WT}$ or

Table 4.1
Normalized Current and Standard Errors of the Mean

Voltage (mV)	CONTROL(n=26)	hSOD1^{WT}(n=23)	hSOD1^{A4V}(n=22)
-40	1 ± 0.29	4.02 ± 1.78	6.23 ± 2.68
-30	1 ± 0.15	1.42 ± 0.37	2.36 ± 0.36
-20	1 ± 0.12	1.34 ± 0.23	1.82 ± 0.24
-10	1 ± 0.12	1.19 ± 0.13	1.73 ± 0.22
0	1 ± 0.12	1.35 ± 0.18	2.01 ± 0.27
10	1 ± 0.14	1.43 ± 0.20	2.22 ± 0.35
20	1 ± 0.18	1.44 ± 0.22	2.63 ± 0.48
30	1 ± 0.23	1.44 ± 0.29	3.20 ± 0.69

mutant hSOD1^{A4V}. Lastly, in Figure 4.3C, voltage-activation curves were calculated from the analyses of dependence of activation on voltage. In this figure, the solid curves illustrate the Boltzmann curves corresponding to the data. Data are presented as the mean ± SEM (n = 14-20 oocytes). The average values of the midpoint of activation $V_{1/2}$ were: control (-30.89 ± 0.44, n = 20); hSOD1^{WT} (-30.64 ± 0.49, n = 18), and hSOD1^{A4V} (-33.79 ± 1.21, n = 14); $V_{1/2}$ for hSOD1^{A4V} differed significantly from $V_{1/2}$ for either hSOD1^{WT} or control ($p < 0.05$). The average values of the activation curve slopes did not differ significantly among control (2.14 ± 0.13, n = 20), hSOD1^{WT} (2.19 ± 0.17, n = 19) and hSOD1^{A4V} (1.85 ± 0.13, n = 13) groups ($p > 0.05$, ANOVA with Tukey‘s post test)

4.2.3 Voltage Dependence of Inactivation

The voltage dependence of inactivation of the $Na_v1.3$- $\beta1$ channel complex was measured. Figure 4.4 shows the traces recorded by step depolarizations to -30 mV from a conditioning test potential between -120 and 0 mV. The resultant currents were normalized to the first current elicited during the protocol, graphed as an exponential function and fit to a Boltzman equation. Neither the average midpoint of inactivation $V_{1/2}$ nor the voltage- dependence (slope) differed significantly between the three groups. In Figure 4.4, SOD1 protein does not affect the voltage dependence of inactivation of

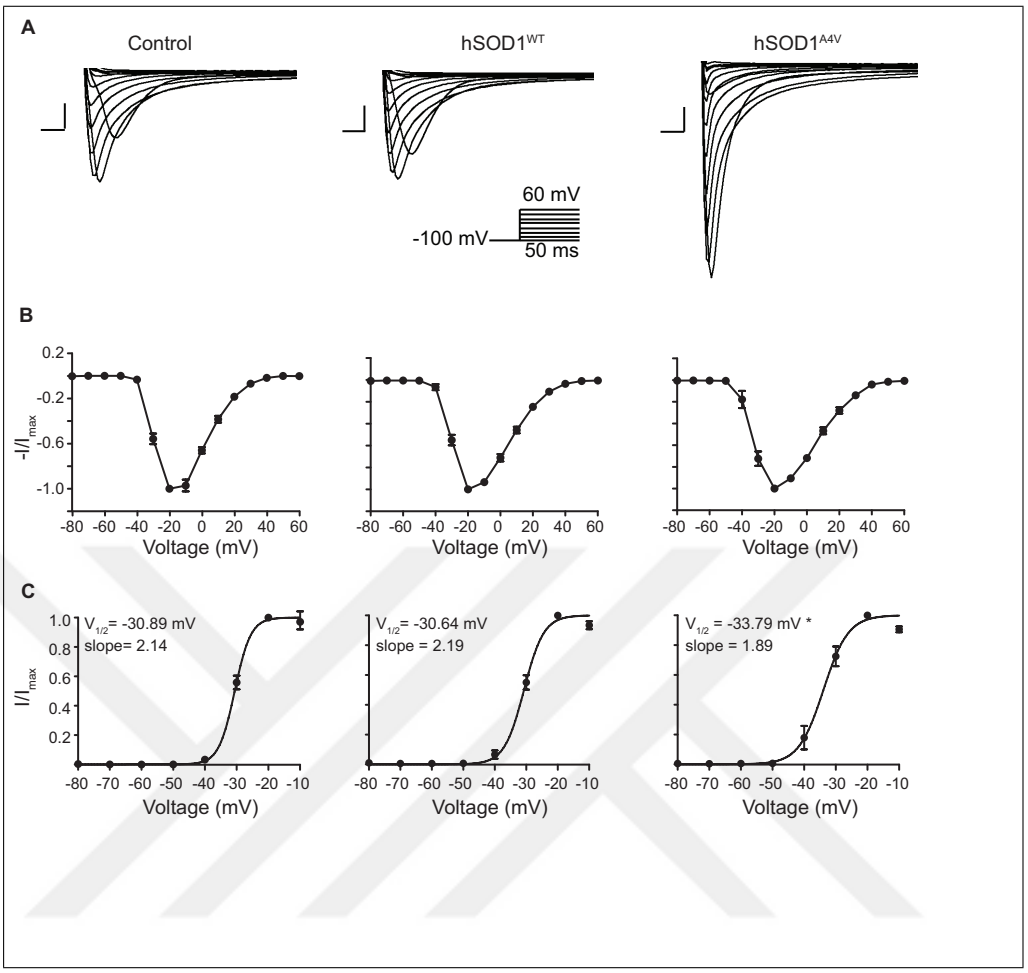

Figure 4.3 SOD1 Protein Induces a Hyperpolarizing Shift in the Voltage Dependence of $Na_v1.3$- $\beta1$ Channel Activation.

$Na_v1.3$- $\beta1$ channel complexes. $Na_v1.3$- $\beta1$ current was recorded by step depolarizations to -30 mV from a conditioning test potential between -120 and 0 mV, in 20 mV steps (scale bar: x = 0.2 ms, y = 1 μA) as shown in Figure 4.4A. Then, inactivation curves were calculated from the data in Figure 4.4A and these curves are indicated in Figure 4.4B. In this figure, the solid lines represent Boltzmann fits to the data. The average midpoint of inactivation $V_{1/2}$ for control (-61.55 $\pm$0.82, n = 19), $hSOD1^{WT}$ (-64.24 $\pm$ 1.82, n = 17), and $hSOD1^{A4V}$ (-61.89 $\pm$ 0.95, n = 13) and the voltage dependency (slope) of inactivation curves for control (-4.88 $\pm$ 0.39, n = 19), $hSOD1^{WT}$ (-5.00$\pm$ 0.31, n = 17), and $hSOD1^{A4V}$ (-5.32 $\pm$ 0.40, n = 13) were similar ($p > 0.05$, ANOVA with Tukey‘s post test).

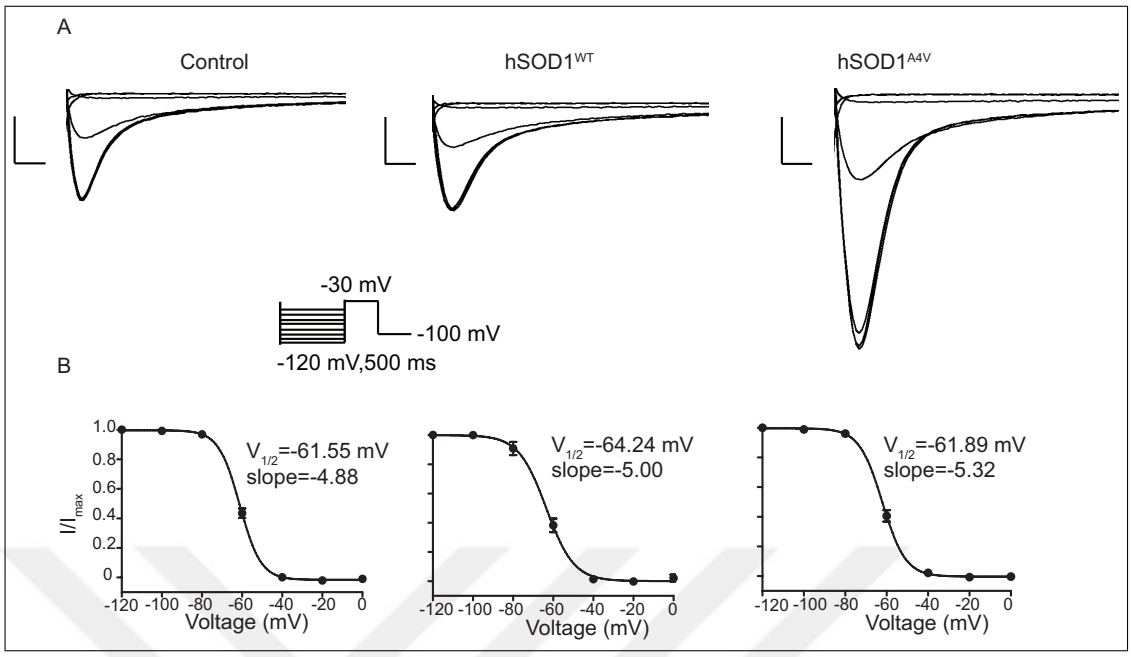

Figure 4.4 SOD1 Protein does not Affect the Voltage Dependence of Inactivation of $Na_v1.3$- $\beta 1$ Channel Complexes.

4.2.4 Kinetics of Fast Inactivation

It has previously been observed in mice expressing hSOD1^{G93A} that cultured neurons demonstrate an increase in the rate of recovery from inactivation [86]. For this reason, it was next determined whether the increase in current caused by hSOD1^{A4V} was due to changes in the inactivation kinetics of $Na_v1.3$- $\beta 1$ channel complexes. To determine the effect hSOD1 had on the kinetics of $Na_v1.3$- $\beta 1$ channel complexes inactivation, the decay phases of activation current traces were fit to a two- phase exponential decay function. As seen in Figure 4.5, these currents had a noticeable fast transient component and a slow persistent component. The fast and slow time constants for all three groups were similar (Figure 4.5, Table 4.2). In Figure 4.5, hSOD1 does not affect the inactivation kinetics of $Na_v1.3$- $\beta 1$ channel complexes. Figure 4.5A are representative $Na_v1.3$ current traces for control, hSOD1^{WT} and mutant hSOD1^{A4V} obtained following depolarization from a holding potential of -100 mV to -20 mV. These currents demonstrated a fast transient component and a slow component (scale bar: x = 0.2 ms, y = 2 μA). Figure 4.5B are the decay phases of activation current traces that were fit to a two-phase exponential decay function. In this figure, bar graphs display the

mean ± SEM of the T_1 and T_2 values of fast inactivation of three groups. Averages of both the fast and slow time constants for all three groups were similar ($p > 0.05$).

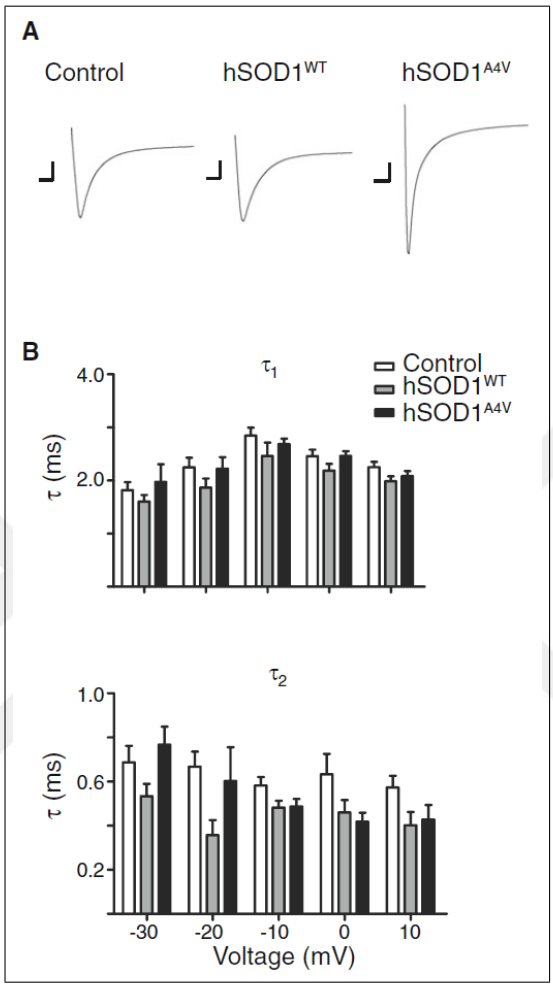

Figure 4.5 hSOD1 does not Affect the Inactivation Kinetics of $Na_v1.3$- $\beta 1$ Channel Complexes.

In the following table, kinetics of fast inactivation are similar for oocytes injected with WT and mutant hSOD1. Rates of inactivation were measured by fitting currents to a double exponential. Data is represented as the mean SEM (-30 mV: n=23 (control), n=15 ($hSOD1^{WT}$), n= 15 (Mutant $hSOD1^{A4V}$); -20 mV: n=20 (control), n=15 ($hSOD1^{WT}$), n= 13($hSOD1^{A4V}$); -10 mV: n=15 (control), n=11 ($hSOD1^{WT}$), n= 13 ($hSOD1^{A4V}$); 0 mV: n=20 (control), n=17 ($hSOD1^{WT}$), n= 16 ($hSOD1^{A4V}$); 10 mV: n=13 (control), n=14 ($hSOD1^{WT}$), n= 15($hSOD1^{A4V}$).

Table 4.2
Kinetics of Fast Inactivation are Similar for Oocytes Injected with WT and Mutant hSOD1.

	CONTROL	hSOD1^{WT}	hSOD1^{A4V}	CONTROL	hSOD1^{WT}	hSOD1^{A4V}
	T_1	T_1	T_1	T_2	T_2	T_2
-30 mV	1.82 ± 0.15	1.60 ± 0.12	1.97 ± 0.34	0.69 ± 0.07	0.53 ± 0.06	0.77 ± 0.08
-20 mV	2.25 ± 0.18	1.86 ± 0.17	2.22 ± 0.21	0.67 ± 0.07	0.36 ± 0.07	0.60 ± 0.15
-10 mV	2.73 ± 0.10	2.27 ± 0.17	2.69 ± 0.10	0.58 ± 0.04	0.49 ± 0.03	0.49 ± 0.03
0 mV	2.46 ± 0.12	2.19 ± 0.13	2.46 ± 0.09	0.63 ± 0.09	0.46 ± 0.06	0.42 ± 0.04
10 mV	2.25 ± 0.10	1.99 ± 0.09	2.08 ± 0.09	0.57 ± 0.05	0.40 ± 0.06	0.43 ± 0.07

4.2.5 Recovery from Fast Inactivation

A two-step protocol was used to measure the effect of hSOD1^{WT} vs hSOD1^{A4V} on the Na$_v$1.3- β1 channel complex recovery from fast inactivation (Figure 4.6).

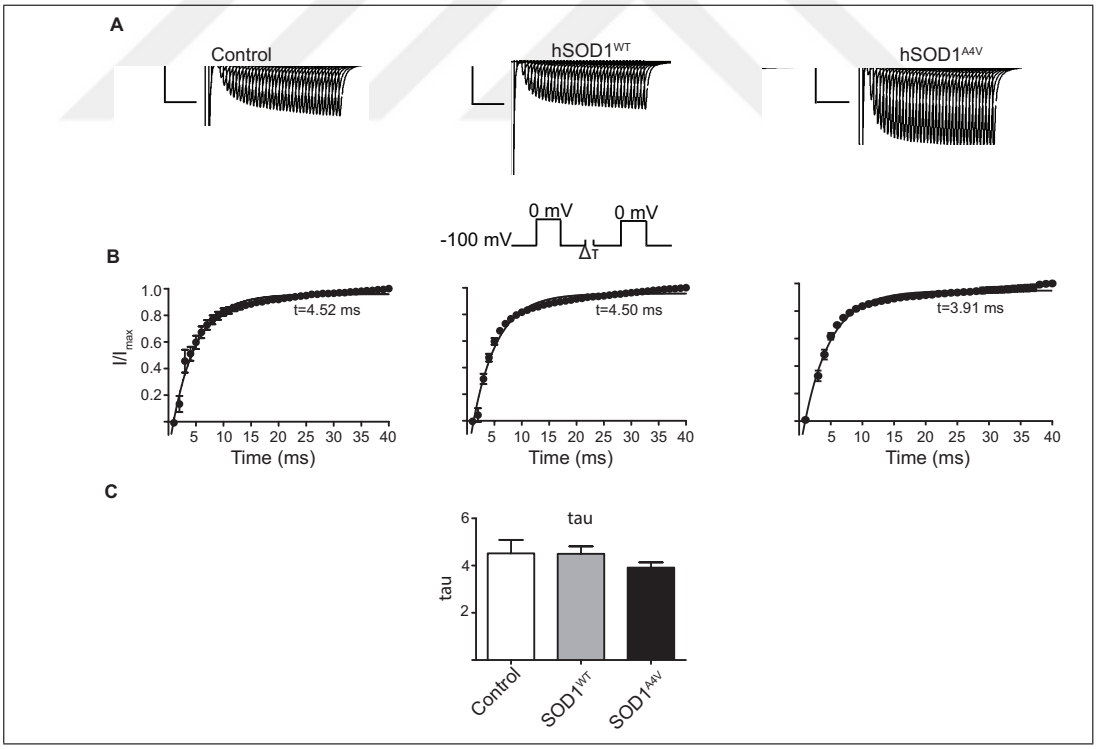

Figure 4.6 A Two-Step Protocol was Used to Measure the Effect of hSOD1 on the Recovery of Na$_v$1.3- β1 Current from Fast Inactivation.

The resultant traces were fit to a single-phase exponential decay function. Although, mutant hSOD1^{A4V} did decrease the rate of recovery from fast inactivation,

this difference was not significant. In Figure 4.6A, current traces for the recovery from fast inactivation in control oocytes and in the presence of either hSOD1^{WT} or hSOD1^{A4V} protein are shown (scale bar: x = 10 ms, y = 2μA). Profile of the peak current traces expressed as a single-phase exponential decay function are indicated in Figure 4.6B. Decay constants from Figure 4.6B were compared in Figure 4.6C. Current amplitude during the second depolarization test pulse was normalized to the current amplitude during the first depolarization test pulse and a recovery value was found for every sweep. The hSOD1^{A4V} protein slightly decreased the rate of recovery from fast inactivation hSOD1^{A4V} (3.91 $\pm$ 0.22, n = 19) but this was not significant compared to control (4.52 $\pm$ 0.57, n=19) or hSOD1^{WT} (4.50 $\pm$ 0.32, n = 12) ($p > 0.05$ ANOVA with Tukey post test).

5. MATHEMATICAL MODELING

5.1 Mathemetical Modeling Using Hodgkin-Huxley Equations

Na_v and K_v channel behaviors are usually modeled by using Hodgkin and Huxley equations. Hodgkin and Huxley were awarded the Nobel award in1952 for developing a set of differential equations depicting the ionic basis of action potentials based on the voltage clamp experiments done on squid axon measuring Na^+ and K^+ conductance [31]. In their model, an equivalent electrical circuit as shown in Figure 5.1 (modified from [104]) represents the neuron.

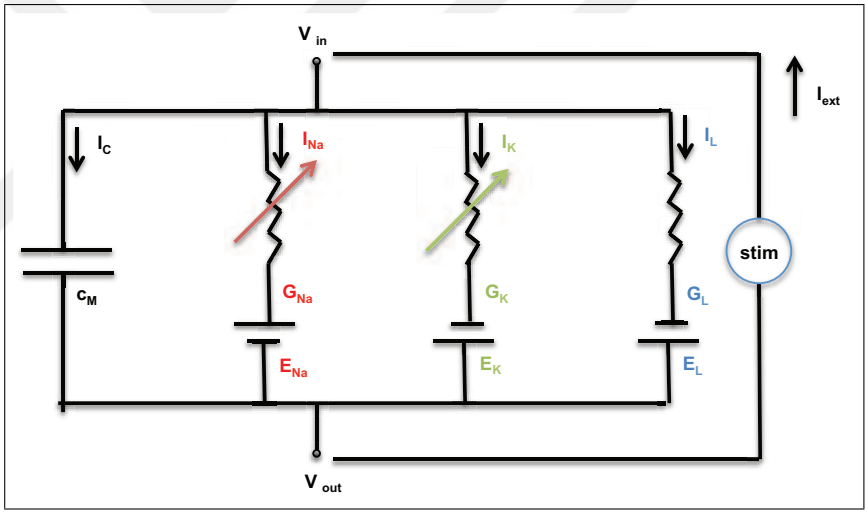

Figure 5.1 Hodgkin-Huxley Circuit

In this figure, electrical equivalent circuit for a neuron is shown. The C_M is the capacitance of the cell membrane; G_{Na} and G_K are the the voltage-dependent conductances of $Na^+$and K^+ respectively, G_L is the voltage independent leakage conductance, and the three batteries show reversal potentials for the corresponding conductance. The "stim" pathway is an externally applied current, such as introduced current via an intracellular electrode

The set of differential equations developed by Hodgkin and Huxley [31] were called as Hodgkin and Huxley models [104]. Because biophysical events crucial for

action potential production in all organisms can be evaluated and modeled by Hodgkin Huxley modeling, it is important to understand their model and related assumptions. This model consists of a set of four differential equations based on some assumptions. The main equation is a nonlinear equation describing membrane circuitry whereas the other three are linear delineating channel characteristics. These equations are:

$$C_m \frac{dV}{dt} = g_{Na}^{-} m^3 h(V_m - E_{Na}) + \bar{g_k}\, n^4 (V_M - E_K) + g_L(V_m - E_L) - I_{ext} \tag{5.1}$$

$$\frac{dm}{dt} = \alpha_m(V)(1-m) - \beta_m(V)m \tag{5.2}$$

$$\frac{dh}{dt} = \alpha_h(V)(1-h) - \beta_h(V)h \tag{5.3}$$

$$\frac{dn}{dt} = \alpha_n(V)(1-n) - \mathrm{B}_n(V)n \tag{5.4}$$

In order to attain these four main equations, The 1^{st} differential equation of the model is where I_{ext} is the externally applied current:

$$C_m \frac{dV_m}{dt} + I_{ion} = I_{ext} \tag{5.5}$$

The total current I_{ion} through the circuit is the sum of all the individual currents through all channels of the membrane. This current is proportional to the conductance times the difference between the membrane potential V_m and equilibrium potential E_k.

$$I_{ion} = \sum_k I_k = \sum_k G_k(V_m - E_k) \tag{5.6}$$

This equation also could be written as;

$$I_{ion} = G_{Na}\,(V_m - E_{Na}) + G_K\,(V_m - E_K) + G_L(V_m - E_L) \tag{5.7}$$

Each individual ion channel can be demonstrated as including one or more gates that regulate the ion flow through that channel. Each gate could be in permissive or impermissive state for the ions. If all the gates of the channels are in permissive state, the channel is open. If any of the gates are in impermissive state, the channel is closed. The probability of a gate to be in permissive state is shown as p_i and this p_i changes between numbers 0 and 1. At some point in time t, if p_i (t) correspond the fraction of gates that are in the permissive state. So, 1- p_i (t) must be in the impermissive state.

$$\frac{dp_i}{dt} = \alpha_i\,(V)\,(1 - p_i) - \beta_i(V)p_i \tag{5.8}$$

If the membrane voltage V_m is clamped at some fixed value V, then the fraction of gates in the permissive state will eventually reach a steady state value

$$p_{i,t\to\infty} = \frac{\alpha_i(V)}{\alpha_i(V) + \beta_i(V)} \tag{5.9}$$

$$t_i(V) = \frac{1}{\alpha_i(V) + \beta_i(V)} \tag{5.10}$$

Concerning the conductance values, the macroscopic conductance G_k (because of the channels of type k) with essential gates of type i is proportional to the product of the individual gate probabilities pi.

$$G_k = g\prod_i^k p_i \tag{5.11}$$

Also, according to Hodgkin and Huxley, the sodium current conductance is represented by three gates named as 'm' and one gate named as 'm' where m is for the activating state and h is for the inactivation state. It is crucial to note that:

1. h is the probability that the gate is not in its inactivating state
2. These m, h,n gating particles are voltage and time dependent.

Next, the previous equation becomes;

$$G_{Na} = g_{Na} p_m^3 p_h = g_{Na} m^3 h \tag{5.12}$$

The potassium conductance is represented by four 'h' gates;

$$G_K = g_K p_n^4 = g_K n^4 \tag{5.13}$$

Then the I_{ion} is;

$$I_{ion} = g_{Na} m^3 h(V_m - E_{Na}) + g_K n^4 (V_m - E_K) + g_L (V_m - E_L) \tag{5.14}$$

Where;

$$\frac{dm}{dt} = \alpha_m(V)(1 - m) - \beta_m(V)m \tag{5.15}$$

$$\frac{dh}{dt} = \alpha_h(V)(1 - h) - \beta_h(V)(h) \tag{5.16}$$

The rate constants α_n and β_n depend on voltage as; Initially, with $V_m = 0$, the state variable n has a steady-state value:

$$n_\infty(0) = \frac{\alpha_n(0)}{\alpha_n(0) + \beta_n(0)} \tag{5.17}$$

And if V_m= V_c, then the equation becomes;

$$n_\infty(V_c) = \frac{\alpha_n(V_c)}{\alpha_n(V_c) + \beta_n(V_c)} \tag{5.18}$$

So, the boundary conditions will be;

$$n(t) = n_\infty(V_c) - (n_\infty(V_c) - n_0(0)) e^{\frac{-t}{t_n(V_c)}} \tag{5.19}$$

There are also some other equations that should be kept in mind;

$$G_K = g_k n^4 = g_k [n_\infty(V_c) - (n_\infty(V_c) - n_0(0)) e^{\frac{-t}{t_n(V_c)}})]^4 \tag{5.20}$$

For the sodium conductance, if the similar idea of potassium conductance and 'm'

activation gate, 'n' inactivation gate are taken into account;

$$m(t) = n_\infty(V_c) - (m_\infty(V_c) - m_0(0))e^{\frac{-t}{t_m(V_c)}} \tag{5.21}$$

$$h(t) = h_\infty(V_c) - (h_\infty(V_c) - h_0(0))e^{\frac{-t}{t_h(V_c)}} \tag{5.22}$$

Also, conductance values and the time constants can be figured out as a function of command voltage by fitting the Hodgkin and Huxley experimental data as;

$$\alpha_n(V) = \frac{n_\infty(V)}{t_n(V)} \tag{5.23}$$

$$\beta_n(V) = \frac{1 - n_\infty(V)}{t_n(V)} \tag{5.24}$$

$$\alpha_n(V) = \frac{0.01(10 - V)}{e^{(\frac{10-V}{10})} - 1} \tag{5.25}$$

$$\beta_n(V) = 0.125e^{(\frac{-V}{80})} \tag{5.26}$$

For the 'm' and 'n' gates of the sodium channel:

$$\alpha_m(V) = \frac{0.1(25 - V)}{e^{\frac{25-V}{10}} - 1} \tag{5.27}$$

$$\beta_m(V) = 4e^{(\frac{-V}{18})} \tag{5.28}$$

$$\alpha_h(V) = 0.07e^{(\frac{-V}{20})} \tag{5.29}$$

$$\beta_h(V) = \frac{1}{e^{(\frac{30-V}{10})} + 1} \tag{5.30}$$

$$\alpha(V) = \frac{A + BV}{C + He(\frac{V+D}{F})} \tag{5.31}$$

All the equations and explanations were taken from [104]. Intense input applied to most

cells result in short voltage pulses, which are also called spikes or action potentials. Action potentials can be in various shapes depending on the cell type and they form according to all or none principle in response to membrane depolarization at voltages more negative than 0 mV. According to this principle, if the voltage is lower than a certain threshold, no spike is formed and potential goes back to its baseline level. If the threshold is surmounted, the membrane initiates a voltage trajectory, which mirrors the membrane features. When a short inward current under the threshold value is applied to a membrane, this current charges membrane capacitance and increases membrane potential. If the capacitance is small, the membrane depolarizes faster. This elevation in potential will increase m and n leading to sodium and potassium activation whereas it diminishes h, resulting in sodium inactivation [104].

5.2 Mathemetical Modeling via NEURON Simulation Program

Experimental results of this study define two specific effects of hSOD1^{A4V} on the Na$_v$1.3- β1 complex: (1) an increase in peak Na^+ current after depolarization and (2) a shift in the voltage dependence of activation in a hyperpolarizing direction. Next, computational studies were undertook to model the impact of these changes, considered individual and together, on overall firing frequency of a mammalian neuron. For this purpose, calculations were run using the open source program NEURON [105], which incorporates mammalian neuronal channel parameters. This model again uses conventional Hodgkin-Huxley simulations [31] involving the neuronal soma and two passive membrane dendrites in order to keep the simulation environment simple, reflecting the study‘s oocyte conditions. The basic equations used for data modeling were mainly the same as classical Hodgkin-Huxley [104].

$$C_m \frac{dV_m}{dt} + I_{ion} = I_{ext} \tag{5.32}$$

$$I_{ion} = G_{Na}\,(V_m - E_{Na}) + G_K\,(V_m - E_K) + G_L(V_m - E_L) \tag{5.33}$$

$$G_{Na} = g_{Na} p_m^3 p_h = g_{Na} m^3 h \tag{5.34}$$

$$G_K = g_K p_n^4 = g_K n^4 \tag{5.35}$$

$$I_{ion} = g_{Na} m^3 h (V_m - E_{Na}) + g_K n^4 (V_m - E_K) + g_L (V_m - E_L) \tag{5.36}$$

However, the gating equations, compared to the equations given in previous section 5.1, were changed as :
"m" sodium activation system:

$$\alpha_m = .1 * exp(-(v + 40), 10) \tag{5.37}$$

$$\beta_m = 4 * exp(-(v + 65)/18) \tag{5.38}$$

"h" sodium inactivation system:

$$\alpha_h = .07 * exp(-(v + 65)/20) \tag{5.39}$$

$$\beta_h = 1/exp(-(v + 35)/10) + 1) \tag{5.40}$$

The parameters used for the simulations are also indicated in Tables 5.1 and 5.2:

Table 5.1
Parameters for Simulations-1

	nseg	diam	L	Ra
Soma	1	18.8	18.8	123
Dentrite#1	5	3.18	701.9	123
Dentrite#2	5	2	549.1	123

Simulations of excitability in the presence of hSOD1^{WT} protein used the baseline parameters which were listed in Tables 5.1 and 5.2. These parameters were derived from the following file: (http://neuron.yale.edu/hg/neuron/nrn/file/tip/src/nrnoc/hh.mod).

Table 5.2
Parameters for Simulations-2

	(S/cm^2)
$\bar{g_{Na}}$(S/cm^2)	0.25
g_I (S/cm^2)	0.0001666
$\bar{g_K}$ (S/cm^2)	0.036
el (mV)	-60

Experimental data was introduced by varying first independently then simultaneously the two parameters that was observed to be experimentally significant:

1. The peak conductance of the Na_v channel $\bar{g_{Na}}$
2. The voltage dependence of activation

5.2.1 The Peak Conductance of the Na_v Channel ($\bar{g_{Na}}$) Simulations

The conductance $\bar{g_{Na}}$ was set at 0.25 S/cm^2 at baseline, reflecting conditions of electrical silence when wild type SOD1 was present. At baseline, which was 0.25 Siemens/cm^2 conductance, the model did not generate action potentials spontaneously (resting potential -62 mV). To model the impact of mutant SOD1, this conductance was increased by 0.04 S/cm^2 to 0.29 S/cm^2. This initiated spontaneous generation of action potentials. Moreover, the firing frequency increased progressively with further increases in Na^+ conductance until an increase of 134 %, at which conductance the membrane became depolarized (-27 mV) and unexcitable. Because the range of conductance changes induced by $hSOD1^{A4V}$ were on the order of 50-200 (Figure 4.2), it could be concluded that $hSOD1^{A4V}$ can exert a pro-excitatory influence on $Na_v1.3$-$\beta1$ conductance, and that this mutant protein might ultimately lead to depolarization arrest of excitability (Figure 5.2).

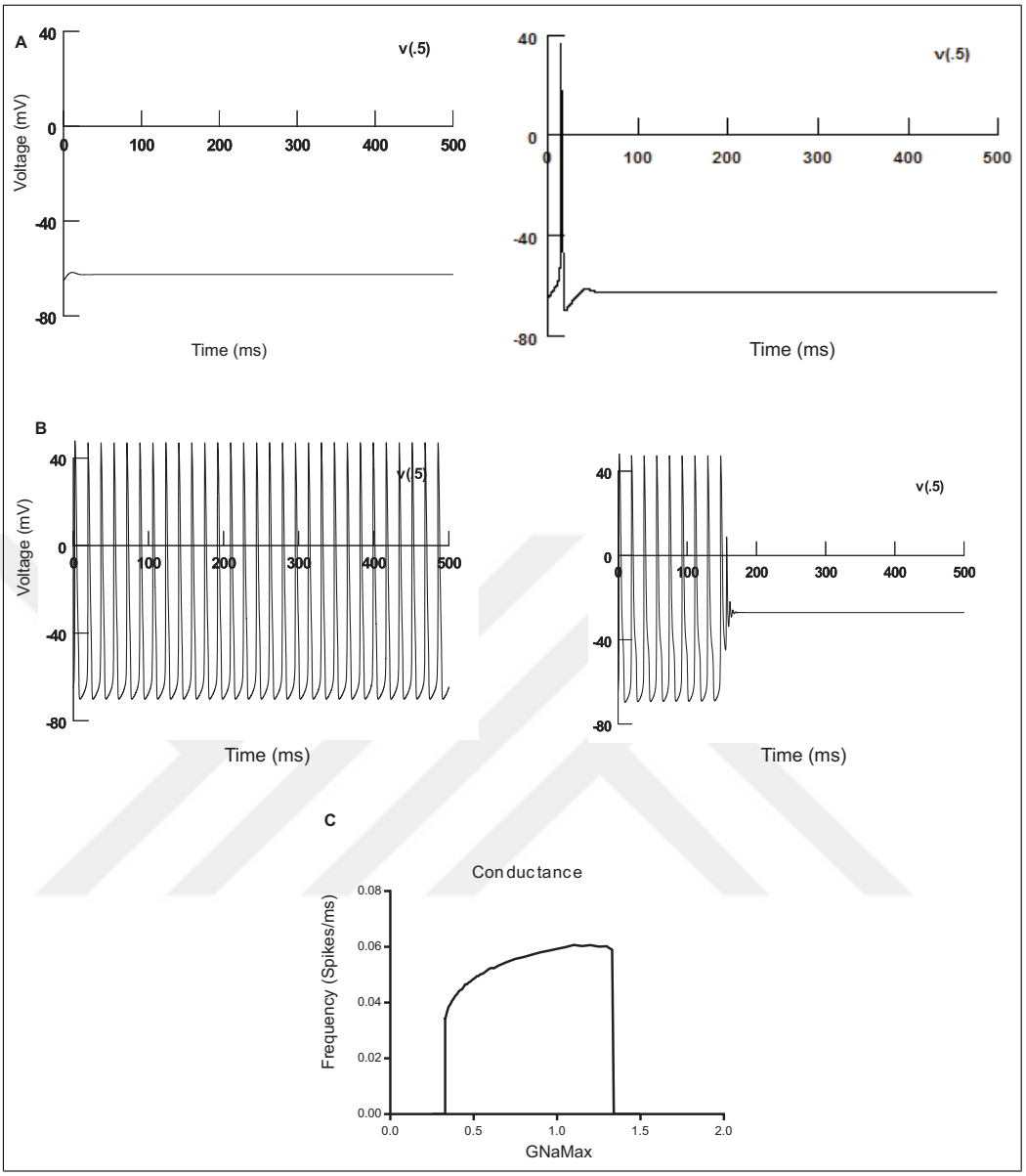

Figure 5.2 Firing Patterns of Mammalian Neuron in Response to Changes in Na_v Conductance

In Figure 5.2, firing patterns of mammalian neuron in response to changes in Na_v conductance and voltage dependence of activation induced by $hSOD1^{A4V}$ is shown. At baseline, there is no predicted spontaneous firing as modeled using NEURON software (Figure 5.2A, left; resting membrane potential -62 mV). Transition from silence to firing up was observed first at conductance of 0.29 Siemens/cm^2 (Figure 5.2A, right). As indicated in Figure 5.2B, when the Na_v conductance in the model is increased by 90 % (from 0.25 to 0.475 Siemens/cm^2, which is the mean increment in conductance recorded experimentally), the model fires spontaneously (left). When this conductance is further

increased to 1.34 Siemens/cm^2 (a 4.4-fold increase), the model is depolarized to -27 mV and becomes unexcitable (right). Lastly, Figure 5.2C demonstrates dependence of firing frequency on Na_v channel conductance, indicating that as the conductance increases there is a progressive increase in frequency until depolarization.

5.2.2 The Voltage Dependence of Activation of the Na^+ Current

Analogously, the impact on firing frequency of hyperpolarizing shifts in the voltage dependence of activation of the $Na_v1.3$ current was modelled. The conductance was left at 0.25 baseline value at all conditions in this model and the baseline activation parameters for the midpoint of m gating (activation) included α_m= -40 mV and β_m= -65 mV. This baseline simulated both the control situation and the experiments in which WT SOD1 was present; in this circumstance the model did not demonstrate spontaneous generation of action potentials. To simulate the impact of mutant SOD1, the observed hyperpolarizing change in the voltage dependence of activation ($V_{1/2}$) was modeled by shifting the gating constant for activation α_m and β_m by 1 mV hyperpolarizing increments. In each instance, the key output was the frequency of spontaneous firing. Although the neuron was electrically quiescent at the baseline $V_{1/2}$; it demonstrated spontaneous generation of trains of action potentials with a 0.6 mV hyperpolarization. A shift of 3 mV α_m= -43 mV; β_m= -68 mV), which was observed experimentally was associated with activation of repetitive firing. In these simulations, gating of the potassium currents was not changed. The firing frequency further increased with additional hyperpolarizing shifts up to 9 mV. With a 10 mV hyperpolarizing shift, the membrane became unexcitable and depolarized (-37 mV) (Figure 5.3).

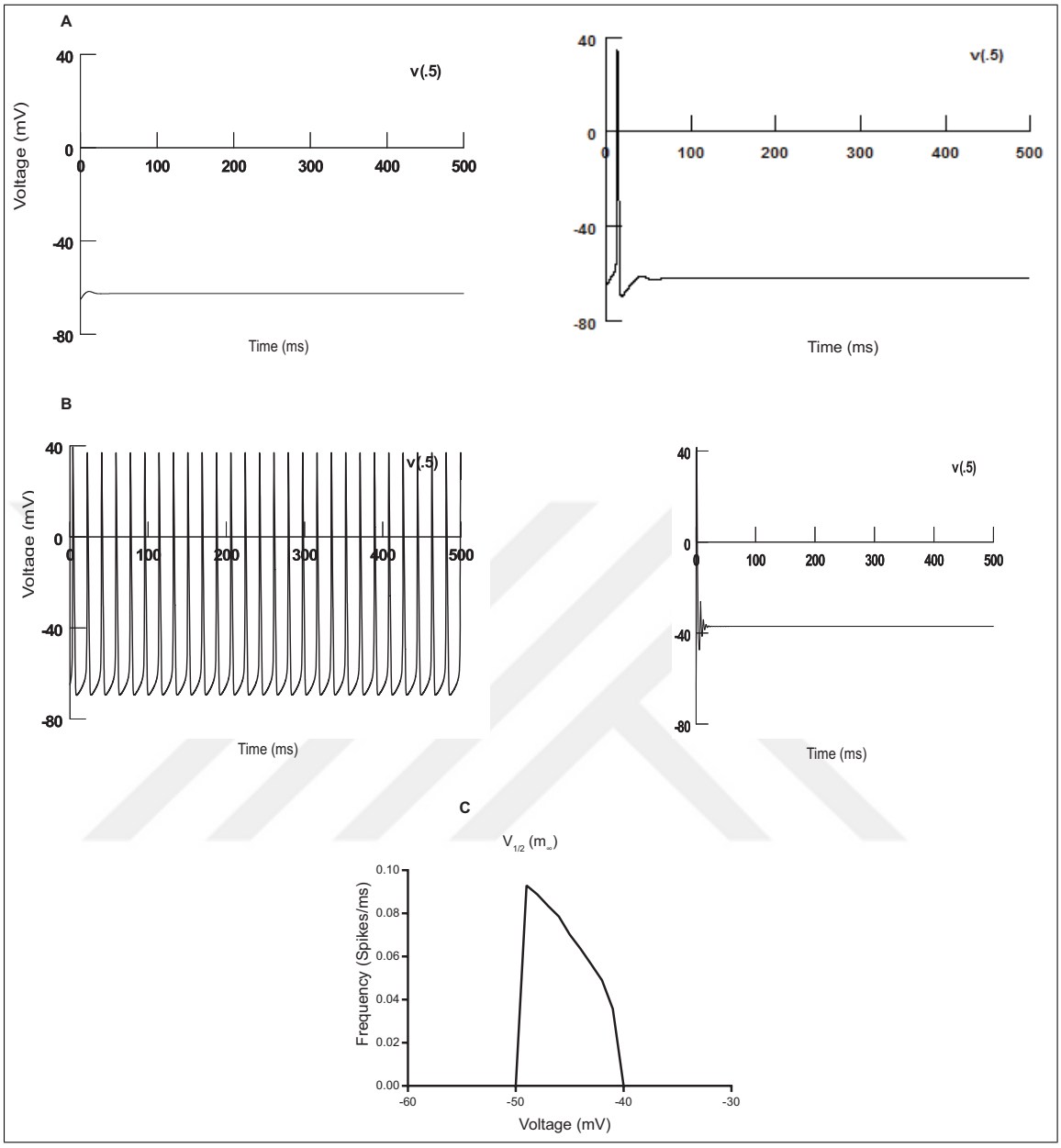

Figure 5.3 Firing Patterns of Mammalian Neuron in Response to Changes in Voltage Dependence of Activation Induced by hSOD1^{A4V}

In Figure 5.3, firing patterns of mammalian neuron in response to changes in voltage dependence of activation induced by hSOD1^{A4V} is demonstrated. The conductance was set at the baseline level of 0.25 S/cm^2 baseline value at all conditions in this model; the baseline $V_{1/2}$ for the steady the state activation curve for the sodium current was -40 mV = α_m, -65 mV= β_m. As seen in Figure 5.3A, the neuron is electrically at rest at the baseline $V_{1/2}$ (left). A single spontaneous action potential is initiated with a 0.6 mV hyperpolarization (right). Then, when the voltage dependence

of Na_v channel activation is shifted 3 mV in the hyperpolarizing direction (as observed experimentally), continuous spontaneous firing is triggered (Figure 5.3B, left). When the hyperpolarizing shift exceeds 10 mV, the model becomes depolarized to -37 mV and inexcitable (Figure 5.3B, right). Lastly, panel C is an equivalent relationship for the dependence of firing frequency on the voltage dependence of Na_v channel activation.

Because hSOD1^{A4V} both augments peak Na^+ current and hyperpolarizes the activation process, also the impact on firing frequency of simultaneous changes in these parameters was modeled. As shown in Figure 5.4, the prediction of this model is that the simultaneous impact of a 90 % increase in g_{Na} and a 3 mV hyperpolarizing shift in moo is a state of stable, repetitively firing action potentials at 0.066/ms (66/sec). The modeled conductance and voltage dependences of Na_v channel activation are indicated in the x and y axes, respectively. The firing frequency is indicated in the z-axis. The yellow dot indicates the estimated position of the frequency in the presence of hSOD1^{A4V}-induced changes (0.475 Siemens/cm^2, -43 mV). This predicts that under the experimental conditions induced by hSOD1^{A4V} the model will fire spontaneously and thus is hyperexcitable as compared to baseline in the presence of hSOD1^{WT} (green dot).

Although the voltage dependence of inactivation did not significantly change with the mutant protein injection, if the 3 mV depolarization shift in the inactivation $V_{1/2}$ at Figure 4.4 would induce neuronal firing was also investigated. At the baseline, steady state half-inactivation, α_h = -65 mV, and β_h = -35 mV. These constants were left at their default value for the control and wild type protein experimental conditions. Analogously to voltage dependence of activation simulations, the conductance was left at 0.25 baseline value. To simulate the effect of a depolarizing shift in the voltage dependence of inactivation, α_h and β_h were in the depolarizing direction; experimentally the shift was -3 mV (α_h = -62 mV; β_h = -32 mV). There were no spontaneous action potential trains at baseline but firing of single action potentials was triggered with a 2.6 mV depolarization. When the depolarizing shift exceeded 5 mV, spontaneous firing was triggered. When the depolarizing shift exceeded 19 mV, the model became depolarized to -25 mV and inexcitable. Gating for potassium activations were left at their default

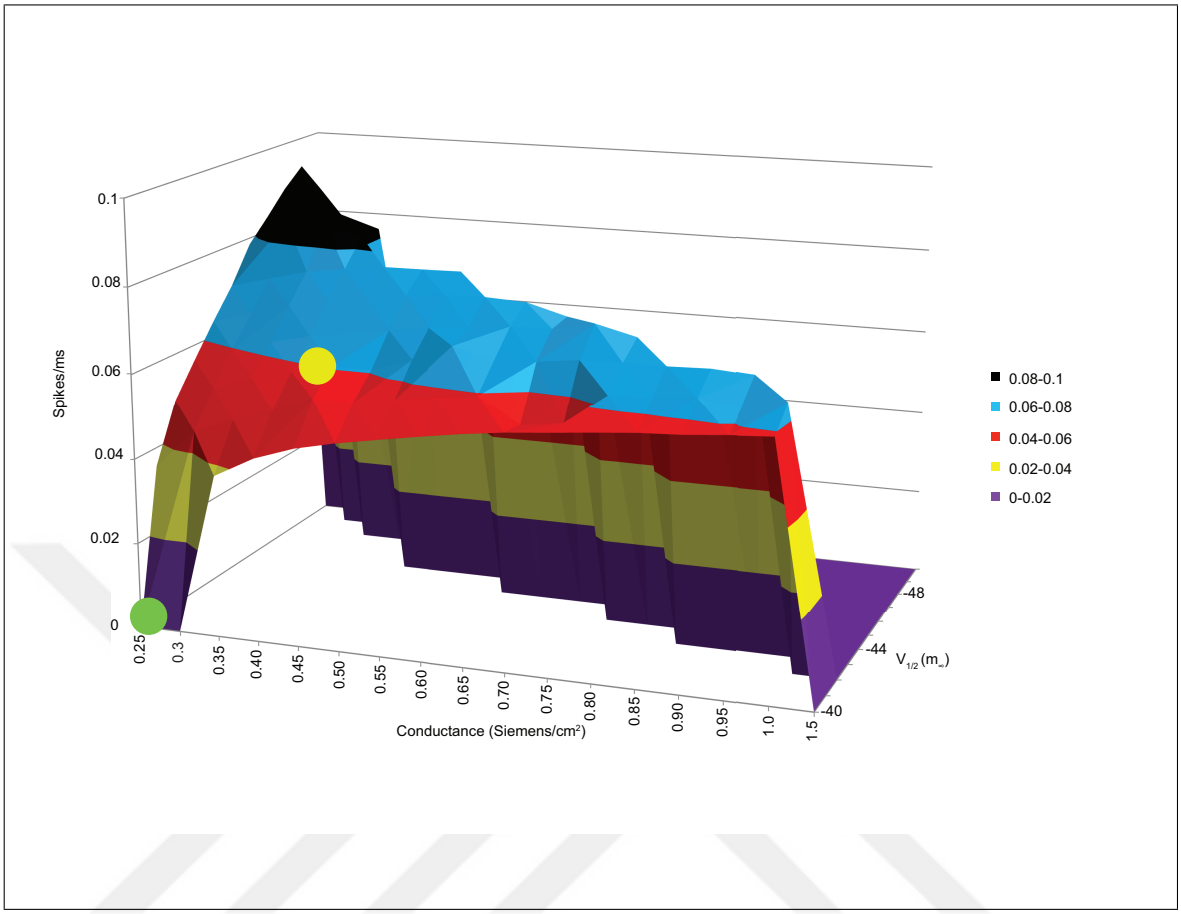

Figure 5.4 Dependence of Firing Frequency on Simultaneous Changes Induced by hSOD1^{A4V} on Na^+ Conductance and Voltage Dependence of Activation

values (Figure 5.5). In Figure 5.5A, the neuron was electrically silent at the baseline $V_{1/2}$ (left); an initial, single action potential was seen with a 2.6 mV depolarization (right). When the voltage dependence of the Na_v channel inactivation is shifted 3 mV in the depolarizing direction (as observed experimentally), no spontaneous firing was observed (resting membrane potential -40 mV) as seen in Figure 5.3B. Lastly, when the depolarizing shift exceeds 5 mV, repetitive spontaneous firing is triggered (5.3C, left). When the depolarizing shift exceeds 19 mV, the model becomes depolarized to -25 mV and inexcitable (5.3C, right).

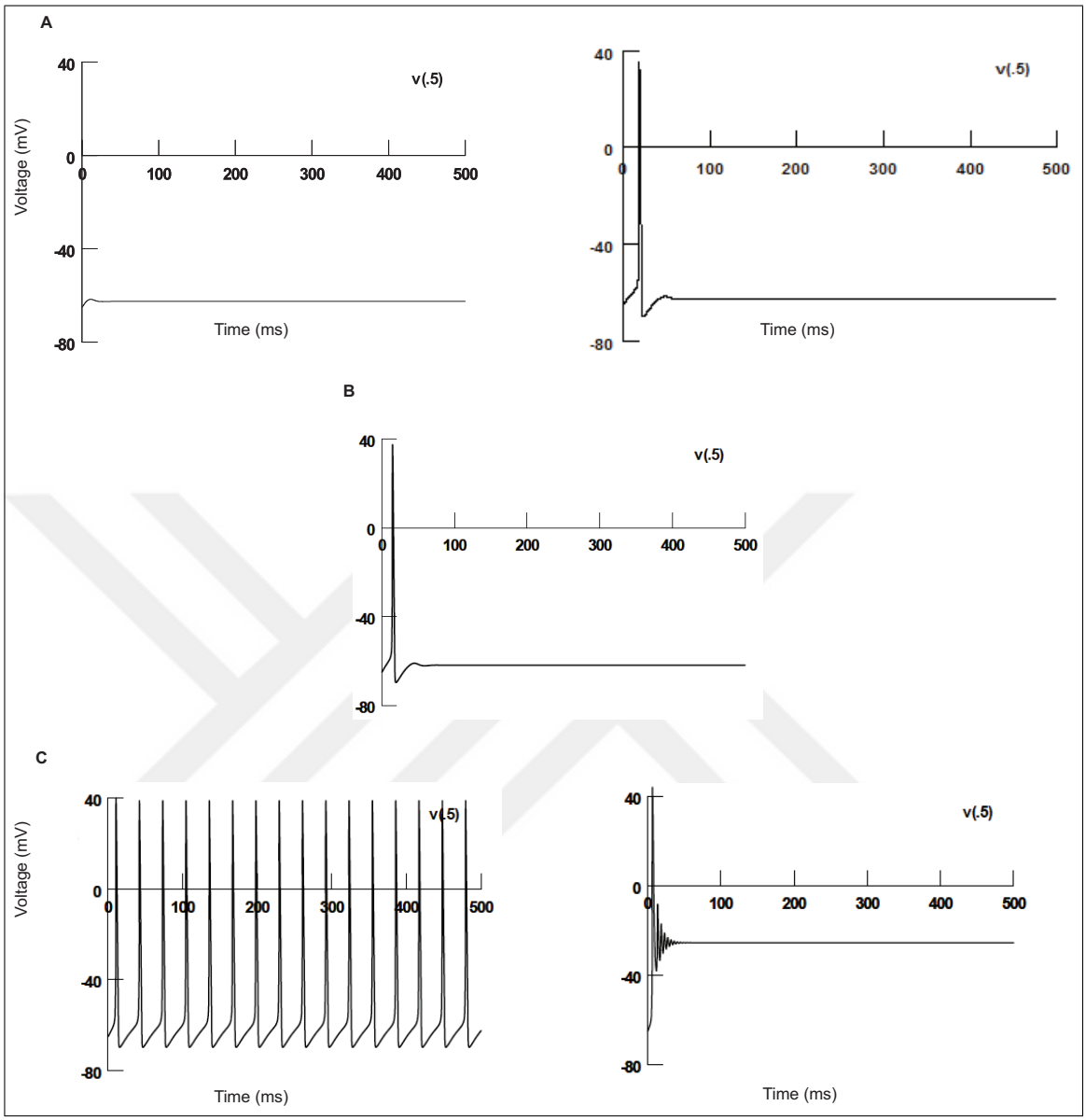

Figure 5.5 Firing Patterns of Mammalian Neuron in Response to Changes in Voltage Dependence of Inactivation Induced by hSOD1^{A4V}

6. DISCUSSIONS

Using an oocyte expression system, the impact of hSOD1^{A4V} protein on physiological parameters of a complex of Na$_v$1.3 consisting of its α and β subunits was examined in this study. This is the first report to examine the impact of mutant SOD1 protein at the level of a specific Na(V) channel complex. Also, it was observed that, as compared to hSOD1^{WT}, the mutant SOD1 protein induced two significant changes in the properties of the Na$_v$1.3 complex: an increase in peak Na^+ current and a hyperpolarizing shift in the voltage dependence of Na$_v$ channel activation. Using the software program NEURON, it was documented that these changes are predicted to increase firing frequency of a simulated model of mammalian neuron. NEURON was selected as this study's model primarily because it has been used extensively to model the behavior of a mammalian neuron [105]. These results suggest that changes in the biophysical properties of voltage-gated sodium channels are important in the genesis of mutant SOD1-induced hyperexcitability in ALS.

6.1 Hypothetical Reasons for ALS Hyperexcitability

Normal neuron signaling requires the activation and inactivation kinetics to be in harmony. Even small oscillations in the normal gating rhythm would change cellular excitability. Ion channel contribution in ALS pathogenesis have been studied in literature, such as AMPA receptor permeability alterations [85, 106] and striatal synaptic plasticity changes [107]. In addition, mutations in the subunits of sodium channel cause channel kinetic alterations and pathologies [108, 48]. For example, sodium channel α subunit mutations lead to hyperexcitability by an accelerated recovery from fast inactivation mechanism [20]. Accelerated firing results in free intracellular calcium and sodium ion concentration increase, together with inability of Na^+/ Ca^{+2} exchanger to eject extra calcium[109].

Observations of this study are consistent with several lines of experimental data

that implicate excessive firing of motor neurons as a central element in the pathogenesis of ALS. These studies have included investigations of human motor cortex [110], murine cell culture and slice preparations of motor cortex [92, 93], spinal cord [83, 60, 86, 84, 79, 100, 80, 85, 62, 101] and brainstem [90, 63, 61]. Most recently, in vitro studies have also shown hyperexcitability of cultured iPSC- derived motor neurons from individuals with SOD1, FUS and C9orf72 gene mutations [94]. The mechanisms whereby neurons in ALS disease are hyperexcitable are multiple, with data implicating both endogenous membrane changes as well as excessively excitatory synaptic inputs [90, 63, 99] and excitatory stimuli from astrocyte conditioned medium [111]. However, recent data have raised the important possibility that early motor neuronal hypoexcitability may be pivotal in ALS and other neurodegenerative disorders, initiating a cascade of events that compromise neuronal viability with hyperexcitability as a compensatory rather than a primary phenomenon [112, 113]. Resolution of these two viewpoints will await further studies, although it is noted that the observation which mutant SOD1 directly augments sodium channel excitability is consistent with a primary, upstream role for hyperexcitability in neuronal pathology in ALS.

The mechanism(s) whereby mutant SOD1 protein affects the biophysical properties of the $Na_v1.3$ complex is not known. Potential mechanisms are numerous and, at this point, speculative. Some potential mechanisms through which mutant SOD1 increases current could be:

1. SOD1 directly affects hyperexcitability: There may be a direct effect on the channel proteins, perhaps mediated via channel oxidation or phosphorylation. Transcriptional modifications of genes special for protein degradation, cell survival and death, immunity and antioxidant response [114, 115] could be given as some reasons for SOD1 related hyperexcitability. For example, oxidative stress can activate protein kinases such as protein kinase C (PKC). This is of potential interest in the context of this study because levels of PKC activity are elevated in $hSOD1^{G93A}$ mice and human ALS patients [58, 116, 117, 118, 90]. Moreover, PKC is known to phosphorylate the α subunit of some Na_v channels [119]. Channels

phosphorylated by PKC open faster and have reduced inactivation which in turn produces elevated PICNa$^+$ [119]. Oxidative stress and elevated [Ca^2] levels via voltage gated calcium channels in mutant SOD1 organisms would activate PKC which would augment PICNa$^+$ and hyperexcitability and also elevate mitochondrial metabolic demands which would further activate PKC [90].The resulting altered excitability may change energy metabolism [120], mitochondrial processes [121], increase oxidative stress [122], which would eventually lead to cell death, structural and functional damage [6] of motor neurons with poor calcium buffering capacity [89]. Consequently, cells producing an increased amount of action potentials per unit of input are more excitable and vulnerable to excitotoxicity. After PKC is activated, Na$^+$channels possess prolonged openings, which are in agreement with the monitored slowing of inactivation of Na$_v$ channel [123]. In this current study, although hSOD1 ^{A4V} did not significantly change the inactivation kinetics of Na$_v$ 1.3 channel complexes, oxidative stress could be playing a role in the increased sodium current. That there might be a direct effect of mutant SOD1 on the channel is further suggested by the observation that mutant SOD1 can interact directly with the cytoplasmic face of the voltage dependent anion channel, VDAC1 [124]. In that study, misfolded mutant SOD1 directly bound to the cytoplasm facing side of VDAC1 and acted like a porin. This mitochondrial pore like structure is the main actor to ATP/ADP import/export [125]. So, misfolded SOD1 somehow, by itself or via interaction with other channels, affects cation flux through those channels.

2. SOD1 indirectly affects hyperexcitability: Alternatively, it is conceivable that mutant SOD1 has an indirect effect on the Na$_v$1.3 complex, by a mechanism such as increased channel trafficking to the membrane. For example, in the study done by Van Zundert et. al., [126] conditioned media from astrocytes expressing mutant SOD1 selectively leads to motor neuron death through voltage-gated sodium channels. The authors of that study also indicated that incubation of the motor neuron cultures in mutant SOD1 and TDP 43 astrocyte conditioned medium with sodium channel blockers such as mexiletine (antiarrythmic drug targeting Na$_v$ channel receptor site,[127]), spermidine (a polyamine acting as an activity

dependent Na_v channel blocker [128]) or riluzole (neural excitability supressor via Na_v channels, [60, 111]) inhibit both motor neuron death and nitroxidative stress. Mentioned study indicates that mutant SOD1 or TDP43 proteins mediate secretion of soluble factors leading to motor neuron cell death via Na_v channels.

It is likely that excessive firing will be detrimental to motor neurons in two ways. In the author‘s view, the primary adverse impact of heightened electrical activity is likely to be mediated by a downstream effect, such as elevations in cytosolic calcium, with subsequent activation of calcium-dependent enzymes (e.g. proteases, lipases). These changes will lead to cytotoxicity, cell death, muscle denervation and paralysis. In addition, it is possible that excessive firing will be adverse at least transiently because it can lead to depolarization arrest, which will prevent motor neuron activation of contraction, even if the neuromuscular junction is intact. The possibility of depolarization arrest of motor neurons (presumably early in the illness) has not been studied. The potentially important implication of this is that in ALS cases there may be populations of neurons that can rapidly be rendered functional by interventions that repolarize the electrically silent cells. Such reagents might include not only Na_v channel blocking compounds (such as mexiletine) but also compounds that augment K^+ channel activity (e.g. retigabine).

6.2 Sodium Channel Inactivation Types and β Subunit Effect on Recovery from Fast Inactivation

Voltage-gated Na^+ channels (Na_v), which underlie neuronal excitation and action potential propagation, consist of a 260 kDa α subunit and one or more 30-40 kDa β subunits. Because α subunits form the actual ion channel as well as sensors of voltage dependence, they are inherently working cores of the excitation process. β subunits modulate the kinetics of voltage dependence activation and inactivation as well as channel localization on the cell membrane [129, 130]. Sodium channels have two types of inactivation as; fast and slow. Fast inactivation is the rapid decay of Na^+

currents in response to short depolarizations, whereas slow inactivation is the depolarization of neurons for seconds or minutes. These two types use also different structural elements [131].

At the very beginning of this study, experiments were executed without β subunit in order to evaluate the α subunit excitability property in isolation. However, the channel inactivated very slowly and even failed to recover from fats inactivation completely (shown in Appendix A) which was consistent with the study demonstrating the fact that Na_v 1.3 channel inactivated crucially slowly without β subunit as it was also noted by Joho et. al., study [132]. Thus, the experiments were reexecuted with the inclusion of β subunit. This result also indicates that the auxiliary subunits are important in sodium channel functionality modification [38, 133, 37].

6.3 hSOD1^{A4V} Mutations

Missense mutant protein SOD1^{A4V} was elected to study because the A4V substitution is the most common and clinically most severe SOD1 mutation in North America [2]. Also, in a previous study examining structure and activity of hSOD1^{A4V} [96], hSOD1^{A4V} forms distinct pore like structures with evident conductance across a lipid membrane. In that study, it was also suggested that mutant hSOD1^{A4V} leads to cellular homeostasis disturbances and also calcium level increase. As suggested in that study, the increase of calcium could be as a result of either voltage sensitive calcium channels activation or mutant SOD1 interaction with other kind of ion channels that effect calcium. In addition, sodium channel interaction with hSOD1^{A4V} could be the main factor actor affecting increase of calcium levels in the cytoplasm. Further experiments with this most mutation should be done to prove that sodium channels are responsible for calcium homeostasis disruption.

6.4 *Xenopus* Oocyte as Isolated Model Organisms

The functional sodium channel activation with mutant hSOD1 ^{A4V} would have reflected presence of numerous α and β subunits inside the cell if motor neurons were used in this study. The alteration of channel activation functionality would reflect endogenous compound modifications on the channel, transcriptional alterations or indirect effectors that could modify the channel. Instead, oocyte model system was used in order to be stable at the variety of α and β subunits and to eliminate different isoform and subunit type factor. In addition to acquiring an isolated system with only the channel and the protein of interest, the oocyte system has some advantages as; being easy to use, fast and economical electrophysiological method especially over small cells transfected with exogenous RNA, where expression levels are not easy to determine with an otherwise technique [78].

6.5 Na_v 1.3 Isoform

Sodium channels are responsible for action potential formation and spread and different subtypes of sodium channels have distinct abilities to form action potentials with distinct electrogenic properties such as refractory period or threshold. Also, each subclass is expressed at different developmental periods in particular temporal and spatial patterns [73]. Distortions in ion channel expression levels also correlate with the selectivity of this subclass expression brings the idea that each isoform is responsible for a specific function for different neuron types at different developmental stages [77].

As noted before, in this study the focus was on $Na_v1.3$, an embryonically expressed isoform, because many of the studies pointing to motor neuron hyperexcitability in ALS are based on embryonic or immediately post-natal motor neurons (particularly in vitro). For example, in transgenic hSOD1^{G93A} ALS mice, heightened excitability is evident before or shortly after birth [84, 134, 81, 55]. Also, embryonic spinal cord cultures of 4-7 DIV (days in vitro) have elevated persistent inward currents

when treated with astrocyte conditioned media from SOD1^{G93A} mice [126]; this study showed that astrocyte conditioned media from hSOD1^{G93A} mice targets $Na_v1.2$ and $Na_v1.3$. In embryonic development, the predominant Na_v isoforms expressed in motor neurons are $Na_v1.2$ and $Na_v1.3$. Expression of $Na_v1.3$ begins very early in embryogenesis and then increases, attaining a maximum level at birth; it then declines after the second postnatal week to very low levels at adulthood [135, 136, 72]. $Na_v1.1$ and 1.6 expression levels predominate at later developmental stages [135]. In the rat, Na_v 1.1, Na_v 1.2, and Na_v 1.6 are expressed at robust levels in the adult CNS while Na_v 1.3 levels are substantially reduced [136]. In addition to being expressed in embryonic stages and rare at adult stages of development, Na_v 1.3 channels cause neuron to be hyperexcitable by persistent current production and hyperexcitability relation could also explain why this channel is abundant at embryonic stages where neural circuit development requires spontaneous activity [137]. Also, these channels recover form inactivation fast so they fire fast. Expression levels of this channel especially are elevated after neural injury which is also related to hyperexcitability, alterations after pain and neural hyperresponsive behaviors [77].

To date, there have been no analyses of the impact of mutant ALS genes and proteins on single channel isoform behavior of voltage-gated Na^+ channels. In the current study, it is shown that a common familial ALS mutant, hSOD1^{A4V}, shifts the voltage dependence and augments total Na^+ currents of Na_v channel, $Na_v1.3$, an isoform that is characteristic of embryonic motor neurons [135], that is documented both to have a persistent inward sodium current and to be implicated in human neurological disease [76, 77].

6.6 Specific Experimental Comments

In this study, a conductance increase of sodium current and a negative shift in $V_{1/2}$ of activation curve in hSOD1^{A4V} mutant oocytes were observed compared to hSOD1^{WT} oocytes. Increased conductance, thus total current through the motor neuron would make it hyperexcitable and the more negative $V_{1/2}$ values of activation of

hSOD1^{A4V} in the experiments would change the activation and inactivation gating harmony involved in action potential. As a result, this modification would cause the hSOD1^{A4V} organisms to begin and propagate at action potentials at more negative values closer to polarized membrane potential value that is around -90 mV in humans and around -60 mV in *Xenopus* oocytes. Initiation of action potentials at more polarized values leads to more frequent action potentials as previously shown [83, 85]. Kuo et. al., also [60] demonstrated that cultured spinal cord motor neurons from embryonic hSOD1^{G93A} mice disclosed an increased persistent current, and is able to fire repetitively with prolonged depolarization. Likewise, Van Zundert et. al., [90] used neonatal mice expressing hSOD1^{G93A} which display higher rates of AP firing and amplitude than mice expressing hSOD1^{WT} and the observed persistent sodium current hyperexcitability responds significantly to riluzole treatment.

Previous studies focused on the effects the familial mutant hSOD1 ^{G93A} has on neuronal excitability and correlated the increased sodium current with changes in kinetics of activation [85]. In the analysis of the fast kinetics of activation in this study, T_1 and T_2 values were not significantly different among three populations. Although T_2 was different at the Pieri study [92], this study's results are consistent with Zona et al., where they found no significant difference [86]. Control and hSOD1^{WT} results were similar however; hSOD1^{A4V} was different, meaning that the findings were specifically attributable to the hSOD1^{A4V} mutation and not to effects of overexpression of SOD1 protein. The slope of the activation curve remained unchanged, indicating a persistent current in mutant oocytes. The $V_{1/2}$ and slope values of the inactivation did not differ between two groups consistent with the Zona et al. [86] study. While analyzing the fast kinetics of activation, Na_v 1.3 was observed to inactivate with biphasic kinetics which is also consistent with the previous study [37] indicating fractional modification by the $\beta 1$ subunit and slow phase of the inactivation is faster significantly indicating the presence of the persistent current in hSOD1^{A4V} oocytes. In the analysis of the fast kinetics of activation, T_1 values were not significantly different among three populations whereas T_1 values of hSOD1^{A4V} was significantly different from the oocytes injected with just sodium channel complex or the oocytes injected with sodium channel complex and hSOD1^{WT} which is consistent with the previous study [92]. According to these

patch clamp studies, motor neurons firing frequency and injected current increased and passive membrane properties remained similar, in the hSOD1^{G93A} mice with respect to control [83, 85]. Also, although recovery form fast inactivation decay constants differed in the previous study [86] with patch clamp with only 1 ms, which would be impossible to analyze with TEVC technique.

The functional change of the activation of Na_v channels may be related to several factors as; the presence of numerous α and β subunits bearing divergent characteristics and distinctly expressed, distinct channel modulations caused by endogenous factors, transcriptional modifications and indirect effectors whose functions could be altered by mutant SOD1. Each of these contributors alters the sodium channel function in the presence of mutant SOD1. Documented modifications on neuronal excitability in the ALS model systems with different hSOD1 mutations could give different results: hSOD1^{G85R} motor neurons are hypo-excitable [84, 97] while those expressing hSOD1^{G93A} are hyper-excitable [60, 90, 97, 92]. So, it could be stated that type of SOD1 mutant, different time course of the disease in each model, type of recordings may contribute to the discrepancies between the excitability changes in the different SOD1 models. It is possible that the A4V mutation will not completely recapitulate what is seen in hSOD1^{G93A} mice. Taken together, this suggests that mutations in SOD1 may differentially affect voltage-gated sodium channel complexes.

In the current study, other than NEURON, alternative simulation programs were also tried to model mathematically model the data. One of them was SimNeuron program; with has been limited in progress because the code is not freely accessible. Next, the simulations were run with the HHSIM Program (shown in Appendix B). This program reproduced the Neuron simulator results qualitatively. However, it had two limitations. First, its parameters are not predicated on the structure and physiology of mammalian motor neurons and, second, it is inherently less flexible than the NEURON program, and so the NEURON Simulation Program was elected to present the data. It should also be noted that the NEURON program has been used in studies covered in more than 300 papers [105]. So, the problem of insignificant firing of mammalian concentrations with Hodgkin-Huxley simulations was overcome with Neuron

program simulations using one soma and two dentritic system with mammalian neuronal concentrations and conditions. Mathematical modeling with NEURON agreed well with the experimental data regarding the conductance increase and the shift in voltage-dependence of the complex with the mutant protein.

7. CONCLUSION

In conclusion, this study sheds light onto the modulation of Na_v channel by SOD1 and suggests that ALS-associated SOD1 mutants may differently modulate Na_v channel complexes. These findings are consistent with the view that excessive neuronal excitability is a potential target for therapy in ALS. A compelling point supporting this view is the fact that riluzole, a compound that blocks neuronal firing (presumably via blockage of Na_v channels) [63, 61, 62] prolongs survival in ALS and is an FDA-approved ALS therapy. Consistent with this, the acquired data showing that another Na_v channel blocking drug, mexiletine, prolongs survival in ALS mice. In this study, intrinsic functional modulation of Na^+ channels displays the compulsion for further research. Also, as a future study, it is important to analyze different channel isoforms with different SOD1 mutations and various action mechanisms of hypothetical drugs. Observations in this study are consistent with several lines of experimental data that implicate excessive firing of motor neurons as a central element in the pathogenesis of ALS. However, recent data have raised the important possibility that early motor neuronal hypoexcitability may be pivotal in ALS and other neurodegenerative disorders, initiating a cascade of events that compromise neuronal viability with hyperexcitability as a compensatory rather than a primary phenomenon [112, 113]. Resolution of these two viewpoints will await further studies, although it should be noted that the observation that mutant SOD1 directly augments sodium channel excitability is consistent with a primary, upstream role for hyperexcitability in motor neuron pathology in ALS.

This study‘s findings are consistent with the view that excessive neuronal excitability is a potential target for therapy in ALS. A compelling point supporting this view is the fact that riluzole, a compound that blocks neuronal firing (presumably via blockage of Na_v channels)[63] prolongs survival in ALS and is an FDA- approved ALS therapy [62, 138]. Conceivably, other Na_v channel blocking compounds may also be beneficial in ALS.

7.1 List of publications produced from the thesis

1. Mutant SOD1 protein increases Nav1.3 channel excitability. E. Kubat Öktem, K. Mruk, J. Chang, A. Akin,W. R. Kobertz, R.H. Brown Jr. *Journal of Biological Physics*, 2016, April 12 [Epub ahead of print].

APPENDIX A. Importance of β1 Subunit in Sodium Channel Dynamics

In a bunch of previous experiments, in order to have a more simple cellular design, the experiments were executed without β1 subunit injection; however, recovery from fast inactivation could not be achieved without β1 subunit as shown in Figure A.1. In Figure A.1, oocytes were injected with (20 ng /oocyte) $Na_v1.3$ α subunit. The protocol began with a conditioning depolarization from a holding potential of -100 to 0 mV for 50 ms, which inactivated the channels. This was followed by a second test pulse at the same depolarizing pulse value delivered to get Na^+ current fraction, whereas the time between the two pulses varied with 1 ms increments to determine the rate of recovery. The sweep number was increased to 101 to have fully recovery. However, the recovery was about 40 %. Upper figure: all of the 101 sweeps of the recovery from fast inactivation. Lower figure: the 101^{th} sweep of the whole protocol, the recovery is about 54 % as shown in the figure.

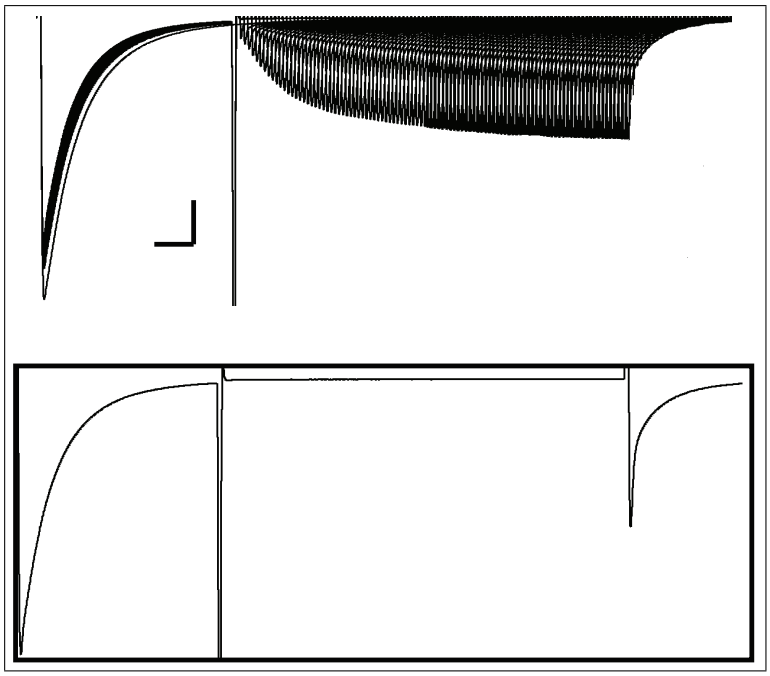

Figure A.1 Recovery from Fast Inactivation Traces without β1 Subunit

It was decided to also inject $\beta 1$ subunit to the oocyte system to solve this problem. New data sets with $\beta 1$ subunit have been taken for all protocols. It has been figured out that β subunit helped the traces to fully recover from inactivation as demonstrated in in Figure A.2. In Figure A.2, oocytes were injected with 6 ng α subunit and 1.2 ng β subunit. The protocol began with a conditioning depolarization from a holding potential of -100 to 0 mV for 50 ms, which inactivated the channels. This was followed by a second test pulse at the same depolarizing pulse value delivered to get Na^+ current fraction, whereas the time between the two pulses varied with 1 ms increments to determine the rate of recovery. The sweep number was 40 because the current had reached to a plateau up to that sweep. The recovery was over 90 %. The current recovery is shown with arrows. Right: full 40 sweeps of the recovery from fast inactivation. Left: the 40^{th} sweep of the whole protocol. The recovery is about 90 % as shown in the figure.

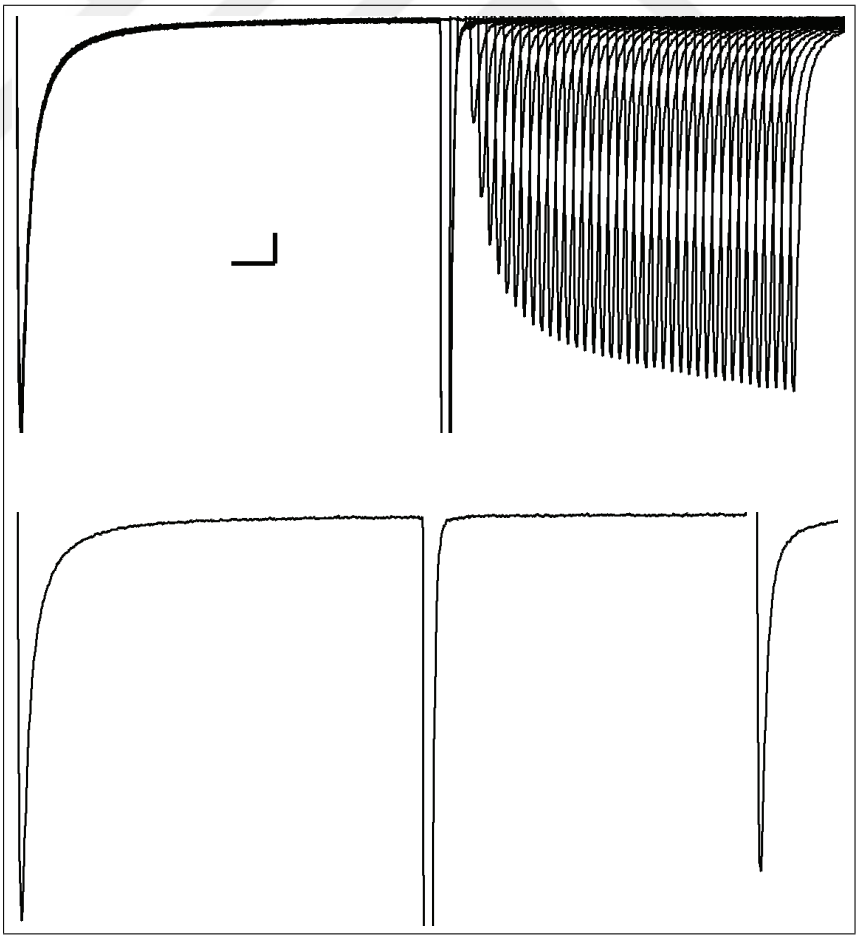

Figure A.2 Recovery from Fast Inactivation Traces with $\beta 1$ Subunit

APPENDIX B. Mathematical Modeling via HHSIM Simulation Program

Before using Neuron Program to mathematically model the experimental data, an open source HH Simulator (HHsim Graphical Hodgkin-Huxley Simulator under MATLAB environment) was used in this study to model the effect hSOD1 protein had on channel complexes acquired from experimental data on the neuronal firing and to provide a better insight to the biophysical changes observed. The experimental data was modeled in three different parameter conditions simulating oocyte, squid and mammalian neurons. Hodgkin and Huxley modeled the sodium conductance with three gating particles called as m and one gating particle named as h. As mentioned before, according to the Hodgkin-Huxley, sodium channel conductance is:

$$\frac{dm}{dt} = \alpha_m(V)(1-m) - \beta_m(V)m \tag{B.1}$$

Where m is the sodium conductance activation state parameter, α_m and β_m are the sodium channel voltage dependent (V) and time (t) independent transfer rate constants [104]. Three models were generated as *Xenopus* oocyte, squid neuron and mammalian neuron to simulate the experimental data. Before evaluating three different cell type conditions in the simulator, all channels were chosen for the action potential firing simulation. Passive G_{Na},G_K, G_{Cl} and delayed rectifier properties were set as default, in both control and mutant protein conditions. To represent hSOD1^{WT} experiments, fast sodium m exponent α_m and β_m constants, and threshold th values were left as default values and called as control protein condition, whereas these constants were shifted by 3 mV in the hyperpolarizing direction at the simulation program to recapitulate mutant hSOD1^{A4V} protein injected complexes and called as mutant protein condition.

B.0.1 Hodgkin-Huxley Squid Condition Simulations

Experimental data was simulated to the original Hodgkin-Huxley squid axon conditions by setting the intracellular ion concentrations to the default intracellular: 50.0 mM Na^+, 400.0 mM K^+ and 52.0 mM Cl^-, extracellular: 440.0 mM Na^+, 20 mM K^+, 560 mM Cl^-, in the simulation program. Membrane capacitance was set to 1 nF and the temperature was set to 6.30° [31]. To model the effect a 3 mV hyperpolarizing shift in the voltage dependence of activation would have on neuronal firing under recording conditions, current stimuli starting from 0 nA to 100 nA (simulation program maximum value) for 50 ms were applied under voltage recording mode for both control and mutant protein conditions. The stimuli were given in 5 nA increments. Figures B.1 and B.2 indicate action potentials at either WT (no attained firing) or mutant protein conditions generated by 0 nA stimulus respectively.

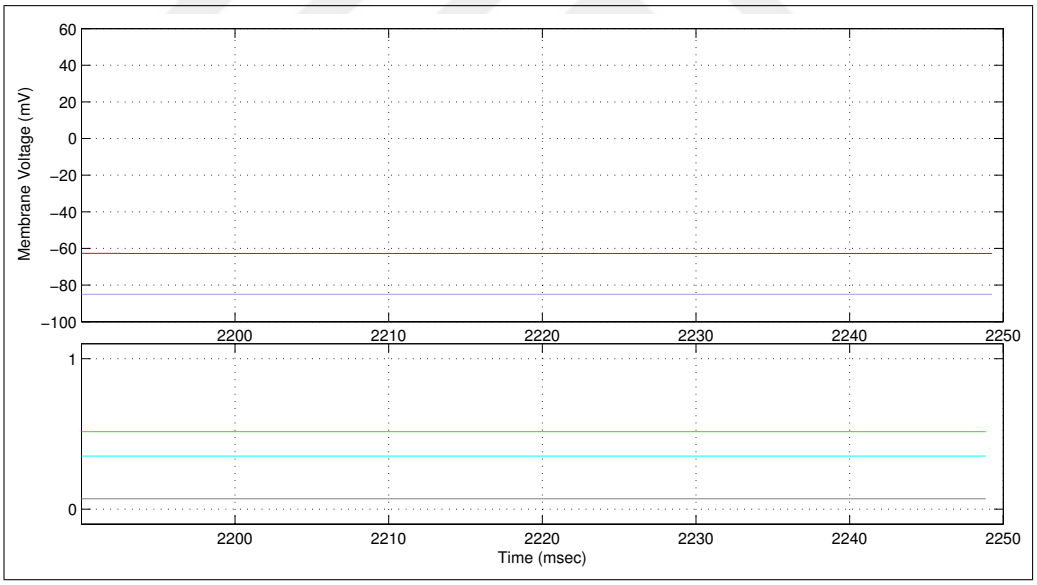

Figure B.1 Unfiring Squid Control Conditions at 0 nA

For the HH squid model, a 3 mV threshold shift of the α_m and β_m constants of sodium channel, which is simulating mutant protein complex effect, has lead to action potential firing even without any current stimulus and this baseline (without stimulus) firing was observed during the entire duration of the simulation. In contrast, action potential firing started at 2 nA with default threshold value, which is simulating Na_v 1.3-β1 channel or WT SOD1 protein-channel complex simulations (Figure B.2).

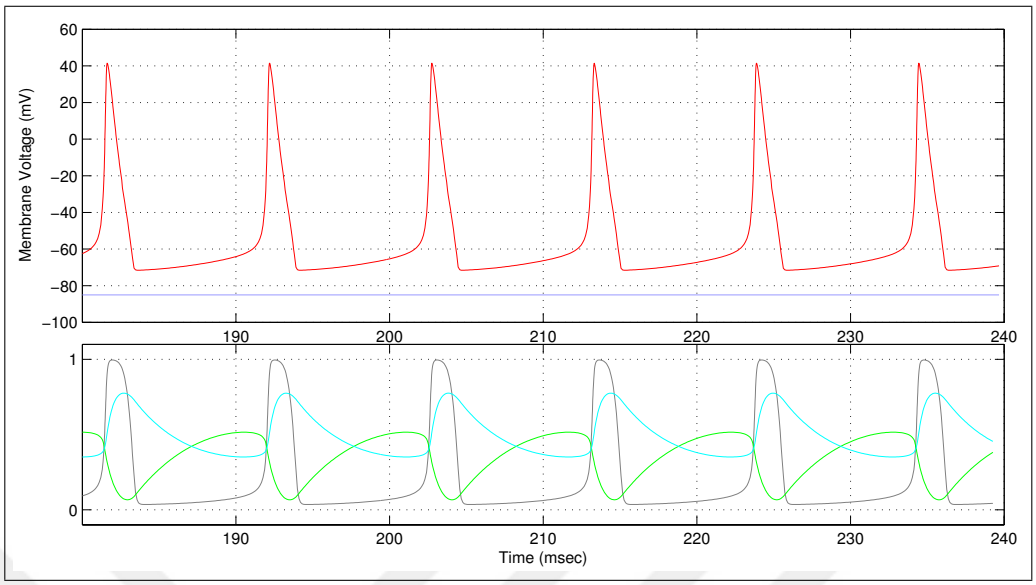

Figure B.2 Firing of Squid Mutant Conditions at 0 nA

In Figure B.3, Hodgkin-Huxley action potential firing simulation data on Hodgkin-Huxley squid conditions is demonstrated. Figure B3.A shows action potential firing which was applied with a current clamp protocol starting from 0 nA and ending with 100 nA in 5 nA increments. Mutant protein complex simulations were applied with 3 mV left shift of fast sodium α_m and β_m. As shown in Figure B3.B, action potential firing increased with this threshold shift. With mutant complex simulation, firing started without stimulus and composed a baseline firing whereas control simulation started firing at 2 nA. Lastly, as indicated in Figure B3.C, firing frequency increased with mutant protein threshold (th) value compared to control.

B.0.2 Hodgkin-Huxley *Xenopus* Oocyte Condition Simulations

In order to mathematically model the experimental findings on *Xenopus* oocyte conditions, the intracellular ion concentrations for Hodgkin-Huxley simulations were set to 14.0 mM Na^+, 122.0 mM K^+, and 49.0 mM Cl^-, [139] whereas the extracellular ion concentrations were adjusted to 96.0 mM Na^+, 2 mM K^+, 100.6 mM Cl^-, in the simulation program. Membrane capacitance was set to 1 nF and the temperature was set to 25°, average room temperature where the experiments executed. The data were

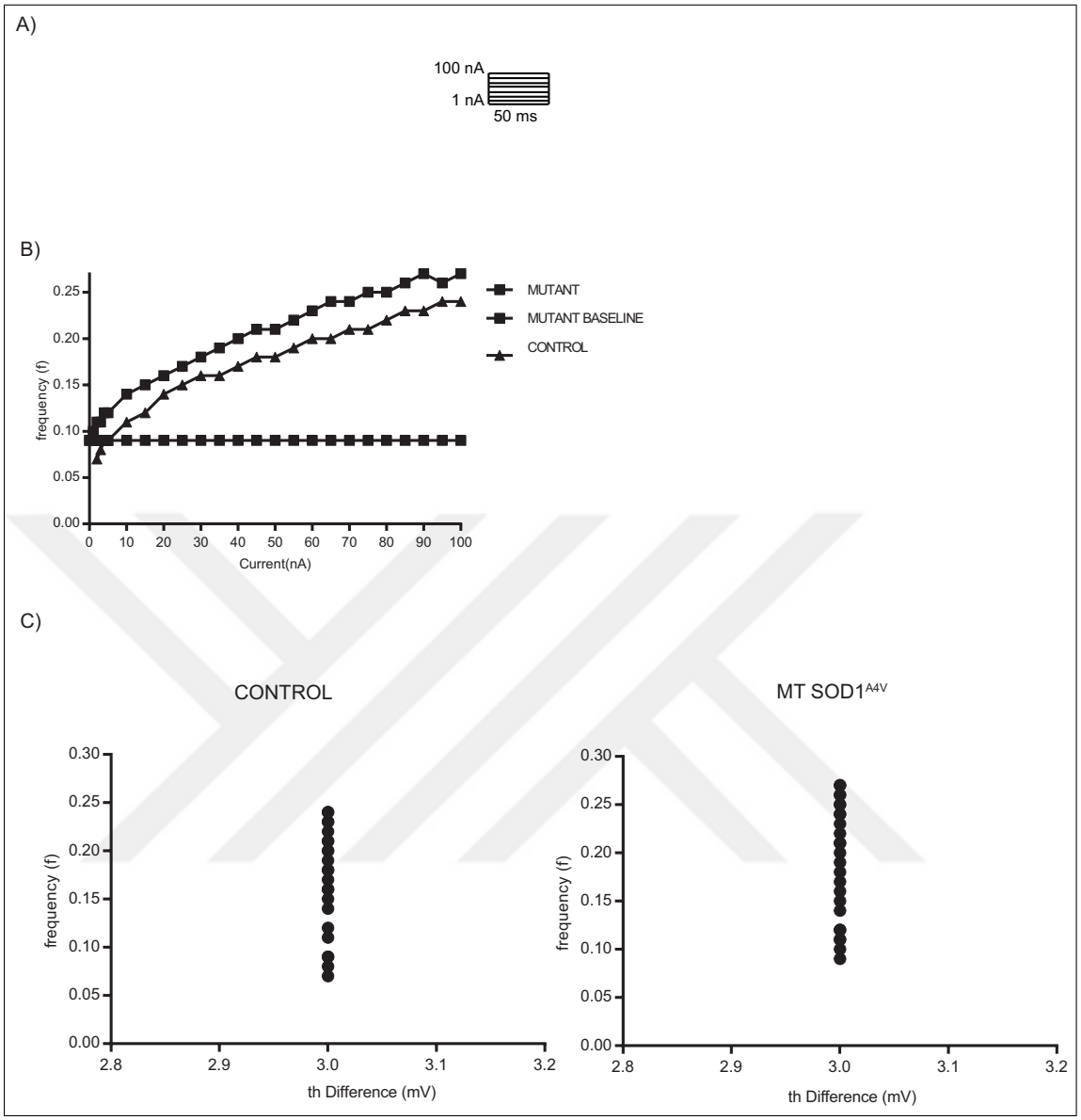

Figure B.3 Firing Data at Hodgkin-Huxley Squid Conditions

modeled similar to the squid modeling. To model the effect a 3 mV hyperpolarizing shift in the voltage dependence of activation would have on neuronal firing under recording conditions, current stimuli starting from 0 nA to 100 nA (simulation program maximum value) for 50 ms were applied under voltage recording mode for both control and mutant protein conditions. The stimuli were given in 5 nA increments.

As a result of this simulation, SOD1 protein complexes were found to have a significant firing rate increase with mutant protein complex. Firing started at around 40 nA for control conditions, whereas it started at around 32 nA for mutant conditions.

In Figure B.4, Hodgkin-Huxley action potential firing simulation data on Xenopus Oocyte conditions is shown. Figure B4.A demonstrates action potential firing which was applied with a current clamp protocol starting from 0 nA and ending with 100 nA in 5 nA increments. Mutant protein complex simulations were applied with 3 mV left shift of fast sodium m exponent α and β components. As seen in Figure B4.B, firing started at around 40 nA for control conditions, whereas it started at around 32 nA for mutant conditions. Firing frequency for mutant was always more than control for all applied currents. Lastly, as shown in Figure B4.C, firing frequency increased with mutant protein threshold (th) value.

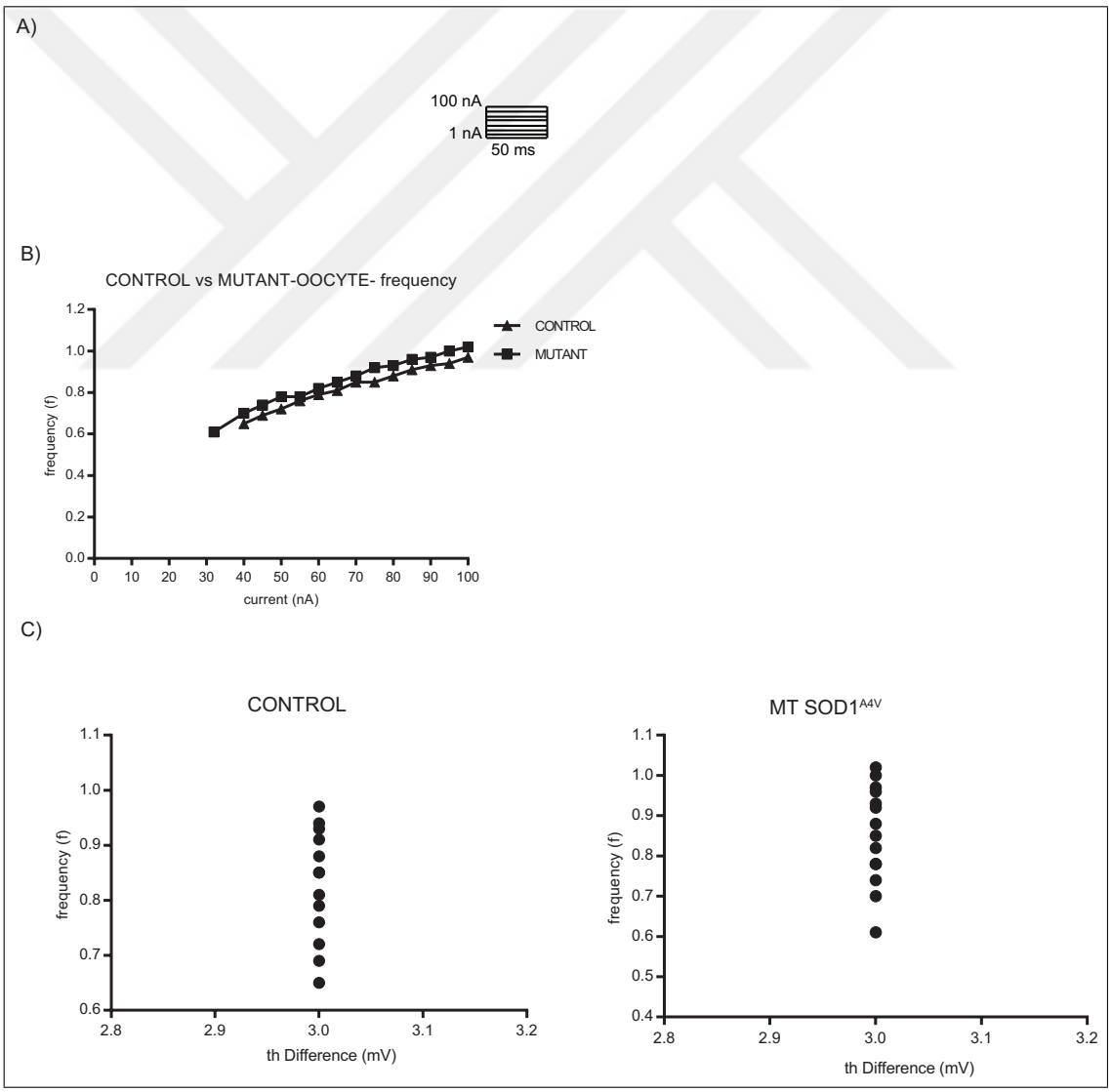

Figure B.4 Firing Data at Xenopus Oocyte Conditions

B.0.3 Hodgkin-Huxley Mammalian Neuron Condition Simulations

To simulate our actual data on the typical mammalian neuron, the extracellular ion concentrations were adjusted to 150.0 mM Na^+, 3 mM K^+, 120 mM Cl^- and the intracellular ion concentrations were set to 18.0 mM Na^+, 135.0 mM K^+ and 7.0 mM Cl^- [140]. Membrane capacitance was set to 1 nF and the temperature was set to 36.3 ° body temperature as the lowest mammalian normal body temperature [141]. The data were modeled similar to the squid modeling. Again, to model the effect a 3 mV hyperpolarizing shift in the voltage dependence of activation would have on neuronal firing under recording conditions, current stimuli starting from 0 nA to 100 nA (simulation program maximum value) for 50 ms were applied under voltage recording mode for both control and mutant protein conditions. The stimuli were given in 5 nA increments.

For the mammalian neuron simulations, the action potential firing even at 100 nA maximum current did not endure until the end of 50 ms stimulus and it vanished. So, no firing frequency could be evaluated for mutant conditions. It was concluded that HHSIM program was not efficient for mammalian neuron conditions. So, instead of HHSIM Program, NEURON Simulation Program was used to mathematically model this study‘s data.

REFERENCES

1. Brown, R. H., "Commentary superoxide dismutase in familial amyotrophic lateral sclerosis," *Current Opinion in Neurobiology*, Vol. 5, pp. 841–846, 1995.

2. Cudkowicz, M. E., P. E. Sapp, W. Chin, B. Geller, and R. H. Brown, "Epidemiology of mutations in superoxide dismutase in amyotrophc lateral sclerosis," *Annals of Neurology*, Vol. 41, no. 2, pp. 210–221, 1997.

3. Cleveland, D. W., and J. D. Rothstein, "From charcot to lou gehrig : Deciphering selective motor neuron death in als," *Nature*, Vol. 2, pp. 806–819, November 2001.

4. Rothstein, J. D., "Current hypotheses for the underlying biology of amyotrophic lateral sclerosis.," *Annals of Neurology*, Vol. 65, pp. 3–9, 2009.

5. Redler, R. L., and N. V. Dokholyan, "The complex molecular biology of amyotrophic lateral sclerosis (als)," *Progress in Molecular Biology and Translational Science*, Vol. 107, pp. 215–262, 2012.

6. Lewinski, F. V., and B. U. Keller, "Ca+2 , mitochondria and selective motoneuron vulnerability : implications for als," *Trends in Neurosciences*, Vol. 28, no. 9, pp. 494–500, 2005.

7. Robberecht, W., and T. Philips, "The changing scene of amyotrophic lateral sclerosis," *Nature Reviews*, Vol. 14, no. 4, pp. 248–264, 2013.

8. de Carvalho, M., R. Dengler, A. Eisen, J. D. Engand, R. Kaiji, J. Kimura, K. Mills, H. Mitsumoto, H. Nodera, J. Shefner, and M. Swash, "The changing scene of amyotrophic lateral sclerosis," *Clinical Neurophysiology*, Vol. 119, no. 3, pp. 497–503, 2008.

9. Sutedja, N., J. H. V. K Fischer, G. J. M. G. van der Heijden, H. Kromhout, D. Heederik, M. H. B. Huisman, J. J. H. Wokke, and L. H. van den Berg, "What we truly know about occupation as a risk factor for als: a critical and systematic review.," *Amyotrophic Lateral Sclerosis*, Vol. 10, no. 5-6, pp. 295–301, 2009.

10. Mattson, M. P., "Infectious agents and age-related neurodegenerative disorders.," *Ageing Research Reviews*, Vol. 3, no. 1, pp. 105–120, 2004.

11. Chio, A., G. Benzi, M. D. R, Mutani, and G. Mora, "Severely increased risk of amyotrophic lateral sclerosis among italian professional football players," *Brain*, Vol. 128, no. 3, pp. 472–476, 2005.

12. Cox, P. A., S. A. Banack, and S. J. Murch, "Biomagnification of cyanobacterial neurotoxins and neurodegenerative disease among the chamorro people of guam.," *Proceedings of the National Academy of Sciences of the United States of America*, Vol. 100, no. 23, pp. 13380–13383, 2003.

13. Bosco, D. A., G. Morfini, N. M. Karabacak, Y. Song, F. Gros-Louis, P. Pasinelli, H. Goolsby, B. A. Fontaine, N. Lemay, D. McKenna-Yasek, M. P. Frosch, J. N. Agar, J. P. Julien, S. T. Brady, and R. H. Brown, "Wild-type and mutant sod1 share an aberrant conformation and a common pathogenic pathway in als.," *Nature Neuroscience*, Vol. 13, pp. 1396–1403, November 2010.

14. Valentine, J. S., P. A. Doucette, and Z. P. Soshanna, "Copper -zinc superoxide dismutase and amyotrophic lateral scletosis," *Annual Review of Biochemistry*, Vol. 74, pp. 563–593, 2005.

15. Sreedharan, J., and R. H. Brown, "Amyotrophic lateral sclerosis: Problems and prospects.," *Annals of Neurology*, Vol. 74, no. 3, pp. 309–316, 2013.

16. Borchelt, D. R., M. K. D. R. Leeo, H. S. Sluntt, M. Guarnierit, Z. H. Xu, P. C. Wong, R. H. Brown, D. L. Price, S. S. Sisodia, and D. W. Clevelandt, "Superoxide dismutase 1 with mutations linked to familial amyotrophic lateral sclerosis possesses significant activity.," *Proceedings of the National Academy of Sciences of the United States of America*, Vol. 91, pp. 8292–8296, August 1994.

17. Hough, M. A., J. G. Grossmann, S. V. Antonyuk, R. W. Strange, P. A. Doucette, M. A. Hough, J. Gu, J. A. Rodriguez, L. J. Whitson, P. J. Hart, L. J. Hayward, J. S. Valentine, and S. S. Hasnain, "Dimer destabilization in superoxide dismutase may result in disease-causing properties : Structures of motor neuron disease mutants," *Proceedings of the National Academy of Sciences of the United States of America*, Vol. 101, no. 16, pp. 5976–5981, 2004.

18. Al-chalabi, A., P. M. Andersen, B. Chioza, C. Shaw, C. Pak, W. Robberecht, G. Matthijs, W. Camu, S. L. Marklund, L. Forsgren, G. Rouleau, N. G. Laing, P. V. Hurse, T. Siddique, P. N. Leigh, and J. F. Powell, "Recessive amyotrophic lateral sclerosis families with the d90a sod1 mutation share a common founder : evidence for a linked protective factor," *Human Molecular Genetics*, Vol. 7, no. 13, pp. 2045–2050, 1998.

19. Rodriguez, J. A., J. S. Valentine, D. K. Eggers, J. A. Roe, A. Tiwari, R. H. Brown, and L. J. Hayward, "Familial amyotrophic lateral sclerosis-associated mutations decrease the thermal stability of distinctly metallated species of human copper/zinc superoxide dismutase.," *Journal of Biological Chemistry*, Vol. 277, no. 18, pp. 15932–15937, 2002.

20. Hayward, L. J., J. A. Rodriguez, J. W. Kim, A. Tiwari, J. J. Goto, D. E. Cabelli, J. S. Valentine, and R. H. Brown, "Decreased metallation and activity in subsets of mutant superoxide dismutases associated with familial amyotrophic lateral sclerosis.," *The Journal of Biological Chemistry*, Vol. 277, no. 18, pp. 15923–15931, 2002.

21. Reaume, A. G., J. L. Elliott, E. K. Hoffman, N. W. Kowall, R. J. Ferrante, D. R. Siwek, H. M. Wilcox, D. G. Flood, M. F. Beal, R. H. Brown, R. W. Scott, and W. D. Snider, "Motor neurons in cu/zn superoxide dismutase-deficient mice develop normally but exhibit enhanced cell death after axonal injury," *Nature Genetics*, Vol. 13, no. 1, pp. 43–47, 1996.

22. Furukawa, Y., and T. V. O'Halloran, "Amyotrophic lateral sclerosis mutations have the greatest destabilizing effect on the apo- and reduced form of sod1, leading to unfolding and oxidative aggregation.," *The Journal of Biological Chemistry*, Vol. 280, no. 17, pp. 17266–17274, 2005.

23. Bystrom, R., P. M. Andersen, G. Grobner, and M. Oliveberg, "Sod1 mutations targeting surface hydrogen bonds promote amyotrophic lateral sclerosis without reducing apo-state stability.," *The Journal of Biological Chemistry*, Vol. 285, no. 5, pp. 19544–19552, 2010.

24. Wang, Q., J. L. Johnson, N. Y. R. Agar, and J. N. Agar, "Protein aggregation and protein instability govern familial amyotrophic lateral sclerosis patient survival," *Plos Biology*, Vol. 6, no. 7, pp. 1508–1526, 2008.

25. Ding, F., and N. V. Dokholyan, "Dynamical roles of metal ions and the disulfide bond in cu, zn superoxide dismutase folding and aggregation," *Proceedings of the National Academy of Sciences of the United States of America*, Vol. 105, no. 50, pp. 19696–19701, 2008.

26. Wang, J., G. Xu, and D. R. Borchelt, "High molecular weight complexes of mutant superoxide dismutase 1 : Age-dependent and tissue-specific accumulation," *Neurobiology of Disease*, Vol. 148, no. 9, pp. 139–148, 2002.

27. Jonsson, P. A., K. Ernhill, P. M. Andersen, D. Bergemalm, T. Brannstrom, O. Gredal, P. Nilsson, and S. L. Marklund, "Minute quantities of misfolded mutant superoxide dismutase-1 cause amyotrophic lateral sclerosis.," *Brain*, Vol. 127, pp. 73–88, 2004.

28. Martin, L. J., N. A. Al-abdulla, A. M. Brambrink, J. R. Kirsch, F. E. Sieber, and C. Portera-cailliau, "Neurodegeneration in excitotoxicity , global cerebral ischemia , and target deprivation : A perspective on the contributions of apoptosis and necrosis," *Brain Research Bulletin*, Vol. 46, no. 4, pp. 181–309, 1998.

29. Yamanaka, K., S. Boillee, E. A. Roberts, M. L. Garcia, M. McAlonis-Downes, O. R. Mikse, D. W. Cleveland, and L. S. B. Goldstein, "Mutant sod1 in cell types other than motor neurons and oligodendrocytes accelerates onset of disease in als mice," *Proceedings of the National Academy of Sciences of the United States of America*, Vol. 105, no. 21, pp. 1–6, 2008.

30. Perlson, E., G. B. Jeong, J. L. Ross, R. Dixit, K. E. Wallace, R. G. Kalb, and E. L. F. Holzbaur, "A switch in retrograde signaling from survival to stress in rapid-onset neurodegeneration.," *The Journal of Neuroscience*, Vol. 29, no. 31, pp. 9903–9917, 2009.

31. Hodgkin, A. L., and A. F. Huxley, "A quantitative description of membrane current and its application to conduction and excitation in nerve," *The Journal of Physiology*, Vol. 117, no. 4, pp. 500–544, 1952.

32. Catterall, W. A., I. M. Raman, H. P. C. Robinson, T. J. Sejnowski, and O. Paulsen, "The hodgkin-huxley heritage: from channels to circuits.," *The Journal of Neuroscience*, Vol. 32, no. 41, pp. 14064–14073, 2012.

33. Hille, B., "Ionic channels in excitable membranes. current problems and biophysical approaches.," *Biophysical Journal*, Vol. 22, no. 2, pp. 283–294, 1978.

34. Beneski, D. A., and W. A. Catterall, "Covalent labeling of protein components of the sodium channel with a photoactivable derivative of scorpion toxin.," *Proceedings of the National Academy of Sciences of the United States of America*, Vol. 77, no. 1, pp. 639–643, 1980.

35. Ogata, N., and Y. Ohishi, "Molecular diversity of structure and function of the voltage-gated na + channels," *The Japanese Journal of Pharmacology*, Vol. 377, no. 88, pp. 365–377, 2002.

36. Patino, G. A., and L. L. Isom, "Electrophysiology and beyond: multiple roles of na+ channel β subunits in development and disease.," *Neuroscience Letters*, Vol. 486, no. 2, pp. 53–59, 2010.

37. Patton, D. E., L. L. Isom, W. A. Catterall, and A. L. Goldin, "The adult rat brain β subunit modifies activation and inactivation gating of multiple sodium channel α subunits," *The Journal of Biological Chemistry*, Vol. 269, no. 26, pp. 17649–17655, 1994.

38. Brackenbury, W. J., and L. L. Isom, "Na channel β subunits: Overachievers of the ion channel family.," *Frontiers in Pharmacology*, Vol. 2, p. 53, September 2011.

39. Sato, C., Y. Ueno, K. Asai, T. Takahashi, M. Sato, A. Engel, and Y. Fujiyoshi, "The voltage-sensitive sodium channel is a bell-shaped molecule with several cavities," *Letters to Nature*, Vol. 409, pp. 1047–1051, 2001.

40. Waxman, S. G., "The neuron as a dynamic electrogenic machine : modulation of sodium-channel expression as a basis for functional plasticity in neurons," *Philosophical Transactions of The Royal Society*, Vol. 355, pp. 199–213, 2000.

41. Ashcroft, F. M., *Ion Channels and Disease*, Academic Press, 1999.

42. Catterall, W. A., "Voltage-dependent gating of sodium channels: correlating structure and function," *Trends in Neurosciences*, pp. 7–10, January 1986.

43. Payandeh, J., T. M. G. El-Din, T. Scheuer, N. Zheng, and W. A. Catterall, "Crystal structure of a voltage-gated sodium channel in two potentially inactivated states.," *Nature*, Vol. 486, no. 7401, pp. 135–139, 2012.

44. Lehmann-horn, F., and K. Jurkat-rott, "Voltage-gated ion channels and hereditary disease," *Physiological Reviews*, Vol. 79, no. 4, pp. 1317–1373, 1999.

45. Hayward, L. J., R. H. Brown, and S. C. Cannon, "Slow inactivation differs among mutant na channels associated with myotonia and periodic paralysis," *Biophysical Journal*, Vol. 72, pp. 1204–1219, March 1997.

46. Liu, X. L., X. J. Huang, X. H. Luan, H. Y. Zhou, T. Wang, J. Y. Wang, S. D. Chen, H. D. Tang, and L. Cao, "Mutations of scn4a gene cause different diseases: 2 case reports and literature review," *Channels (Austin)*, Vol. 9, no. 2, pp. 82–87, 2015.

47. Catterall, W. A., "Ion channel voltage sensors: structure, function, and pathophysiology.," *Neuron*, Vol. 67, pp. 915–928, September 2010.

48. Meisler, M. H., and J. A. Kearney, "Review series sodium channel mutations in epilepsy and other neurological disorders," *The Journal of Clinical Investigation*, Vol. 115, no. 8, pp. 2010–2017, 2005.

49. Cannon, S. C., "Pathomechanisms in channelopathies of skeletal muscle and brain," *Annual Review of Neuroscience*, Vol. 29, pp. 387–415, 2006.

50. George, A. L., "Inherited disorders of voltage-gated sodium channels," *The Journal of Clinical Investigation*, Vol. 115, August 2005.

51. Eijkelkamp, N., J. E. Linley, M. D. Baker, M. S. Minett, R. Cregg, R. Werdehausen, F. Rugiero, and J. N. Wood, "Neurological perspectives on voltage-gated sodium channels," *Brain*, Vol. 135, pp. 2585–2612, 2012.

52. Crill, W. E., "Persistent sodium current in mammalian central neurons," *Annual Reviews of Physiology*, Vol. 58, no. 31, pp. 349–362, 1996.

53. French, C. R., and P. Sah, "A voltage-dependent persistent sodium current in mammalian hippocampal neurons.," *The Journal of General Physiology*, Vol. 95, pp. 1140–1157, June 1990.

54. Brown, A. M., P. C. Schwindt, and W. E. Crill, "Different voltage dependence of transient and persistent na + currents is compatible with modal-gating hypothesis for sodium channels," *Journal of Neurophysiology*, Vol. 71, pp. 2562–2565, June 1994.

55. VanZundert, B., P. Izaurieta, E. FritZ, and F. J. Alvarez, "Early pathogenesis in the adult-onset neurodegenerative disease amyotrophic lateral sclerosis.," *Journal of Cellular Biochemistry*, Vol. 3312, pp. 3301–3312, June 2012.

56. Goldin, A., "Mechanisms of sodium channel inactivation," *Current Opinion in Neurobiology*, Vol. 13, no. 3, pp. 284–290, 2003.

57. Hammarstrom, A. K. M., and P. W. Gage, "Oxygen-sensing persistent sodium channels in rat hippocampus," *The Journal of Physiology*, Vol. 591, no. 1, pp. 107–118, 2000.

58. Franceschetti, S., S. Taverna, G. Sancini, F. Panzica, R. Lombardi, and G. Avanzini, "Protein kinase c-dependent modulation of na currents increases the excitability of rat neocortical pyramidal neurones," *Journal of Physiology*, Vol. 2, pp. 291–304, 2000.

59. Zona, C., A. Siniscalchi, N. B. Mercuri, and G. Bernardi, "Riluzole interacts with voltage-activated sodium and potassium currents in cultured rat cortical neurons.," *Neuroscience*, Vol. 85, pp. 931–938, Aug 1998.

60. Kuo, J. J., T. Siddique, R. Fu, and C. J. Heckman, "Increased persistent na(+) current and its effect on excitability in motoneurones cultured from mutant sod1 mice," *The Journal of Physiology*, Vol. 563, no. 3, pp. 843–854, 2005.

61. Cifra, A., F. Nani, and A. Nistri, "Riluzole is a potent drug to protect neonatal rat hypoglossal motoneurons in vitro from excitotoxicity due to glutamate uptake block.," *European Journal of Neuroscience*, Vol. 33, pp. 899–913, Mar 2011.

62. Schuster, J. E., R. Fu, T. Siddique, and C. J. Heckman, "Effect of prolonged riluzole exposure on cultured motoneurons in a mouse model of als.," *Journal of Neurophysiology*, Vol. 107, no. 1, pp. 484–492, 2012.

63. Bellingham, M. C., "Pre- and postsynaptic mechanisms underlying inhibition of hypoglossal motor neuron excitability by riluzole.," *Journal of Neurophysiololgy*, Vol. 110, pp. 1047–1061, Sep 2013.

64. Dascal, N., "The use of xenopus oocytes for the study of ion channel," *Critical Reviews in Biochemisty*, Vol. 22, no. 4, pp. 317–387, 187.

65. Gurdon, J. B., C. D. Lane, H. R. Woodland, and G. Marbaix, "Use of frog eggs and oocytes for the study of messenger rna and its translation in living cells.," *Nature*, Vol. 233, pp. 177–82, September 1971.

66. Clare, J. J., and D. J. Trezise, *Expression of Ion Channels in Xenopus Oocytes*, Weinheim, FRG: Wiley-VCH Verlag GmbH, 2006.

67. Taylor, M. A., A. D. Johnson, and L. D. Smith, "Growing xenopus oocytes have spare translational capacity," *Proceedings of the National Academy of Sciences of the United States of America*, Vol. 82, pp. 6586–8589, October 1985.

68. Dibhajj, S. D., T. R. Cummins, J. A. Black, and S. G. Waxman, "From genes to pain: Nav1.7 and human pain disorders," *Trends in Neuroscience*, Vol. 30, pp. 555–563, 2007.

69. Helbig, I., I. E. Scheffer, J. C. Mulley, and S. F. Berkovic, "Navigating the channels and beyond: unravelling the genetics of the epilepsies," *The Lancet Neurology*, Vol. 7, pp. 231–245, 2008.

70. Noebels, J. L., "How a sodium channel mutation causes epilepsy," *Epilepsy Currents*, Vol. 3, pp. 70–71, 2003.

71. Sisodia, S., J. H. Cross, I. Blumcke, D. Chadwick, J. Craig, P. B. crino, P. Debenham, N. Delanty, F. Elmslie, and M. Gardiner, "Genetics of epilepsy: epilepsy research foundation workshop report," *Epileptic Disorders*, Vol. 9, pp. 194–236, 2007.

72. Beckh, S., M. Noda, H. Lubbert, and S. Numa, "Differential regulation of three sodium channel messenger rnas in the rat central nervous system during development," *EMBO Journal*, Vol. 8, pp. 3611–3616, 1989.

73. Felts, P. A., S. Yokohama, S. Dib-Hajj, J. A. Black, and S. G. Waxman, "Sodium channel α-subunit mrnas i, ii, iii, nag, na6 and hne (pn1): different expression patterns in developing rat nervous system," *Molecular Brain Research*, Vol. 45, pp. 71–82, 1997.

74. Waxman, S. G., J. D. Kocsis, and J. A. Black, "Type iii sodium channel mrna is expressed in embryonic but not adult spinal sensory neurons, and is reexpressed following axotomy," *Journal of Neurophysiology*, Vol. 72, pp. 466–470, 194.

75. Estacion, M., A. Gasser, S. D. Dib-Hajj, and S. G. Waxman, "A sodium channel mutation linked to epilepsy increases ramp and persistent current of nav1.3 and induces hyperexcitability in hippocampal neurons," *Experimental Neurology*, Vol. 224, no. 2, pp. 362–368, 2010.

76. Holland, K. D., J. A. Kearney, T. A. Glauser, G. Buck, M. Keddache, J. R. Blankston, I. W. Glaaser, R. S. Kass, and M. H. Meisler, "Mutation of sodium channel scn3a in a patient with cryptogenic pediatric partial epilepsy," *Neuroscience Letters*, Vol. 433, no. 1, pp. 65–70, 2008.

77. Lampert, A., B. C. Hains, and S. G. Waxman, "Upregulation of persistent and ramp sodium current in dorsal horn neurons after spinal cord injury," *Experimental Brain Research*, Vol. 174, no. 4, pp. 660–666, 2006.

78. Dascal, N., "Voltage clamp recordings from xenopus ooytes," *Current Protocols in Neuroscience*, Vol. 6, no. 12, pp. 2–20, 2000.

79. Hadzipasic, M., B. Tahvildari, M. Nagy, M. Bian, A. L. Horwich, and D. A. McCormick, "Selective degeneration of a physiological subtype of spinal motor neuron in mice with sod1-linked als," *Proceedings of the National Academy of Sciences of the United States of America*, Vol. 111, pp. 16883–16888, November 2014.

80. Martin, E., W. E. Cazenave, D. Cattaert, and P. Branchereau, "Embryonic alteration of motoneuronal morphology induces hyperexcitability in the mouse model of amyotrophic lateral sclerosis," *Neurobiology of Disease*, Vol. 54, pp. 116–126, 2013.

81. Quinlan, K. A., J. E. Schuster, R. Fu, T. Siddique, and C. J. Heckman, "Altered postnatal maturation of electrical properties in spinal motoneurons in a mouse model of amyotrophic lateral sclerosis," *Journal of Physiology*, Vol. 589, no. 9, pp. 2245–2260, 2011.

82. Chang, Q., and L. J. Martin, "Glycine receptor channels in spinal motoneurons are abnormal in a transgenic mouse model of amyotrophic lateral sclerosis," *The Journal of Neuroscience*, Vol. 31, pp. 2815–2827, February 2011.

83. Kuo, J. J., M. Schonewille, T. Siddique, A. N. A. Schults, R. Fu, P. R. Bar, R. Anelli, C. J. Heckman, and A. B. A. Kroese, "Hyperexcitability of cultured spinal motoneurons from presymptomatic als mice," *Journal of Neurophysiology*, Vol. 91, pp. 571–575, 2004.

84. Bories, C., J. Amendola, B. L. d'Incamps, and J. Durand, "Early electrophysiological abnormalities in lumbar motoneurons in a transgenic mouse model of amyotrophic lateral sclerosis.," *The European Journal of Neuroscience*, Vol. 25, no. 2, pp. 451–459, 2007.

85. Pieri, M., F. Albo, C. Gaetti, A. Spalloni, C. P. Bengtson, P. Longone, S. Cavalcanti, and C. Zona, "Altered excitability of motor neurons in a transgenic mouse model of familial amyotrophic lateral sclerosis," *Neuroscience Letters*, Vol. 351, pp. 153–156, 2003.

86. Zona, C., M. Pieri, and I. Carunchio, "Voltage-dependent sodium channels in spinal cord motor neurons display rapid recovery from fast inactivation in a mouse model of amyotrophic lateral sclerosis.," *Journal of Neurophysiology*, Vol. 96, no. 6, pp. 3314–3322, 2006.

87. Carter, J. R., and M. Mynlieff, "Amyotrophic lateral sclerosis patient igg alters voltage dependence of ca+2 channels in dissociated rat motoneurons," *Neuroscience Letters*, Vol. 353, pp. 221–225, 2003.

88. Damme, P. V., M. Leyssen, G. Callewaert, and W. Robberecht, "The ampa receptor antagonist nbqx prolongs survival in a transgenic mouse model of amyotrophic lateral sclerosis," *Neuroscience Letters*, Vol. 343, pp. 81–84, 2003.

89. Vanselow, B. K., and B. U. Keller, "Calcium dynamics and buffering in oculomotor neurones from mouse that are particularly resistant during amyotrophic lateral sclerosis (als) -related motoneurone disease," *Journal of Physiology*, Vol. 525, no. 2, pp. 433–445, 2000.

90. van Zundert, B., M. H. Peuscher, M. Hynynen, A. Chen, R. L. Neve, R. H. Brown, M. C. Paton, and M. C. Bellingham, "Neonatal neuronal circuitry shows hyperexcitable disturbance in a mouse model of the adult-onset neurodegenerative disease amyotrophic lateral sclerosis.," *The Journal of Neuroscience*, Vol. 28, no. 43, pp. 10864–10874, 2008.

91. Zona, C., A. Siniscalchi, N. B. Mercuri, and G. Bernardi, "Riluzole interacts with voltage-activated sodium and potassium currents in cultured rat cortical neurons.," *Neuroscience*, Vol. 85, pp. 931–938, August 1998.

92. Pieri, M., I. Carunchio, L. Curcio, N. B. Mercuri, and C. Zona, "Increased persistent sodium current determines cortical hyperexcitability in a genetic model of amyotrophic lateral sclerosis.," *Experimental Neurology*, Vol. 215, no. 2, pp. 368–379, 2009.

93. Pieri, M., S. Caioli, N. Canu, N. B. Mercuri, E. Guatteo, and C. Zona, "Over-expression of n-type calcium channels in cortical neurons from a mouse model of amyotrophic lateral sclerosis," *Experimental Neurology*, Vol. 247, pp. 349–358, 2013.

94. Wainger, B. J., E. Kiskinis, C. Mellin, O. Wiskow, S. S. W. Han, J. Sandoe, N. P. Perez, L. A. Williams, S. Lee, G. Boulting, J. D. Berry, R. H. Brown, M. E. Cudkowicz, B. P. Bean, K. Eggan, and C. J. Woolf, "Intrinsic membrane hyperexcitability of amyotrophic lateral sclerosis patient-derived motor neurons.," *Cell Reports*, Vol. 7, no. 1, pp. 1–11, 2014.

95. Palma, E., M. Inghilleri, L. Conti, C. Deflorio, V. Frasca, A. Manteca, F. Pichiorri, C. Roseti, G. Torchia, C. Limatola, F. Grassi, and R. Miledi, "Physiological characterization of human muscle acetylcholine receptors from als patients," *Proceedings of the National Academy of Sciences of the United States of America*, Vol. 108, no. 50, pp. 20184–20188, 2011.

96. Allen, M. J., J. J. Lacroix, S. Ramachandran, R. Capone, J. L. Whitlock, G. D. Ghadge, M. F. Arnsdorf, R. P. Roos, and R. Lal, "Mutant sod1 forms ion channel : Implications for als pathophysiology," *Neurobiology of Disease*, Vol. 45, no. 3, pp. 831–838, 2012.

97. Pambo-Pambo, A., J. J Durand, and J. P. Gueritaud, "Early excitability changes in lumbar motoneurons of transgenic sod1g85r and sod1g(93a-low) mice.," *Journal of Neurophysiology*, Vol. 102, no. 6, pp. 3627–3642, 2009.

98. Andjus, P. R., Z. Stevic-marinkovic, and E. Cherubini, "Immunoglobulins from motoneurone disease patients enhance glutamate release from rat hippocampal neurones in culture," *Journal of Physiology*, Vol. 504, no. 1, pp. 103–112, 1997.

99. McGown, A., J. R. McDearmid, N. Panagiotaki, H. Tong, S. A. Mashhadi, N. Redhead, A. N. Lyon, C. E. Beattie, P. J. Shaw, and T. M. Ramesh, "Early interneuron dysfunction in als : Insights from a mutant sod1 zebrafish model," *Annals of Neurology*, Vol. 73, no. 2, pp. 246–258, 2013.

100. Jiang, M., J. E. Schuster, R. Fu, T. Siddique, and C. J. Heckman, "Progressive changes in synaptic inputs to motoneurons in adult sacral spinal cord of a mouse model of amyotrophic lateral sclerosis," *Neurobiology of Disease*, Vol. 29, no. 48, pp. 15031–15038, 2009.

101. Damme, P. V., E. Bogaert, M. Dewil, N. Hersmus, D. Kiraly, W. Scheveneels, I. Bockx, D. Braeken, N. Verpoorten, K. Verhoeven, V. Timmerman, P. Herijgers, G. Callewaert, P. Carmeliet, L. V. D. Bosch, and W. Robberecht, "Astrocytes regulate glur2 expression in motor neurons and their vulnerability to excitotoxicity," *Proceedings of the National Academy of Sciences of the United States of America*, Vol. 204, no. 37, pp. 14825–14830, 2007.

102. Rotunno, M. S., J. R. Auclair, S. Maniatis, S. A. Shaffer, J. Agar, and D. A. Bosco, "Identification of a misfolded region in superoxide dismutase 1 that is exposed in amyotrophic lateral sclerosis.," *The Journal of Biological Chemistry*, Vol. 289, no. 41, pp. 28527–38, 2014.

103. O'Connell, D., K. Mruk, J. M. Rocheleau, and W. R. Kobertz, "Xenopus laevis oocytes infected with multi-drug-resistant bacteria: implications for electrical recordings.," *The Journal of General Physiology*, Vol. 138, no. 2, pp. 271–7, 2011.

104. Nelson, M. E., *Hodgkin-Huxley Models*, pp. 1–12. Electrophysiological Models, New York: Wiley, New York, 2004.

105. Carnevale, N. T., and M. L. Hines, *The NEURON Book*, Cambridge, UK: Cambridge University Press, 2006.

106. Spalloni, A., F. Albo, F. Ferrari, N. Mercuri, G. Bernardi, and C. Zona, "Cu/zn-superoxide dismutase (gly93-ala) mutation alters ampa receptor subunit expression and function and potentiates kainate-mediated toxicity in motor neurons in culture.," *Neurobiology of Disease*, Vol. 15, no. 2, pp. 340–350, 2004.

107. Geracitano, R., ECPaolucci, S. Prisco, E. Guatteo, C. Zona, P. Longone, M. Ammassari-Teule, G. Bernardi, N. Berretta, and N. B. Mercuri, "Altered long-term corticostriatal synaptic plasticity in transgenic mice overexpressing human cu/zn superoxide dismutase (gly93-ala) mutation," *Neuroscience*, Vol. 118, pp. 399–408, 2003.

108. Rook, M. B., C. B. Alshinawi, W. A. Groenewegen, C. V. I. Gelder, A. C. G. V. Ginneken, H. J. Jongsma, M. M. A. M. Mannens, and A. A. M. Wilde, "Human scn5a gene mutations alter cardiac sodium channel kinetics and are associated with the brugada syndrome," *Cardiovascular Research*, Vol. 44, pp. 507–517, 1999.

109. Reuter, H., and H. Porzig, "Localization and functional significance of the na + / ca 2+ exchanger in presynaptic boutons of hippocampal cells in culture," *Neuron*, Vol. 15, pp. 1077–1084, 1995.

110. Vucic, S., and M. C. Kiernan, "Novel threshold tracking techniques suggest that cortical hyperexcitability is an early feature of motor neuron disease.," *Brain*, Vol. 129, pp. 2436–4236, 2006.

111. Fritz, E., P. Izaurieta, A. Weiss, F. R. M. FR, P. Rojas, D. Gonzalez, F. Rojas, R. H. jr Brown, R. Madrid, and B. van Zundert, "Mutant sod1-expressing astrocytes release toxic factors that trigger motoneuron death by inducing hyperexcitability," *Journal of Neurophysiology*, Vol. 109, pp. 2803–2814, June 2013.

112. Roselli, F., and P. Caroni, "From intrinsic firin g properties to selective neuronal vulnerability in neurodegenerative diseases," *Neuron*, Vol. 85, pp. 901–910, 2015.

113. Saxena, S., F. Roselli, K. Leptien, and J. P. Julien, "Neuroprotection through excitability and mtor required in als motoneurons to delay disease and extend survival.," *Neuron*, Vol. 80, pp. 80–96, 2013.

114. Kirby, J., E. Halligan, M. J. Baptista, S. Allen, P. R. Heath, H. Holden, S. C. Barber, L. Loynes, C. A. Wood-Allum, J. Lunec, and P. J. Shaw, "Mutant sod1 alters the motor neuronal transcriptome: implications for familial als.," *Brain*, Vol. 128, pp. 1686–1706, 2005.

115. Ryu, H., K. Smith, S. I. Camelo, I. Carreras, J. Lee, A. H. Iglesias, F. Dangond, K. A. Cormier, M. E. Cudkowicz, R. H. Brown, and R. J. Ferrante, "Sodium phenylbutyrate prolongs survival and regulates expression of anti-apoptotic genes in transgenic amyotrophic lateral sclerosis mice.," *Journal of Neurochemistry*, Vol. 93, pp. 1087–1098, 2005.

116. Hongpaisan, J., C. A. Winters, and S. B. Andrews, "Strong calcium entry activates mitochondrial superoxide generation, upregulating kinase signaling in hippocampal neurons.," *The Journal of Neuroscience*, Vol. 24, no. 48, pp. 10878–10887, 2004.

117. Hu, J. H., K. Chernoff, S. Pelech, and C. Krieger, "Protein kinase and protein phosphatase expression in the central nervous system of g93a msod over-expressing mice," *The Journal of Neurochemistry*, Vol. 85, pp. 422–431, 2003.

118. Knapp, L. T., and E. Klann, "Superoxide-induced stimulation of protein kinase c via thiol modification and modulation of zinc content.," *The Journal of Biological Chemistry*, Vol. 275, pp. 24136–24145, 2000.

119. Numann, R., W. A. Catteral, and T. Scheuer, "Functional modulation of brain sodium channels by protein kinase c phosphorylation," *Science*, Vol. 254, pp. 115–118, October 1991.

120. Ellis, D. Z., J. Rabe, and K. J. Sweadner, "Global loss of na , k-atpase and its nitric oxide-mediated regulation in a transgenic mouse model of amyotrophic lateral sclerosis," *Journal of Neuroscience*, Vol. 23, no. 1, pp. 43–51, 2003.

121. Heath, P. R., and P. J. Shaw, "Update on the glutamatergic neurotransmitter system and the role of excitotoxicity in amyotrophic lateral sclerosis.," *Muscle and Nerve*, Vol. 26, pp. 438–458, October 2002.

122. Hand, C. K., and G. A. Rouleau, "Familial amyotrophic lateral sclerosis," *Muscle Nerve*, Vol. 25, no. 2, pp. 135–159, 202.

123. Cantrell, A. R., and W. A. Catterall, "Neuromodulation of na+ channels: an unexpected form of cellular plasticity.," *Nature Reviews Neuroscience*, Vol. 2, pp. 397–407, June 2001.

124. Israelson, A., N. Arbel, S. Cruz, H. Illieva, K. Yamanaka, V. Shoshan-Barmatz, and D. W. Cleveland, "Misfolded mutant sod1 directly inhibits vdac1 conductance in a mouse model of inherited als.," *Neuron*, Vol. 67, August 2010.

125. Lemasters, J. J., and E. Holmuhamedov, "Voltage-dependent anion channel (vdac) as mitochondrial governator–thinking outside the box.," *Biochimica et Biophysica Acta*, Vol. 1762, pp. 181–190, 2006.

126. Rojas, F., N. Cortes, S. Abarzua, A. Dyrda, and B. van Zundert, "Astrocytes expressing mutant sod1 and tdp43 trigger motoneuron death that is mediated via sodium channels and nitroxidative stress," *Frontiers in Neuroscience*, Vol. 8, Feb 2014.

127. Catterall, W. A., E. Perez-Reyes, T. P. S. TP, and J. Striessnig, "International union of pharmacology. xlviii. nomenclature and structure-function relationships of voltage-gated calcium channels," *Pharmacological Reviews*, Vol. 57, pp. 411–425, Dec 2005.

128. Fleidervish, I. A., and L. Libman, "How cesium dialysis affects the passive properties of pyramidal neurons: implications for voltage clamp studies of persistent sodium current.," *New Journal of Physics*, Vol. 10, pp. 35001–35013, 2008.

129. Chen-Izu, Y., R. M. Shaw, G. S. Pitt, V. Yarov-Yarovoy, J. T. Sack, H. Abriel, R. W. Aldrich, L. Belardinelli, M. B. Cannell, W. A. Catterall, W. J. Chazin, N. Chiamvimonvat, I. D. I, E. Grandi, T. J. Hund, L. T. Izu, L. S. Maier, V. A. Maltsev, C. Marionneau, P. J. Mohler, S. Rajamani, R. L. Rasmusson, E. A. Sobie, C. E. Clancy, and D. M. Bers, "Na(+) channel function, regulation, structure, trafficking and sequestration," *Journal of Physiology*, Vol. 593, pp. 1347–1360, March 2015.

130. Catterall, W. A., "Structure and function of voltage-gated sodium channels at atomic resolution," *Experimental Physiology*, Vol. 99, pp. 35–51, January 2014.

131. Ellerkmann, R. K., V. Riazanski, C. E. Elger, B. W. Urban, and H. Beck, "Slow recovery from inactivation regulates the availability of voltage-dependent na + channels in hippocampal granule cells , hilar neurons and basket cells," *Journal of Physiology*, Vol. 532, pp. 385–397, April 2001.

132. Joho, R. H., J. R. Moorman, A. M. VanDongen, G. E. Kirsch, H. Silberberg, G. Schuster, and A. M. Brown, "Toxin and kinetic profile of rat brain type iii sodium channels expressed in xenopus oocytes," *Molecular Brain Research*, Vol. 7, pp. 105–113, February 1990.

133. Isom, L. L., "Sodium channel β subunits: Anything but auxiliary," *The Neuroscientist*, Vol. 7, no. 1, pp. 42–54, 2001.

134. ElBasiouny, S. M., J. E. Schuster, and C. J. Heckman, "Persistent inward currents in spinal motoneurons: Important for normal function but potentially harmful after spinal cord injury and in amyotrophic lateral sclerosis," *Clinical Neurophysiology*, Vol. 121, p. 1669, 2010.

135. Alessandri-Haber, N., G. Alcaraz, C. Deleuze, F. Jullien, C. Manrique, F. Couraud, M. Crest, and P. Giraud, "Molecular determinants of emerging excitability in rat embryonic motoneurons.," *Journal of Physiology*, Vol. 541, pp. 25–39., May 2002.

136. Goldin, A. L., "Diversity of mammalian voltage-gated sodium channels," *Annals of the New York Academy of Sciences*, Vol. 1, no. 868, pp. 38–50, 1999.

137. Katz, L. C., and C. J. Shatz, "Synaptic activity and the construction of cortical circuits," *Science*, Vol. 703, no. 1963, pp. 1133–1138, 1995.

138. Bensimon, G., L. Lacomblez, and V. Meininger, "A controlled trial of riluzole in amyotrophic lateral sclerosis. als/riluzole study group," *N Engl J Med*, Vol. 330, pp. 585–591, March 1994.

139. Zeuthen, T., E. Zeuthen, and D. A. Klaerke, "Mobility of ions, sugar, and water in the cytoplasm of xenopus oocytes expressing na+-coupled sugar transporters (sglt1)," *The Journal of Physiology*, Vol. 542, no. 1, pp. 71–87, 2002.

140. Squire, L., D. D, F. B. F, S. D. Lac, A. Ghosh, and N. Spitzer, *Fundamental Neuroscience*, USA: Academic Press, 3rd ed., 2008.

141. Lu, S. H., and Y. T. Dai, "Normal body temperature and the effects of age, sex, ambient temperature and body mass index on normal oral temperature: a prospective, comparative study.," *International Journal of Nursing Studies*, Vol. 46, no. 5, pp. 661–668, 2009.